UNIVERSITÀ DEGLI STUDI DI MESSINA

Dottorato di Ricerca in Fisica

"Earthquake kinematics and seismogenic stress fields in the Calabrian Arc region"

Tesi di Dottorato di:

Silvia Scolaro

Tutor:

Prof.ssa Barbara Orecchio

XXXI ciclo

ABSTRACT

L'obiettivo di questa tesi è contribuire al miglioramento delle conoscenze sismotettoniche e geodinamiche relative all'area dell'Arco Calabro, fornendo stime accurate dei meccanismi focali e dei campi di sforzo sismogenetico e proponendo nuovi approcci per lo studio dei terremoti storici.

L'Arco Calabro è uno dei settori a più alto rischio sismico in Italia, colpito nei secoli scorsi da numerosi terremoti distruttivi. Inoltre, l'alta eterogeneità cinematica che lo caratterizza, dovuta alla coesistenza di diversi domini tettonici, lo raffigura come uno dei domini geodinamicamente più complessi del Mediterraneo, oggetto di vari dibattiti nella letteratura scientifica recente.

In questa tesi viene utilizzata la tecnica di inversione CAP per il calcolo dei meccanismi focali dei terremoti dell'Arco Calabro. La qualità delle soluzioni ottenute con questo metodo, anche per terremoti di magnitudo relativamente bassa ($2.5 \leq M_w \leq 3.5$), è stata dimostrata tramite vari test di stabilità appositamente costruiti che hanno anche permesso di stimare errori dei parametri focali minori di 10°. L'applicazione di questa tecnica ha consentito la realizzazione del database, ad oggi più aggiornato, dei meccanismi focali dei terremoti dell'Arco Calabro espandendolo in un range di magnitudo non incluso nei cataloghi ufficiali. Il nuovo database, composto da più di 400 meccanismi focali, ha fornito un quadro della cinematica dei diversi settori dell'area in studio ed è stato fondamentale per il calcolo dei campi di sforzo sismogenetico effettuato tramite la tecnica di Arnold e Townend (2007). I risultati ottenuti hanno permesso di ben vincolare il dominio estensionale lungo la catena e quello compressivo nel Tirreno meridionale. Inoltre, è stato caratterizzato per la prima volta un dominio trascorrente nel settore del Mar Ionio.

A fronte di una sismicità storica energeticamente significativa lo studio della sismicità recente dell'Arco Calabro evidenzia l'assenza di

terremoti di particolare rilevanza energetica (M>5), in grado di fornire informazioni più dirette sui processi tettonici a scala regionale. I recenti sviluppi dei metodi di localizzazione e di inversione delle forme d'onda e le nuove tecniche di processamento delle registrazione analogiche forniscono l'opportunità di analizzare gli eventi del passato e di recuperare, quindi, un patrimonio di informazioni particolarmente significativo. A tal proposito è stato analizzato il terremoto avvenuto in Calabria l'8 Settembre 1905 ($M_w \geq 7$), identificato da alcuni autori come il più forte terremoto italiano. La rilocalizzazione tramite la tecnica Bayloc ha consentito di ottenere per la prima volta una stima ipocentrale dell'evento, collocandolo nella zona off-shore della Calabria ad una profondità compresa tra 35-55 km. Tale risultato e l'attenta valutazione delle informazioni da letteratura suggeriscono che il terremoto sia avvenuto nella zona di flessione dello slab ionico in subduzione e che la sua magnitudo sia dell'ordine di 7.5. Tale risultato permette, inoltre, di fare nuove valutazioni sulla possibile relazione causale fra il terremoto del 1905 e quello verificatosi nello Stretto di Messina nel 1908.

Un differente approccio è stato applicato per analizzare il terremoto di Ferruzzano dell' 11 Marzo 1978, il più recente evento $M_w>5$ dell'area di studio, verificatosi prima dell'avvento della rete sismica digitale e per il quale la letteratura propone soluzioni focali e localizzazioni alquanto discordanti tra loro. Lo studio qui riportato mostra i risultati di una complessa modellazione dei sismogrammi analogici raccolti, la rilocalizzazione e l'analisi tramite inversione delle forme d'onda per il calcolo del meccanismo focale e del momento sismico. La soluzione ottenuta indica una profondità focale di 8 km ed un orientamento circa N-S per il piano di faglia normale, in buon accordo con il regime estensionale riconosciuto in Calabria meridionale da dati sismologici, geodetici e geologici. La magnitudo stimata, $M_w=4.7$, denota una sovrastima delle precedenti analisi dimostrando la capacità dell'algoritmo di inversione di analizzare terremoti del passato anche di magnitudo medio-bassa.

CONTENTS

INTRODUCTION

The present PhD thesis was carried out in the framework of research activity of the geophysical team of the Mathematical and Computer Sciences, Physical Sciences and Earth Sciences Department of the University of Messina, and it was developed thanks to the close cooperation with teams of University of Granada, Cartographic and Geological Institute of Catalonia, University of Malta and Istituto Nazionale di Geofisica e Vulcanologia.
The results of my work have been published on international journals and were also discussed in the framework of national and international congresses.

The main aim of this thesis is to improve the knowledge of the seismotectonics of the Calabrian Arc region (South Italy) through a more accurate investigation of earthquake focal mechanisms and seismogenic stress fields. In particular new approaches for the inversion of seismogenic stress fields and for the study of individual historical earthquakes have been carried out.

The Calabrian Arc, (**Chapter 1**), is one of the more interesting area of the central Mediterranean because of a complex geodynamic scenario due to the coexistence of Africa-Eurasia plate convergence and rollback of the Ionian subduction slab. In historical times a relevant number of destructive earthquakes (up to 7-7.5 magnitude and XI–XII MCS intensities) occurred in the Calabrian Arc region, for example in 1638, 1783, 1905, 1908 (Rovida et al., 2016). Furthermore, the 1905 Calabria earthquake and the 1908 Messina Straits earthquake are among the largest events occurred in Italy. These events provoked thousands casualties, the destruction of many towns and cities in northeastern Sicily and Calabria, and also triggered environmental effects (Baratta, 1910). Despite the large amount of geological and geophysical studies

carried out in this area, the seismotectonic scenario is still argued, in particular concerning the actual setting of the rollback process of the Ionian subducting slab, the fault geometry of the strongest earthquakes and the relationship between large-scale geodynamics and more localized seismogenic processes (Neri et al., 2004; Galli et al., 2008; Billi et al., 2010; Palano, 2015; Presti et al., 2017; Tiberti et al., 2017).

In this framework earthquake focal mechanisms are a very powerful tool for studing the interactions among earthquakes, seismic faults and active tectonics. Focal mechanisms are geometrical representations of the faulting during an earthquake then, they provide essential information on local tectonic styles and they are prerequisite to compute the seismogenic stress fields of a region. The inversion of earthquake waveforms is a widely used approach, based on wave-field modeling, to extract quantitative information from seismograms and to estimate focal mechanism solutions. However, the reliability of focal mechanisms may decrease for low magnitude earthquakes (M<4) and their analysis is limited to the temporal range of earthquake instrumental recording. It follows that continuous processing and improvements of earthquake focal mechanisms are necessary to increase their reliability and to expand the temporal and magnitude range of focal mechanism databases.

In this thesis, the "Cut and Paste" (CAP) waveform inversion method of Zhao and Helmberger (1994) and Zhu and Helmberger (1996) has been used to estimate the focal mechanisms, moment magnitude and depths of the earthquakes of the Calabrian Arc region (**Chapter 2**). For its features this technique can be considered as a step forward on source parameters determination allowing to obtain reliable and high-quality focal mechanism solutions also for relatively low-magnitude earthquakes (down to a minimum of 2.6), usually not reported in the official catalogues (see e.g. CMT, RCMT, TDMT). In Chapter 2 new resolution and stability tests are shown with the aim to properly verify robustness and reliability of the focal mechanism parameters estimated for the study region by the CAP method. The obtained results reveal

that focal mechanism solutions are robustly determined also in very unfavourable conditions, then they respesent useful high-quality constraints for the analysis of the regional stress fields acting in southern Italy.

As shown in **Chapter 3**, thanks to the application of the CAP method the number of available solutions for the Calabrian Arc region is more than doubled by adding earthquakes of magnitude as small as 2.6 without overlooking the reability of results. The resulting focal mechanism database furnishes previous lacking data and basic information for investigating the actual dynamics of southern Italy by the computation of seismogenic stress. Taking benefit from the enhanced focal mechanism set, the seismogenic stress tensor variations over the study region have been investigated by a Bayesian technique (Arnold and Townend, 2007) deployed for estimating tectonic stress parameters from primary seismological observations. The stress distributions allowed to identify the subvolumes characterized by homogeneous behaviors, thus providing a detail picture of the main regional engines acting in this very complex area.

The focal mechanisms of relatively small earthquakes (M_w>2.6) have then furnished an important contribution for characterizing local tectonics and constraining stress orientation; moreover, moderate-to-major earthquakes (e.g., M_w≥5) may also provide a more direct evidence of regional-scale processes and main structural systems. Especially in a complex area as Calabrian Arc, the study of these events is crucial to fix new constraints in order to better characterize regional seismotectonics and seismic hazard. A quite small number of moderate-to-major earthquakes occurred in the Calabrian Arc region in the last ca. thirty years while numerous M_w≥5 earthquakes were recorded in the early phases of instrumental monitoring (e.g. 1900-1980; Rovida et al., 2016) and this makes very precious every effort aimed to accurately investigate past earthquakes. In the last years many authors have proven the effectiveness to analyze original seismograms by means of modern techniques to obtain quantitative information (e.g. Okal and

Reymond, 2003; Pino et al., 2008; Batlló et al., 2010; Vannoli et al., 2016; Stich et al., 2018). The efforts to recover and analyze past earthquakes through modern seismological techniques, main goal of Chapters 4 and 5 of the present thesis, allow obtaining information actually not available from the recent seismicity of southern Italy.

Chapter 4 is focused on the study of the September 1905 earthquake that several investigators identified as the strongest earthquake ever occurred in Italy, and for which quite different views exist concerning location, magnitude, and the causative process. The Bayloc location method proposed by Presti et al. (2004, 2008) has been used to estimate hypocenter location of the event. Bayloc is a Bayesian non-linear algorithm that estimates a probability density function for the location of a seismic event by using body wave arrival times. This method furnishes more accurate estimates of hypocenter parameters and location uncertainties with respect to the more commonly used linearized techniques. For this study, Bayloc has been applied to the original seismic wave arrival times recorded at the seismic observatories existing at that epoch. Despite the limitations of the seismometric network existing at the beginning of the past century, the hypocenter location obtained for the 1905 earthquake have suitable quality to investigate the process that generated the earthquake itself. Then, the obtained results allowed to examine possible generation process of the event and to estimate the stress perturbation that it may have induced in the area of the forthcoming 1908 Messina Straits earthquake. In particular, the study highlights that gravity pull of the Ionian subducting slab may have determined the 1905 earthquake rupture in the bending zone of the slab and this rupture has likely perturbed the shallow normal faults of the Tyrrhenian overriding plate in the Messina Straits area favoring the occurrence of the other major earthquake three years later.

The approach proposed in **Chapter 5** is based on instrumental data recovering and on analysis and modelling of original recorded waveforms of the latest M_w>5 earthquake occurred in southern

Calabrian, that is the 11 March 1978 Ferruzzano earthquake. The information available from literature for this event is quite contrasting and not well framed in the local seismotectonic scenario. A relevant work of data collection through the SISMOS (Michelini et al., 2005) and EuroSismos (Ferrari and Pino, 2003) archives has been carried out and a careful processing of the seismograms was needed for successful vectorialization. Thanks to the quality of the obtained data it was possible to re-analyze this event by applying the Bayloc technique and a modern-standard time-domain algorithm to determine hypocentral location, focal mechanism and seismic moment of the event. The time-domain waveform inversion analysis of Stich et al., (2005) has been applied for the first time in Italy. This technique allows a more stable waveform modeling of original analog data by directly processing the original un-rotated horizontal component seismograms and by applying the convolution of the corresponding instrument response to the synthetic Green's Functions. This procedure reduces errors due to the uncertainties of estimated transfer functions, to the misalignment of time signals from component to component, uneven drum speed and wrong polarities. In order to prove feasibility and effectiveness of both the inversion procedure and the results obtained in this study several tests have been performed. Thanks to the application of these advanced modern techniques it has been possible to re-evaluate the 1978 Ferruzzano earthquake furnishing a new hypocenter location and focal mechanism better framed in the local seismotectonic scenario, and a new moment magnitude estimate.

CHAPTER 1

GEODYNAMIC AND SEISMOTECTONIC FRAMEWORK OF THE CALABRIAN ARC REGION

1.1 Geodynamic setting

The Calabrian Arc (South Italy) is a Cenozoic-Quaternary curved orogenic belt shaped during the opening of the Tyrrhenian Sea, and running from the NW–SE-trending Southern Apennines to the E–W-trending Sicilian Maghrebides (Fig. 1.1. Malinverno and Ryan, 1986; Carminati et al., 1998; Wortel and Spakman, 2000; Rosenbaum and Lister, 2004; Billi et al., 2011; Faccenna et al., 2011). The geodynamic evolution in this area of the Central Mediterranean is the result of different and very complex geodynamic processes driven in the last 30-35 Ma by the NW-trending Nubia-Eurasia convergence and the residual southeastward rollback of the Ionian slab beneath the Tyrrhenian lithosphere (Fig. 1.1; Malinverno and Ryan, 1986; Catalano et al., 1996; Gueguen et al., 1998; Faccenna et al., 2001, 2004; Rosenbaum and Lister, 2004; Billi et al., 2011). Current plate convergence velocity in this region has been estimated to be on the order of ~5 mm/yr (Palano et al., 2012; Nocquet, 2012 and references therein) while subduction trench retreat has been progressively decreasing in the last million years until reaching at present time values as small as 2 mm/yr (Hollenstein et al., 2003; Devoti et al., 2008; D'Agostino et al., 2011; Palano et al., 2012).

The complex geodynamic scenario of the Calabrian Arc is also reflected in the different deformation patterns of the whole region (Fig. 1.2). Geological, seismological and geodetic observations highlight a

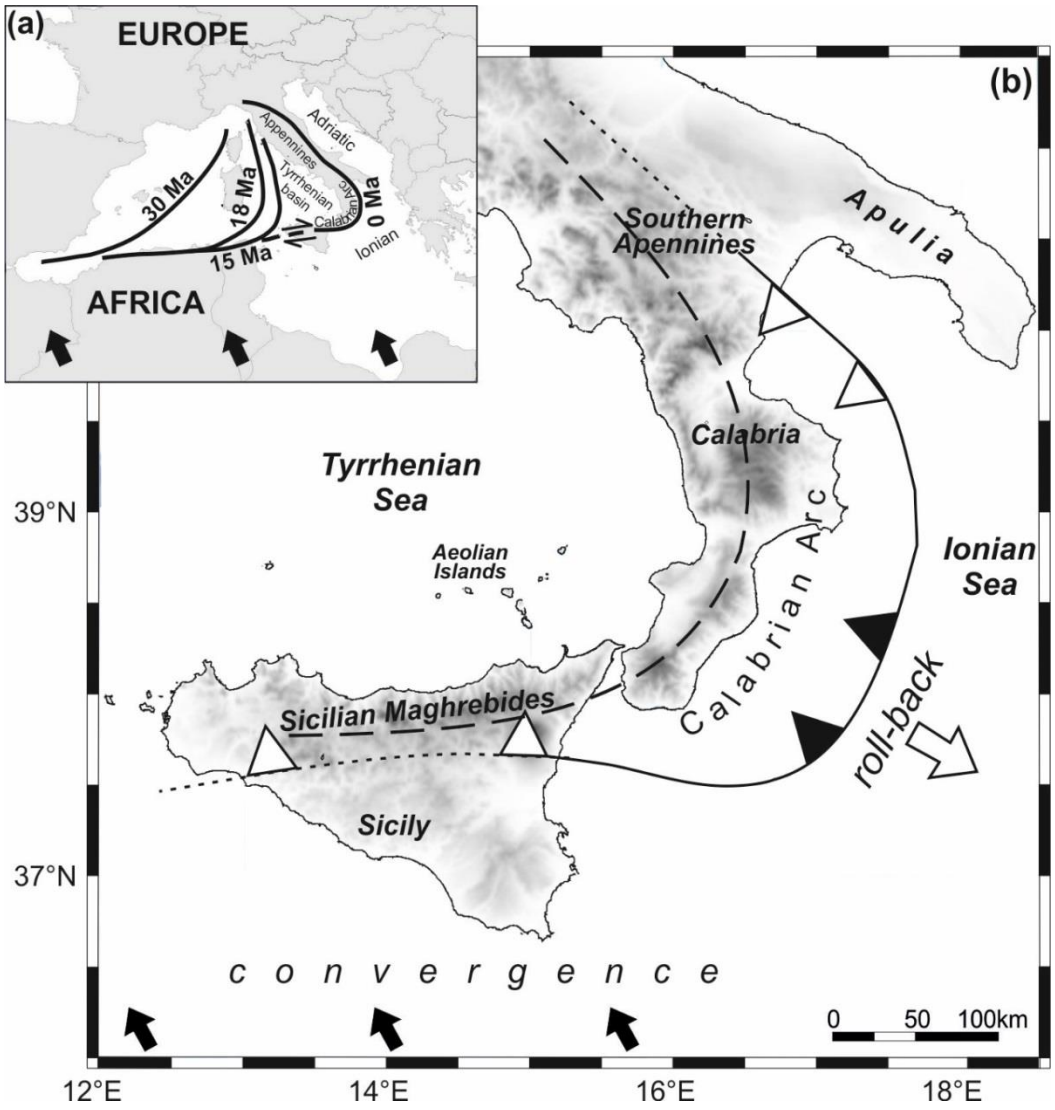

Figure 1.1 (a) Map of the Mediterranean region with the western Mediterranean plate boundary evolution in the last 30 Myrs (redrawn from Wortel and Spakman, 2000). The space-time evolution of the boundary marks the process of rollback of the subducting lithosphere and the related trench retreat until the present-day location near the Ionian shoreline of Calabria. Black arrows indicate the present motion of Africa relative to Europe (Nocquet, 2012; Nocquet and Calais, 2004). **(b)** Map view of the study area. The solid curve with the sawtooth pattern, pointing in the direction of subduction, indicates the present-day location of the Ionian subducting system. According to recent literature (see, among others, Neri et al. 2009, 2012 and Orecchio et al., 2014), black sawteeth indicate the continuous subducting slab while white sawteeth the plate boundary segments where slab has already undergone detachment. The white arrow shows the sense of the subducting slab rollback. The black arrows indicate the present motion of Africa relative to Europe (Nocquet, 2012 and references therein). The large dashed curve running from Southern Apennines to Sicilian Maghrebides through Calabria indicates the Apennine-Maghrebian chain.

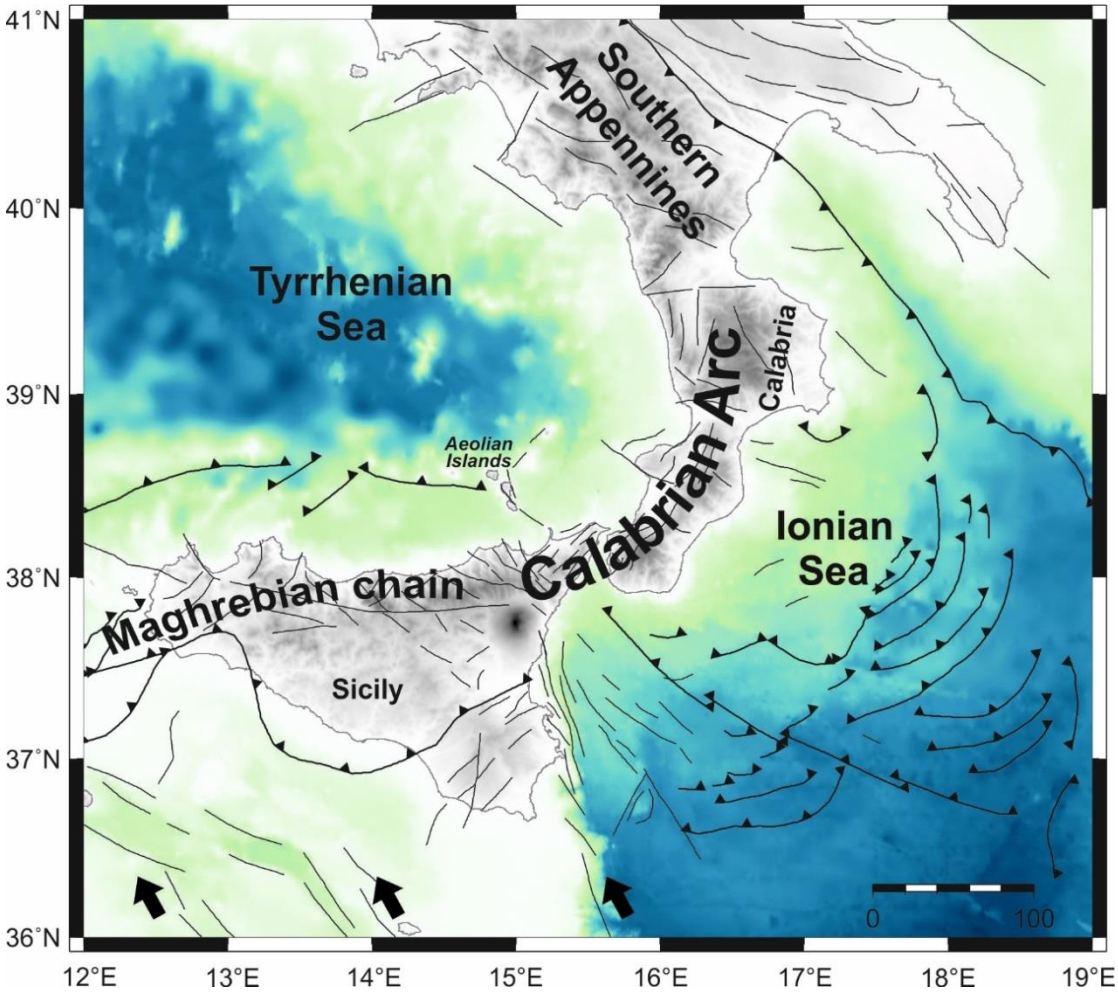

Figure 1.2 Simplified tectonic map of the study area and surrounding areas (redrawn by Palano et al., 2015).

crustal shortening accommodated in southern Tyrrhenian and an extensional deformation in northern Sicily and southern Calabria, perpendicular to the direction of the Calabrian Arc (Neri et al., 2004, 2005; Pondrelli et al., 2006; Serpelloni et al., 2010; Presti et al., 2013; Totaro et al., 2016). The compressional domain, in agreement with NW-SE Africa-Eurasia plates convergence, reveals a broadly E-W trending thrust belt parallel to the north Sicily coast while the extensional one, in northeastern Sicily and southern Calabria, is controlled by southeastward rollback of the Ionian subducting slab (Figure 1.2; Neri et al., 2004, 2012; Palano et al., 2012, 2015; Orecchio et al., 2014,

2017). The transition between these main seismotectonic domains seems to be mainly accommodated along a heterogeneous fault system running from the Aeolian Islands to the Ionian Sea (Figure 1.2; Neri et al., 2005; Argnani, 2009; Polonia et al., 2011; Gallais et al., 2013; Palano et al., 2015).

According to the regional geodynamic models the rollback of the Ionian lithospheric slab has been identified as the primary tectonic source for the (i) southern Tyrrhenian basin opening, the (ii) SE-ward kinematics of the southern Tyrrhenian unit and (iii) its thinning and over thrusting onto the Ionian lithosphere (e.g. Malinverno and Ryan 1986; Barberi et al., 2004; Faccenna et al., 2004; Pepe et al., 2005; Billi et al., 2011). The question on whether and eventually where the subduction slab is still continuous in depth or already detached beneath the Calabrian Arc is subject of debate in literature (Spakman and Wortel, 2004; Guarnieri, 2006; Pontevivo and Panza, 2006; Chiarabba et al., 2008; Monna and Dahm, 2009; Neri et al., 2009, 2012). The most recent analyses of different geophysical data (gravity anomalies, seismotomographic structure, and seismicity of crust and uppermost mantle) argue that the Ionian subducting slab is still in-depth continuous beneath the central part of the Calabrian Arc corresponding approximately to southern Calabria, while detachment of the deepest portion of descending lithospheric body has already occurred with tear processes propagating from the edges of the Arc itself (i.e. northern Calabria and northeastern Sicily) to the center (Neri et al., 2009, 2012; Orecchio et al., 2011, 2014). This scenario identify the Messina Straits and the Sila Massif as transitional areas from continuous to detached subduction mode along the Arc (Neri et al., 2012). Moreover, several analyses of the GPS velocity fields seem to indicate a very slow residual trench retreat compatible with the ongoing subduction process (e.g. Hollenstein et al., 2003; Devoti et al., 2008; D'Agostino et al., 2011; Palano et al., 2012). In this framework subduction activity is now close to end but the very slow trench retreat is considered however still capable of causing strong normal faulting

earthquakes especially in southern Calabria region (Argnani, 2000; D'Agostino et al., 2011; Neri et al., 2009, 2012; Orecchio et al., 2014).

In this framework the earthquake kinematics and dynamics may help to better understand the geodynamic engines acting in different domains of the Calabrian Arc region. In particular, earthquake focal mechanisms are key-element to properly estimate the stress tensor variations and to study the deformation zones and related boundaries. This seismological contribution is particularly useful in region like the Calabrian Arc characterized by wide offshore area and therefore lacking of GPS data usually furnishing essential information for defining the different kinematic regimes (Serpelloni et al., 2010; D'Agostino et al., 2011; Devoti et al., 2008; Billi et al., 2011; Palano et al., 2012, 2017).

1.2 Historical and recent seismicity

The Calabrian Arc represent one of the most seismically active regions of the entire Mediterranean area, with magnitudes of up to 7.1 and intensities of up to XI–XII MCS (Amoruso et al., 2006; Galli et al., 2008; Guidoboni et al., 2007; Monaco and Tortorici, 2000; Neri et al., 2006; Rovida et al., 2016). In the complex tectonic settings that characteryze the Calabrian Arc area the role of moderate-to-major earthquake (e.g. M≥5), directly related to the regional scale processes, can be crucial to clarify regional seismotectonics and seismic hazard of the area. To furnish an overall view of the seismotectonic settings of the Calabrian Arc we focus both on the historical and recent seismic activity. For this purpose, in Figure 1.3 are reported the moderate-to-large earthquakes (M≥5) occurred in the study region from 1000 AD to 2014 included in the Italian Parametric Earthquake Catalogue (CPTI15; Rovida et al., 2016). The epicentral distribution of the M≥5 earthquakes delineates a seismic belt which runs along the Tyrrhenian side of Calabria and, southward, along the Ionian coast of Sicily. Normal faults located along the belt are considered to be major seismogenic faults

believed to have generated the largest earthquakes ever occurred in southern Italy: the June 1638 Calabrian earthquake (M_w 7.0; Galli and Bosi, 2003); the January 1693 Sicilian earthquake (M_w 7.3; Piatanesi and Tinti, 1998; Visini et al., 2009); the Calabrian seismic sequence of February-March 1783 (up to M_w=7.1; Jacques et al., 2001; Tiberti et al., 2017); the December 1857 Val D'Agri earthquake (M_w 7.0; Cello et al., 2003; Burrato and Valensise, 2008) the September 1905 earthquake in the Tyrrhenian shore (M_w 7.0; Riuscetti and Shick, 1975; Galli and Molin, 2009; Presti et al., 2017), and the last catastrophic event the December 1908 earthquake in the Messina Straits (M_w 7.1; Billi et al., 2008; Pino et al., 2009).

To characterize the seismicity of the study area is necessary to evaluate also the recent active tectonics. In spite of the strong historical seismicity a light to moderate seismic activity has been recorded in the Calabria Arc region with no M>5 earthquakes in the last thirty years (Figure 1.4). Figures 1.4(a) and (b) show the epicenter distribution of the M≥2.5 earthquakes occurred between January 1985 and May 2018 at different depths in the Calabrian Arc area, included in the Italian Seismological Instrumental and Parametric Data-Base (www.ingv.it). In Figure 1.4(a) a very wide diffusion of low-energy earthquakes (M<4) is evident at shallow depths ($z \leq 40$ km). The crustal seismicity is mainly distributed i) along the whole Calabrian Arc, ii) in the offshore Tyrrhenian region along the northern coastal area of Sicily up to the central Aeolian archipelago, and iii) in eastern Sicily and its associated offshore area. On the contrary, the earthquakes in the higher magnitude ranges are few and sparse. Deep and intermediate-depth seismicity ($40 < z \leq 350$), shown in Figure 1.4(b), is mainly concentrated in the Tyrrhenian side of the Calabrian Arc, delineating a well-defined Benioff zone (Selvaggi and Chiarabba, 1995), and more diffused in the Ionian Sea. This epicenter distribution is expression of active processes within the Ionian slab (Selvaggi and Chiarabba, 1995; Neri et al., 2009; Orecchio et al., 2014).

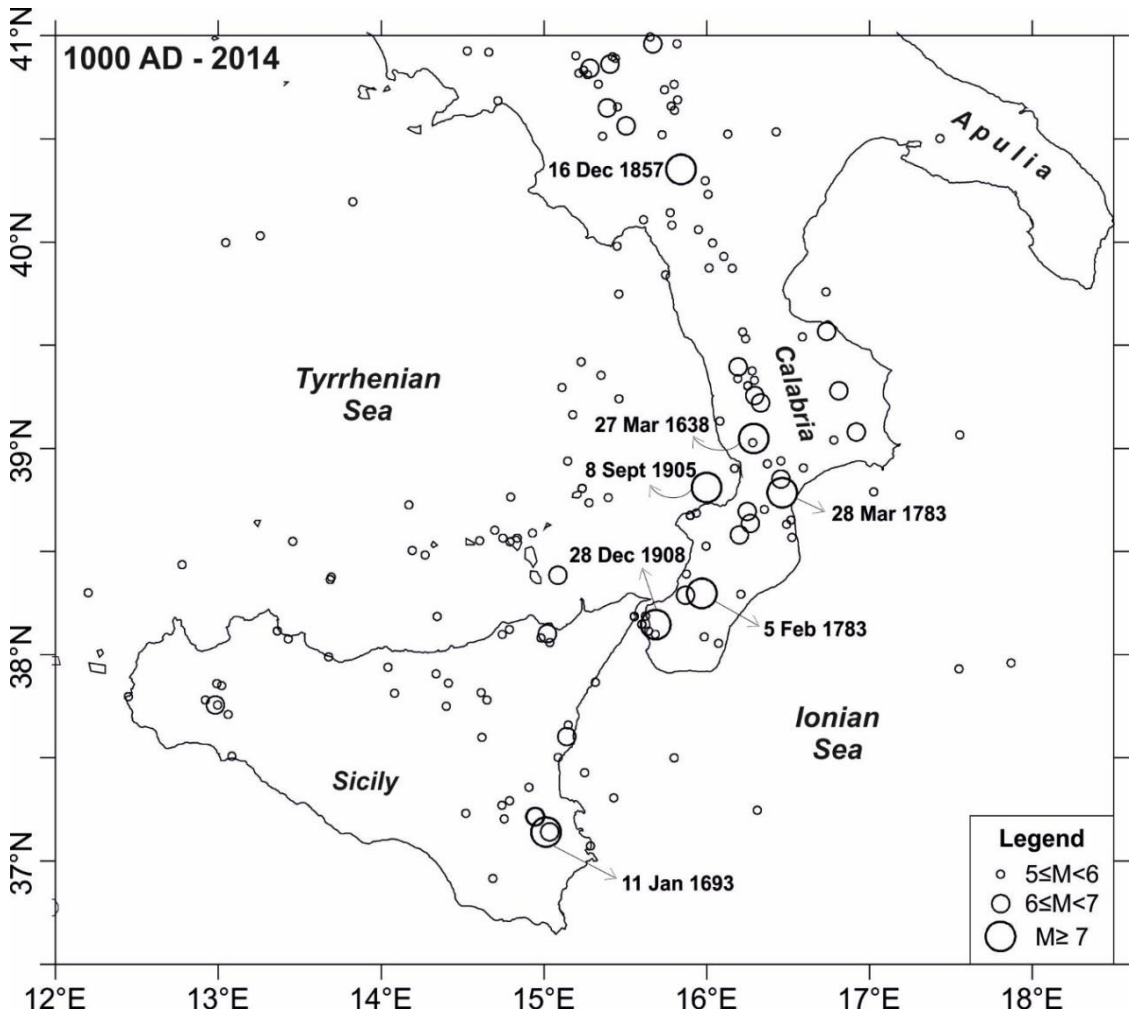

Figure 1.3 Circles show the locations of the M≥5 earthquakes that have occurred in the investigated area after 1000 A.D. according to the CPTI15 catalogue (Rovida et al., 2016;). The symbol size is proportional to earthquake magnitude range (see legend). Labels indicate the date of occurrence of M≥7 earthqaukes.

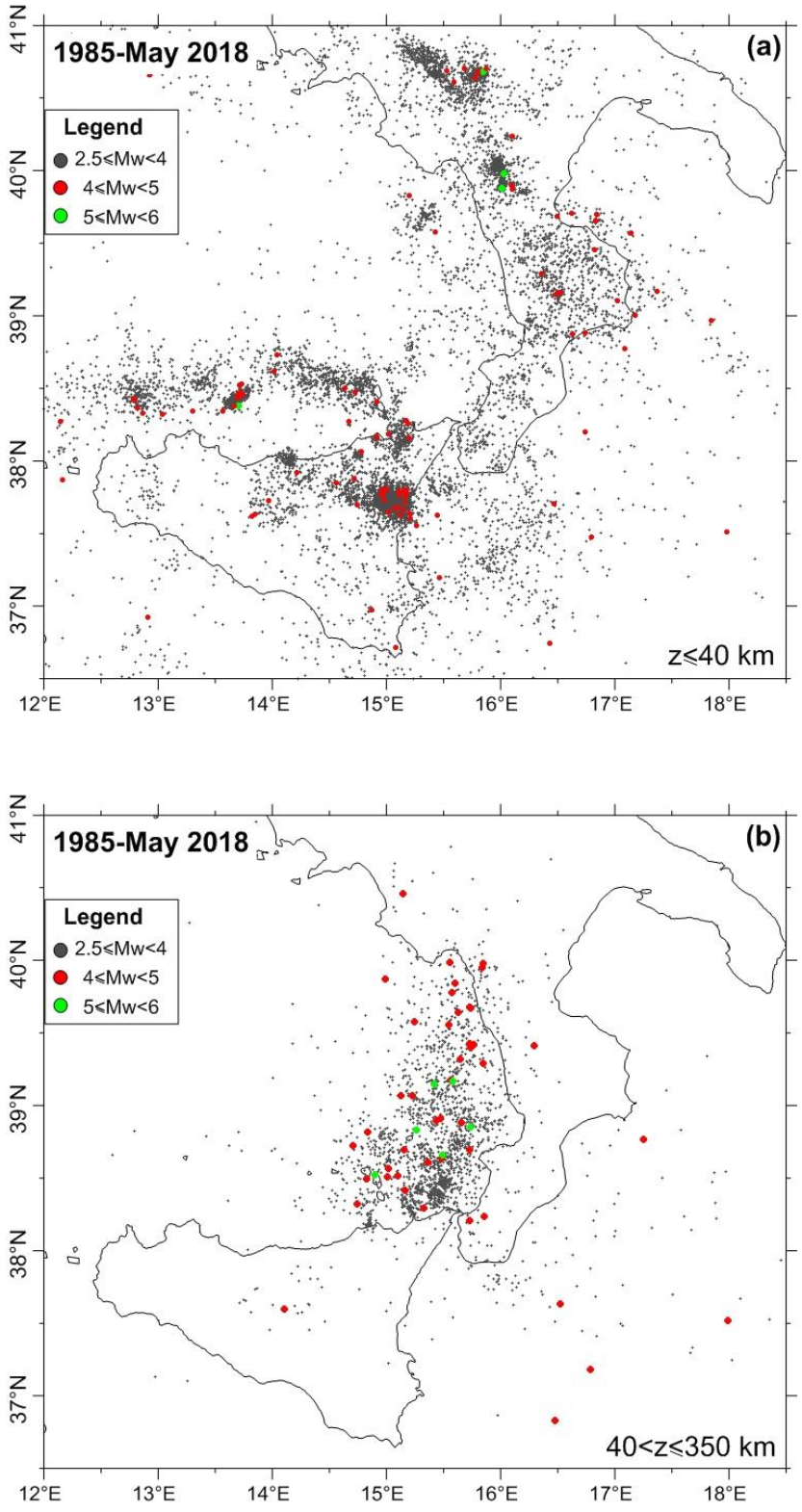

Figure 1.4 The maps **(a)** and **(b)** show the epicenter locations of the earthquakes of M≥ 2.5 occurring between 1985 January and 2018 May at different depths 'z' (kilometres b.s.l.) in the investigated area. Colors are for different magnitude ranges (see legend). Data are from the Italian Seismological Instrumental and Parametric Data-Base.

CHAPTER 2

ESTIMATING STABILITY AND RESOLUTION OF WAVEFORM INVERSION FOCAL MECHANISMS

2.1 Introduction

In this chapter several tools for testing the stability and resolution of waveform inversion focal mechanisms of crustal earthquakes occurred in the Calabrian Arc region (Figure 1.1) are described. It is well known that focal mechanism quality can decrease for low magnitude earthquakes and that, on overall, several factors can influence the results of seismic waveform inversion, for example seismic network coverage, earth model uncertainties and inaccurate earthquake location (Valentine and Trampert, 2012; Brandmayr et al., 2013; Chen et al., 2013; Silwal and Tape, 2016).

The methods traditionally used to compute focal mechanism solutions are based on the polarity of P-wave first motion. First-motion focal solutions reflect only the initial stages of faulting and strongly suffer from both uncertainty on velocity models used to reconstruct the wave path and inadequate azimuthal coverage of seismic networks (Lay and Wallace, 1995; Pondrelli et al., 2006; Scognamiglio et al., 2009; D'Amico et al., 2010; Presti et al, 2013). Moreover, errors in first-motion observations may occur because of station polarity reversals or incorrect direct P-arrival picks due to low signal-to-noise ratio. Much more powerful methods capable to furnish more stable and reliable focal mechanisms with respect to the traditional techniques are those based on waveform inversion. On this regards, the most relevant catalogues furnishing waveform inversion solutions for the Italian

region are Harvard Centroid Moment Tensor, Regional Centroid Moment Tensor and Time Domain Moment Tensor. The Harvard Centroid Moment Tensor (CMT, hereafter) is one of the most popular methodologies for calculating moderate to strong earthquake focal mechanisms and ideally suited to study global seismicity (Dziewonski et al., 1981; Ekström et al., 2012). It provides robust and reliable seismic source mechanisms through the inversion of long period (T > 45 s) body-waves and very-long period (T > 125 s) surface waves recorded at the global scale and, starting from 2003, even teleseismic surface waves with period 50-150 s (Hjörleifsdóttir and Ekström, 2010; Ekström et al., 2012). The CMT catalog includes focal mechanism parameters of worldwide earthquakes with M_w>4.5 occurred since 1976. The Regional Centroid Moment Tensor (RCMT, hereafter) procedure is instead based on the inversion of intermediate and long period surface waves recorded at regional and teleseismic distances (Pondrelli et al., 2002, 2004, 2006, 2007, 2011). The RCMT catalog collects focal mechanisms for earthquakes with magnitude approximately between 4.5 and 5.5 occurred in the Euro-Mediterranean region since 1997 and not well studied at global scale. The Time Domain Moment Tensor (TDMT, hereafter) algorithm performs long-period full waveform inversion for local and regional events with magnitude M_w≥3.5 using broadband recordings (T=40 s) from the seismic network of *Istituto Nazionale di Geofisica e Vulcanologia* since 2006 (Dreger and Helmberger, 1993; Dreger, 2003; Scognamiglio et al., 2009).

During the last years, the research team of University of Messina made continuous processing and improvements on Calabrian Arc earthquake focal mechanisms in order to increase their reliability and to expand the temporal and magnitude range of focal mechanism database. Several studies have proven the capability of the “Cut and Paste” waveform inversion method (CAP hereafter; Zhao and Helmberger, 1994; Zhu and Helmberger, 1996) to furnish reliable and high-quality focal mechanism solutions also for relatively low-magnitude earthquakes (down to a minimum of ca. 2.6) not reported in

the national catalogues and often not well resolved by using P-wave first motions (Neri et al., 2003, 2004, 2005; D'Amico et al., 2010, 2011; Orecchio et al., 2015; Presti et al., 2013; Totaro et al., 2013, 2015, 2016). Because of their frequent occurrence, these small earthquakes are particularly important for characterizing local tectonics and constraining stress orientations, especially in the Calabrian Arc region characterized by high heterogeneity in terms of seismotectonics and kinematics.

2.2 Data and method

Since it is widely accepted that waveform inversion focal solutions are much better constrained than P onset polarity ones (see, among others, Pondrelli et al., 2006; Scognamiglio et al., 2009; Presti et al., 2013), we are going to use only waveform inversion solutions in order to build a new focal mechanism database of the Calabrian Arc region (which will be shown in the next chapter of this thesis). In addition to the solutions reported by the official national and international catalogues we will include in the new database focal mechanisms estimated by the CAP method. The CAP algorithm has been applied to earthquakes of magnitude $M_w \geq 2.6$ that originated at depths shallower than 40 km in the study region between January 2006 and October 2015.

We carried out several analyses on CAP focal mechanisms aiming to evaluate stability and resolution of the used algorithm. In addition, we also performed different tests in order to estimate error on focal mechanism parameters.

In the CAP method (Zhao and Helmberger 1994; Zhu and Helmberger 1996) each waveform is broken up into P_{nl} (P_n waves followed by train of crust-trapped reflected/converted P-SV) and surface wave segments, which are weighted differently during the inversion procedure. Besides, each segment of synthetic seismogram is allowed to

be time-shifted to better match the observed seismogram and a misfit error between observed and synthetic data is define. The use of different portions of the waveform increases the stability of the final solution since different phases are sensitive to different parts of crustal structure and have different amplitude decay with distances. The surface waves, although large in amplitudes, are easily influenced by shallow crustal heterogeneities whereas P_{nl} waves are controlled by the averaged crustal velocity structure and are therefore more stable.

For the data inversion procedure, waveforms are converted in ground velocity and preferred to ground displacement in order to avoid the influence of long-period noise embedded in ground displacements. Furthermore, working with ground velocity rather than ground displacement reduces the influence of a low frequency site or instrument noise on the deconvolution. The same frequency bands have been used to filter synthetic and observed ground velocities, in detail 0.02–0.1 Hz for surface waves and 0.05–0.3 Hz for P_{nl} waves. All these features make the CAP method effective for earthquakes over a wide range of magnitudes (down to a minimum of 2.6; D'Amico et al., 2010, 2011; Zhu et al., 2006) as also proven by several tests and comparisons (Zhao and Helmberger, 1994; Tan et al., 2006; D'Amico et al., 2010, 2011; Totaro et al., 2016).

2.3 Stability tests and resolution estimates

The use of the CAP method in the Calabrian Arc region has allowed to estimate focal mechanism solutions also for low magnitude events (down to a minimum of 2.6) and therefore to significantly increase the number of focal mechanisms based on waveform inversion method. A relevant increase of focal mechanism solutions has important implications for better constraining local stress conditions and geodynamic interpretations in the study area (Totaro et al., 2016

and references therein). Hence it is necessary to carefully check quality and stability of waveform inversion solutions estimated by CAP method. Starting from these considerations and by also taking into account concerned literature information (see e.g., D'Amico et al., 2010, 2011; Presti et al., 2013; Orecchio et al., 2014) several resolution and stability tests have been performed to properly verify the robustness of CAP results.

In this chapter are reported the tests performed on a subset of 5 earthquakes chosen as representative of different network condition, magnitude value, location area and focal depth. For each earthquake we observed how the moment tensor varies as function of focal depth in order to evaluate its stability around the global misfit minimum. The depth increment in the grid search is 5 km and for each depth we report the best-fit solution obtained by searching over the full space of orientations and magnitudes and the relative misfit value. Then, we repeated the inversion procedure by considering different seismic network distributions. Seismic network geometry is fundamental in the earthquake analysis. In particular, in our study region the network configuration is often limited by the presence of wide off-shore sectors and the substantial lack of OBS (Ocean Bottom Seismometer) data. This factor can reduce the quality of solutions and therefore we verify CAP results even with not-optimal azimuthal coverage and few available records by using earthquake located both on-shore and off-shore in the Calabrian Arc area. Also, we investigated the influence of epicentral errors on the waveform inversion. Non-linear earthquake locations performed in the study area using the method by Presti et al. (2004, 2008) and consequent hypocentral error evaluation indicate that the mean epicentral uncertainty is in the range of 4-6 km (Orecchio et al., 2014). Then we forced the epicenter to lie 5 km away from the true location in order to test the solution even taking into account the mean uncertainty on earthquake location.

An important role in waveform inversion procedure is also played by the seismic velocity model that is used for the calculation of Green's

Functions basically for the double-couple mechanism estimates. Each focal mechanism considered in this study has been computed by using a specific 1D velocity model for each target area. To take into account the lithospheric heterogeneities of the Calabrian Arc region we used the most detailed 3D velocity models available from the literature (Barberi et al., 2004; Orecchio et al., 2011; Totaro et al., 2014) to compute theoretical travel times for properly defined target area and to build from these specific 1D velocity models (D'Amico et al., 2011). Even if the time-shift allowed in the CAP algorithm can partly reduce the influence introduced by the velocity model uncertainties, we further verified the stability of the solution with respect to velocity structure by using different velocity models representative of structure heterogeneities of the study region (Figure 2.1). Generally, waveform inversion methods give a standard error for each focal mechanism parameter (e.g., strike, dip and rake) derived from linearized techniques. It provides an important and useful measure of quality of focal mechanism solution but, as shown by several authors, linearized inversion methods tend to underestimate formal errors on focal mechanism parameters (Bevington and Robinson, 2003; Tan et al., 2006). In this study a procedure aimed to assess more reliable confidence limits of estimated strike, dip and rake is presented. Following the approach described by Stich et al., (2003a), we used a grid search for error analysis in the full range of focal parameter space. For each earthquake a set of “artificial” focal mechanisms have been obtained by moving around the best-fit solution in all directions of the focal parameter space with a sampling step of 10°. Then we estimated the misfit for all artificial focal mechanisms and compared these values with the global minimum misfit of the best solution obtained by CAP. In this way it is possible to observe how the misfit value changes with respect to strike, dip and rake, respectively. This comparison can assess the confidence limits and the range of potential alternative solutions over fault plane parameters, allowing us to define the accuracy of the focal mechanism solution. According to Stich et al., (2003a), we assumed that the uncertainty region of the

solution includes all the artificial focal mechanisms having misfit < 10% above the global minimum. By application of this procedure to CAP moment tensor solutions we are able to estimate that our focal mechanism solutions are characterized by fault parameter errors of the order of 8°-10°.

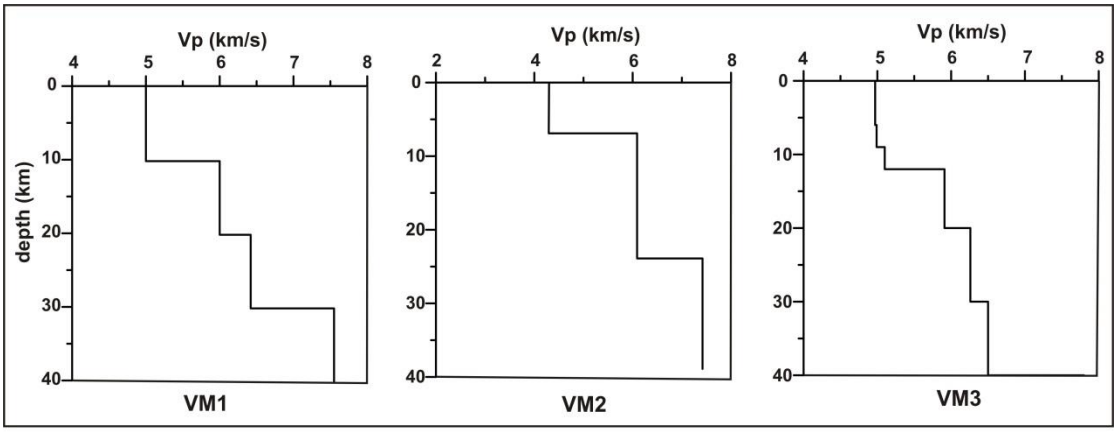

Figure 2.1. Different velocity models used to compute the Green's functions for tests on the influence of possible crustal structure heterogeneities in the study area.

2.4 Results and Discussion

In Figure 2.2 the results of the above described tests are reported for the 5 events listed in Table 2.1 and chosen to fairly represent dataset heterogeneities. For each event the epicenter location (black star) and the recording seismic network (triangles) are shown on plots (a). The earthquakes are located both on-shore and off-shore (ID 2,4 and 1,3,5 in Figure 2.2, respectively) in the Calabrian Arc area and they are also characterized by different network coverage. We display on plots (b) thebest focal mechanism solution in the waveform misfit versus depth curve obtained by the grid search procedure. From plot (b) we can observe that, in general, the focal solution does not change significantly

ID event	DATE yy/mm/dd	TIME hh:mm:ss	Lat (°)	Lon (°)	Depth Km	Strike	Dip	Rake	M_w
1	20090701	17:58:54	38.34	15.01	2	40	90	19	3.1
2	20111119	10:19:16	16.00	37.81	14	121	70	-25	3.4
3	20140323	18:31:52	37.47	16.48	38	177	61	21	3.6
4	20140708	05:02:43	39.90	16.12	2	347	51	-83	2.9
5	20150329	10:48:46	38.09	16.21	12	52	76	-83	3.5

Table 2.1. Events used in this study.

near the minimum misfit value. Only for the earthquake ID 3, located in the Ionian Sea, the curve of waveform misfit is almost flat around the minimum indicating that the network coverage does not provide a tight depth constraint. As already mentioned, we assess inversion results also by using different station configurations as indicated in the left column of plots (c) of Figure 2.2 where we also report the respective best focal mechanism solution. In all cases the focal mechanisms are very similar to that obtained from the inversion with the real station network. Even in this case some differences between the focal mechanisms calculated by test and the true one are visible for earthquake ID 3 and may be probably related to the position of the epicenter with respect to the recording stations. By also taking into account these small differences, this test shows the good stability of CAP results even in case of poor station distribution or quite low magnitude. By way of example see events ID 3, ID 4, and ID 5: for these earthquakes, in fact, the seismic network configuration has an azimuthal gap as large as 180° and also the simulation in extremely bad conditions characterized by only 2 recording stations show very stable solutions. Plots (c) of Figure 2.2 also report (right side) the focal mechanisms obtained by varying of 5 km the epicenter location (grey star in plots a). It clearly appears that a mislocation compatible with the hypocenter location uncertainties does not produce significant differences between true and simulated solution, further supporting the

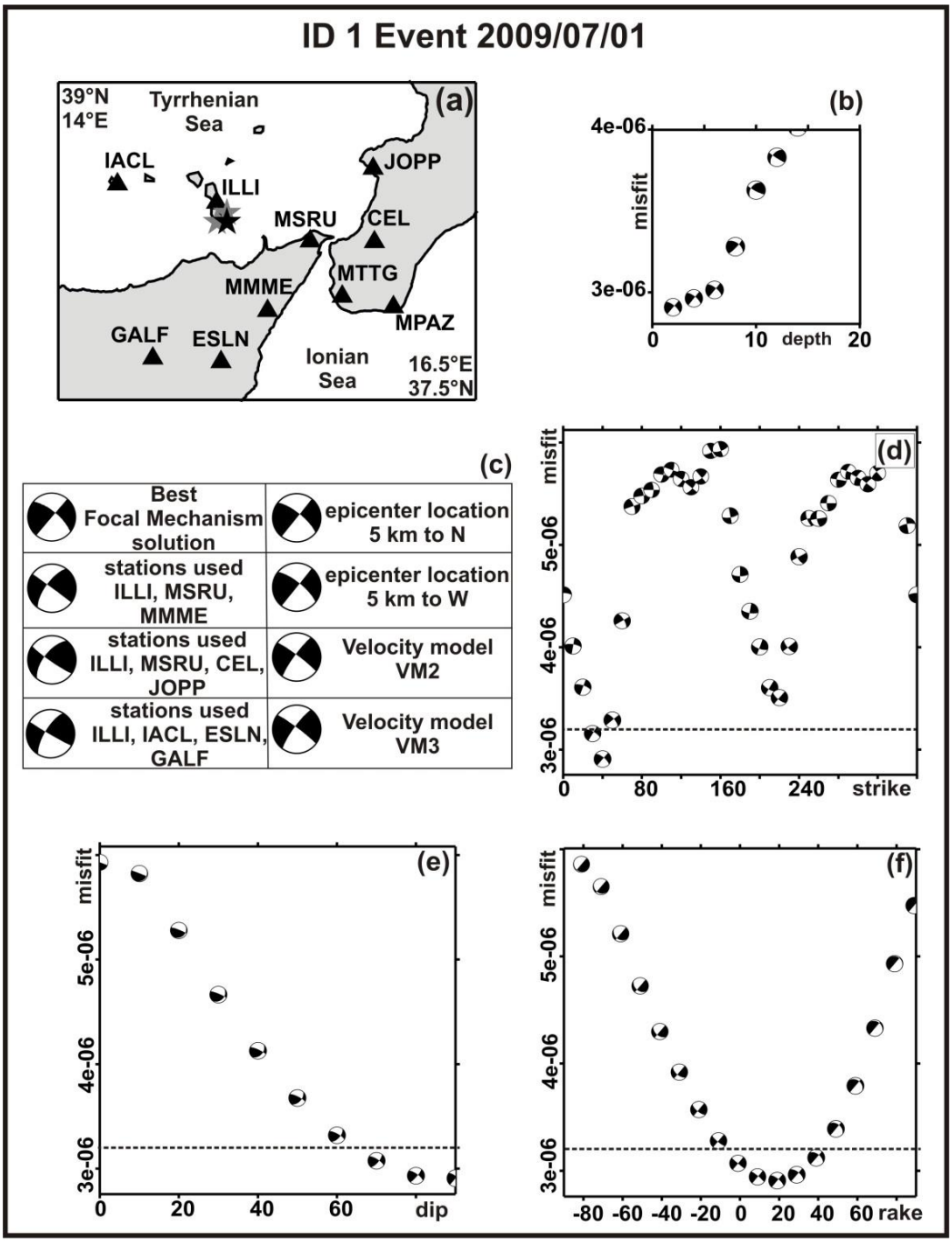

Figure 2.2. The figure shows results obtained after tests performed to verify the stability and the error on CAP focal mechanism solutions. Plot **(a)**: map reporting recording stations (black triangles) and epicentral location (black star) used in the waveform inversion procedure together with two biased epicentral locations used for synthetic tests (grey stars) for each event. Plot **(b)**: misfit error as function of depth. Plot **(c)** reports the best focal mechanisms solution for each earthquake and the results of different tests performed by changing the recording networks (also using very unfavourable conditions), the velocity models for the study area (see Figure 2.1) and by forcing the epicenters to lie 5 km away from the "true" locations. Plots **(d)**, **(e)**, **(f)** reports the graph of RMS versus strike, dip and rake, respectively. The dashed line marks the 10 % threshold of RMS. The minimum shown in each diagram is the best solution of the event.

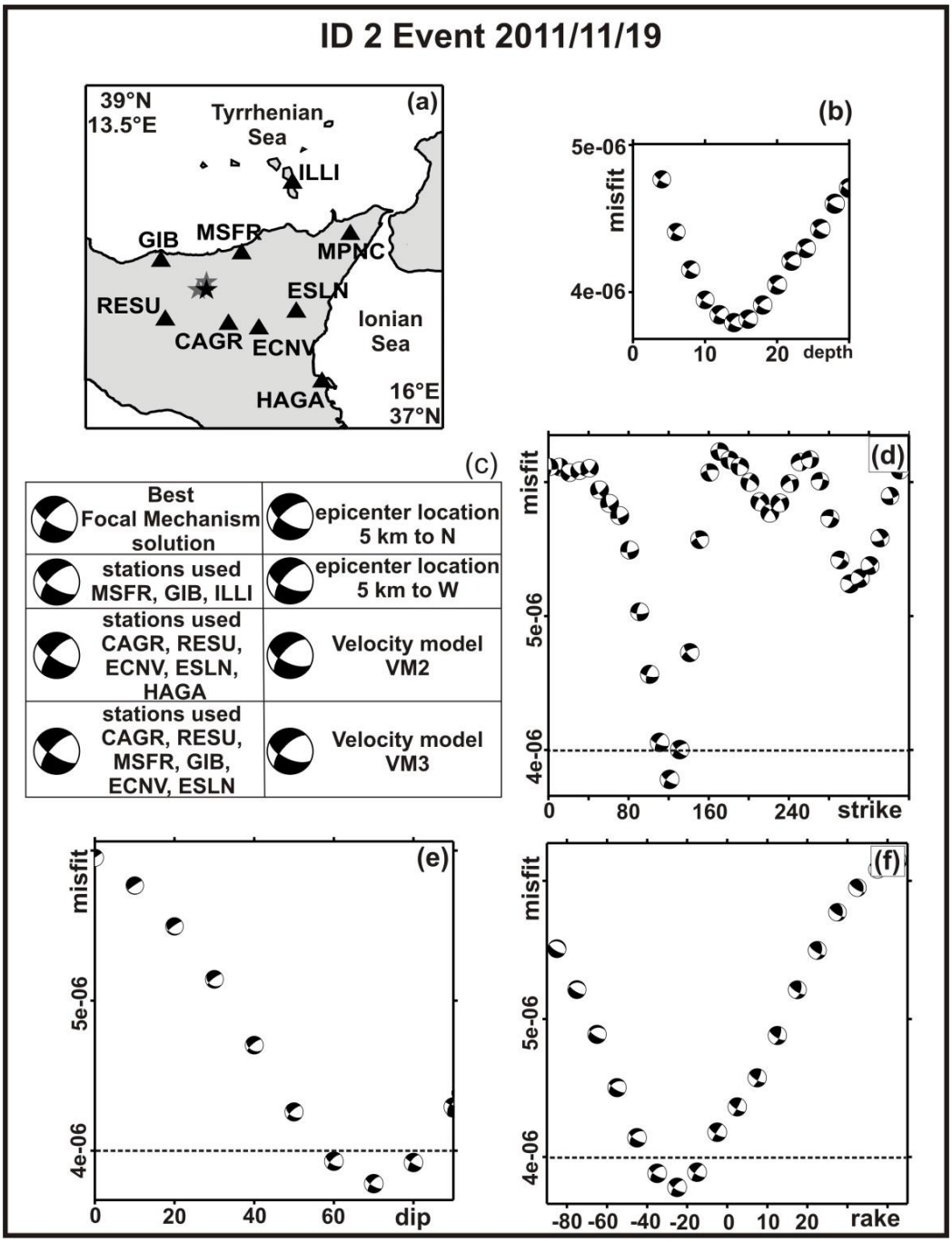

Figure 2.2. *Continued*

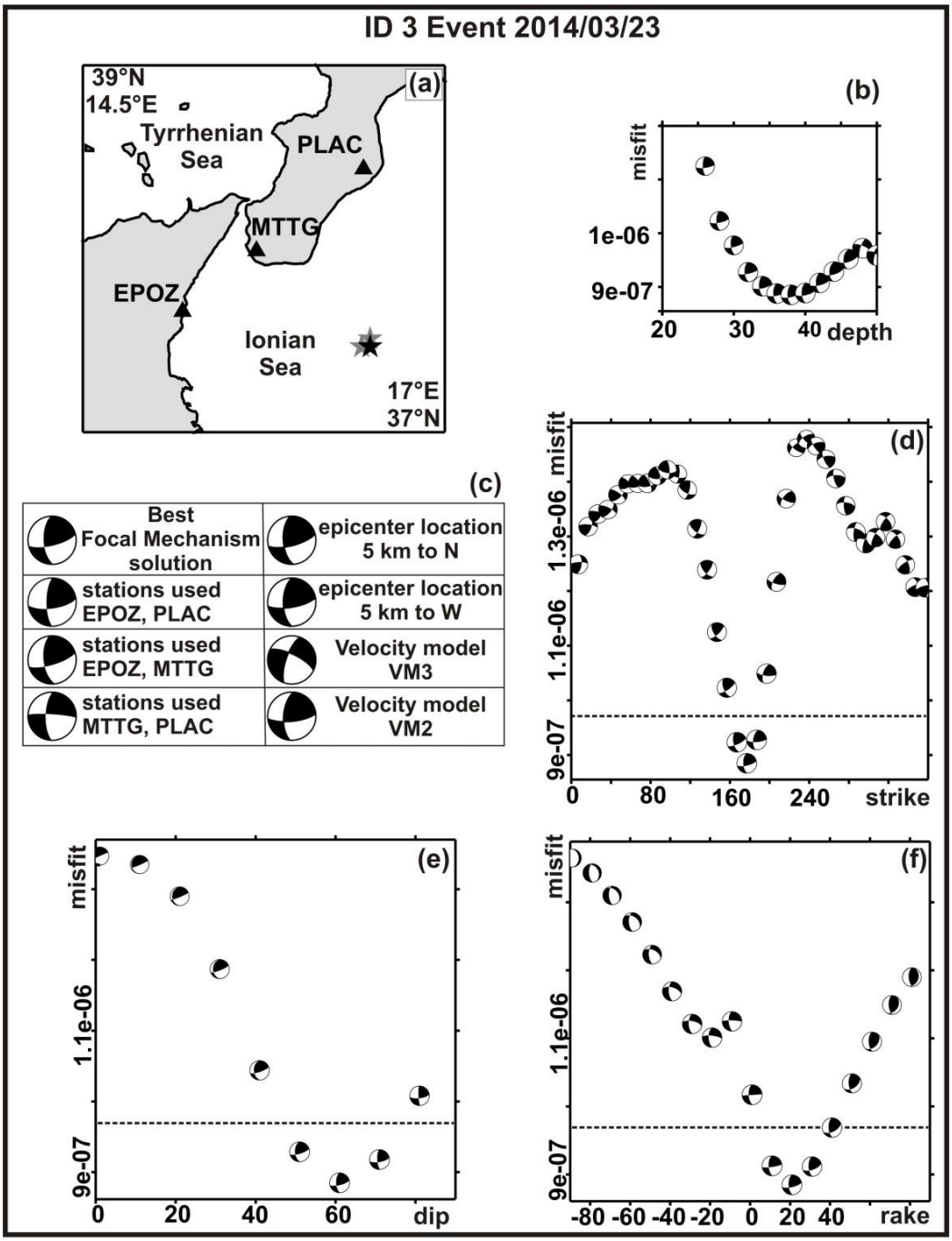

Figure 2.2. *Continued*

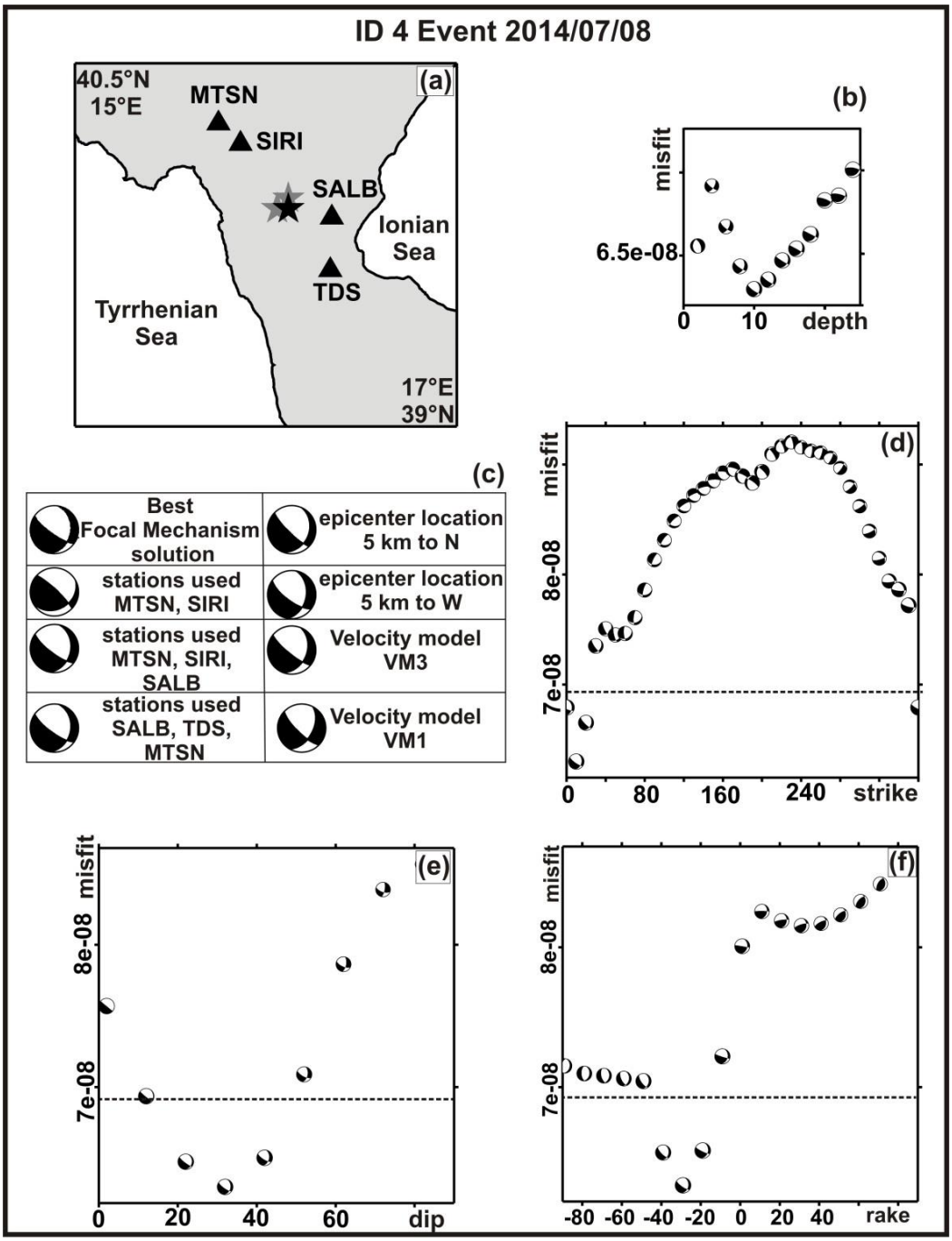

Figure 2.2. *Continued*

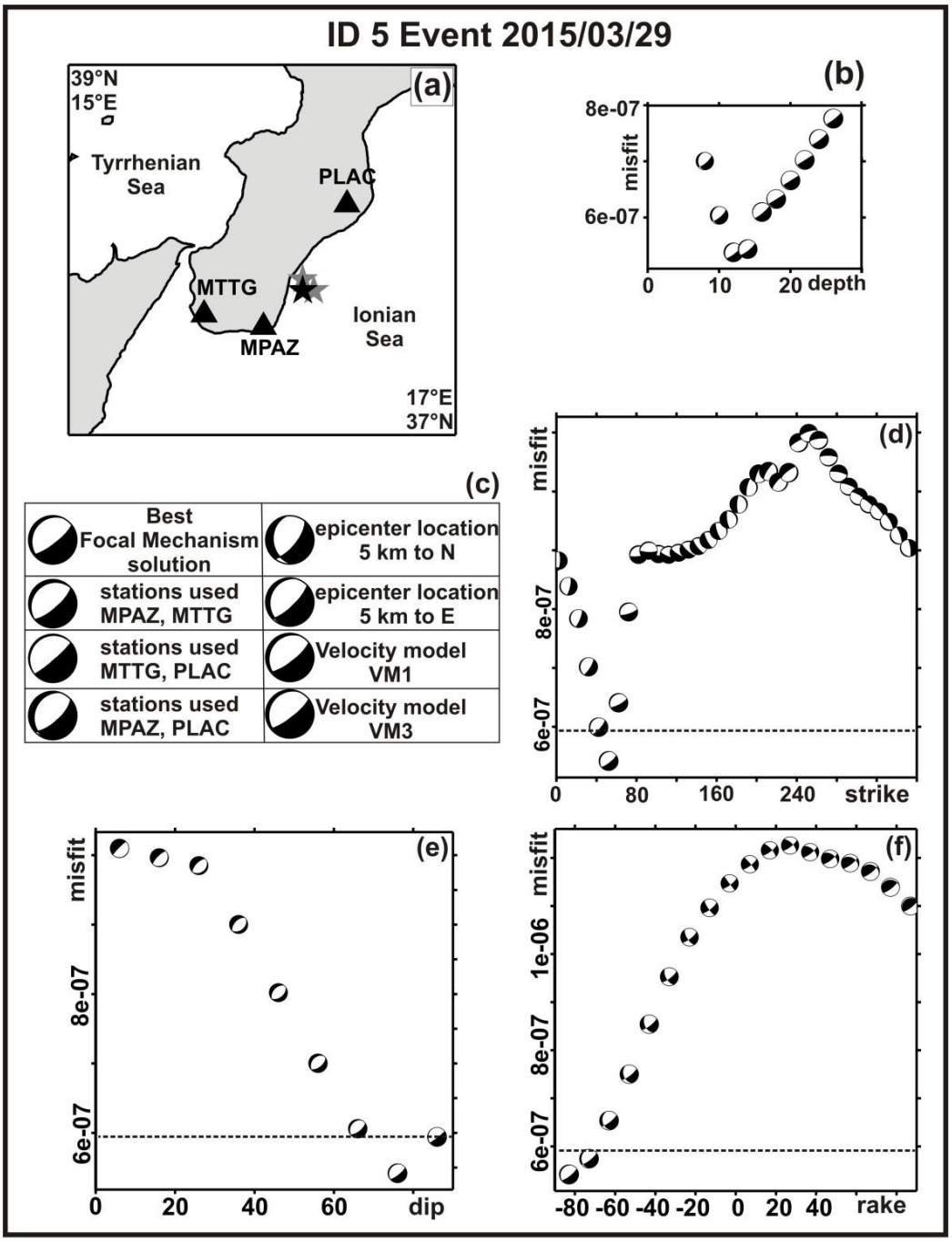

Figure 2.2. *Continued*

stability of our results. In the same plots we compare the solutions estimated using different 1D velocity models, VM1, VM2 and VM3 (Figure 2.1), used for computation of the focal mechanisms. Even in these examples the high stability of the mechanisms is evident. More pronounced differences affect the results of event ID 3, probably due to inaccuracy of the model VM2 and VM3 for the Ionian Sea area. Plots (d), (e) and (f) of Figure 2.2 report the misfit values versus strike, dip and rake respectively. These diagrams useful to study the uncertainties of the focal mechanism solution have been built by estimating the misfit values throughout the space of moment tensor orientations. As the uncertainly volume is defined by misfit lower than 10% respect to the best moment tensor solution all the focal mechanisms under the dashed line are acceptable solutions. Usually, relying on focal mechanisms that follow the 10% threshold we can estimate that our focal parameter errors are on average of 8°-10°, like in the examples here reported.

2.5 Concluding remarks

In order to check the method robustness, the quality and stability of CAP focal mechanism solutions have been proven by mean of several tests also for low magnitude earthquakes. We performed tests taking into account (1) recording station geometry, (2) different velocity models, (3) the misfit error as a function of depth, (4) epicenter uncertainty, and (5) strike, dip and rake variations as function of waveform misfit. Through these tests we verified that CAP solutions are robustly determined and just a few stations provide enough information to properly constrain the earthquake focal mechanism. Furthermore, the application of CAP method can provide good-quality solutions in a magnitude range (i.e. $2.6 \leq M_w \leq 3.5$) not properly represented in the official catalogues and where the solutions estimated from P-onset polarities are often poorly constrained. The procedures described in this

study could be applied to different datasets in order to verify the robustness of estimated focal mechanisms and, consequently, to properly improve the knowledge of the seismotectonic regime, regional stress field features as well as the seismic hazard of different investigation areas.

Analyses and results reported in this chapter have been also published by Scolaro S., Totaro C., Presti D., D'Amico S., Neri G., & Orecchio B. (2018). Estimating Stability and Resolution of Waveform Inversion Focal Mechanisms. In *Moment Tensor Solutions*, 93-109, Springer.

CHAPTER 3

SEISMOGENIC STRESS FIELD ESTIMATION IN THE CALABRIAN ARC REGION FROM A BAYESIAN APPROACH

3.1 Introduction

Seismic faulting is strictly related to tectonic stress acting in the lithosphere (Dziewonski et al., 1981; Anderson et al., 1993). Various seismological methods and analyses for determining the components of tectonic stress tensor have been reported in the literature, and stress fields in many regions of the world are today known (see, e.g., Heidbach et al., 2010). Earthquake focal mechanisms are among the most used data for stress inversion (McKenzie, 1969 and Gephart and Forsyth, 1984 among many others). However, relatively low accuracy of focal mechanisms of older and/or lower magnitude earthquakes due in particular to limitations of seismic monitoring systems has prevented accurate stress estimates in many regions, and southern Italy is one of these. In this chapter a new database of shallow earthquake focal mechanisms relative to the Calabrian Arc region is compiled. The new database has been compiled by adding 146 waveform inversion solutions estimated in this work to 292 selected from literature and official catalogs (see Table 3.1).

The inclusion of original solutions computed by the CAP method (Zhao and Helmberger, 1994; Zhu and Helmberger, 1996) has permitted us to expand the existing set of data adding earthquakes of magnitude as small as 2.6 still keeping high quality of data (see Chapter 2; D'Amico et al., 2010, 2011; Orecchio et al., 2015). Taking benefit from the enhanced set of focal mechanisms, we have investigated the

seismogenic stress tensor variations over the study region. For this purpose, we have used a very effective Bayesian technique introduced for estimating tectonic stress parameters from primary seismological observations (Arnold and Townend, 2007) never applied in southern Italy before the present study. This technique allows to incorporate nodal plane ambiguity and observational errors in the computational process and furnishes the posterior density function for the principal components of stress tensor and the stress-magnitude ratio (Townend et al., 2012). The main aim of the present work is that of improving the knowledge of seismotectonic domains of Calabrian Arc and surrounding areas in south Italy.

3.2 Data and Methods

An updated high-quality database of 438 crustal earthquake focal solutions has been compiled by taking from literature and catalogs the highest-quality waveform inversion solutions and adding 146 solutions computed in the present study (Figure 3.1). All the focal mechanisms we selected are waveform inversion solutions (i) computed by the CAP method or (ii) coming from Italian centroid moment tensor (CMT), Regional CMT, and time domain moment tensor catalogs (Pondrelli et al., 2006, 2011). Focal mechanisms estimated by CAP are for earthquakes of magnitude $M_w \geq 2.6$ that originated at depths shallower than 40 km in the study region between January 2006 and October 2015 (Figure 3.1).

As shown in Chapter 2, the robustness of CAP in our applications has been verified through rigorous tests in which recording network configuration, velocity model, focal depth, and epicenter location are varied. Furthermore, additional tests has been performed following the approach by Stich et al. (2003a) for estimating formal errors on focal mechanism parameters. By application of this procedure to the solution

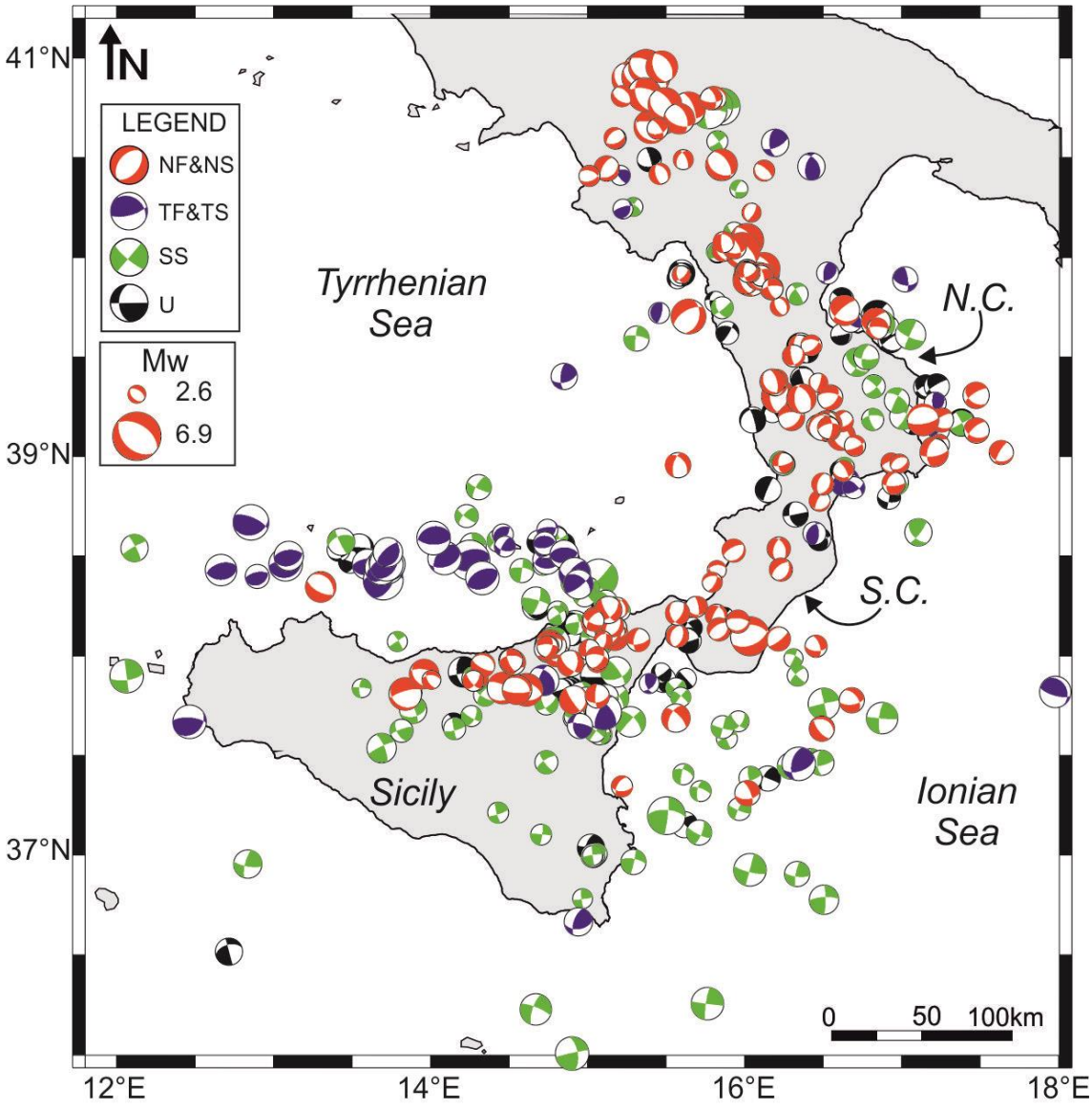

Figure 3.1. Database of crustal earthquake focal mechanisms for the study area. Different colors identify different types of mechanisms following Zoback's (1992) classification based on values of plunges of P and T axes: red = normal faulting (NF) or normal faulting with a minor strike-slip component (NS); green = strike-slip faulting (SS); blue = thrust faulting (TF) or thrust faulting with a minor strike-slip component (TS); black = unknown stress regime (U). "U" includes all focal mechanisms which do not fall in the other five categories (Zoback, 1992). The beach ball size is proportional to the earthquake magnitude (see legend). "N.C." and "S.C." stand for Northern Calabria and Southern Calabria, respectively.

estimated by CAP in the present study, we found that uncertainties of solutions estimated by CAP in the present study, we found that uncertainties of focal mechanisms of our data set are of the order of 8°–10°. These solutions have been combined with the focal mechanisms selected from literature and official catalogs for earthquakes occurring at depth <40 km in southern Italy between 1977 and 2015 (Figure 3.1 and Table 3.1). In order to estimate the stress distribution over the study region, this high-quality database has been used for stress tensor inversion by applying, for the first time in south Italy, the method by Arnold and Townend (2007). These authors developed a Bayesian method for tectonic stress computation which furnishes the posterior density function of the principal components of stress tensor (maximum σ_1, intermediate σ_2, and minimum σ_3 compressive stress, respectively) and the stress-magnitude ratio (R). The parameter R is used to determine the axis of maximum horizontal compressive stress (SH_{max}). Each focal mechanism is characterized by four parameters: strike, dip, rake, and a weight factor or precision τ. The τ value estimate is based on the assumption that fault parameter errors follow a Matrix-Fisher distribution (see, for more details, Arnold and Townend, 2007 and Mazzotti and Townend, 2010). This Bayesian approach enables to incorporate nodal plane ambiguity, focal mechanism uncertainties, and similarity of the focal mechanisms included in each seismic zone (Arnold and Townend, 2007). The latter criterion is important because additional similar solutions add little to the constraints on the stress than is provided by a single solution (McKenzie, 1969; Hardebeck, 2006; Townend et al., 2012). Some of the most common algorithms for stress computation (see, e.g., Gephart and Forsyth, 1984) tend to be misleading in this regard (Hardebeck and Michael, 2004; Townend, 2006). Before starting with stress computations, we applied the k-means nonhierarchical clustering algorithm (see, e.g., Hartigan, 1975) to subdivide the focal mechanism data set according to hypocentral locations. This algorithm is not guaranteed to furnish a globally optimal, or even unique, solution, but by fixing the number of clusters

"k," it assures that each event is closer to the centroid of the cluster to which it is assigned than to the ones of all k-1 other clusters. It has already been applied by other investigators to focal mechanism data specifically (see, e.g., Holt et al., 2013). Since clustering obtained by the k-means algorithm is based only on earthquake locations and not on faulting type, this approach allows identifying the sectors to be investigated without any "a priori" constraint from focal mechanism distribution. For our data set we have tested several values of k and run the k-means algorithm 1000 times randomly selecting various starting points for each k. At last, we have chosen k = 12 which appeared the most appropriate number of clusters for our data set according to the "elbow criterion" based on analysis of data variance versus k (Thorndike, 1953). We therefore report in Figure 3.2 the results obtained by using k=12 clusters: the clusters contain on average 37 focal solutions and a minimum of 20, with the only exception of two clusters containing, respectively, 15 and 5 focal solutions (boxes 7 and 12 in Figure 3.2). For each cluster the stereonet reporting the contours of the σ_1, σ_2, and σ_3 axes at the 90% confidence level is shown (Figure 3.2b). The confidence areas of obtained stress fields appear, in general, quite concentrated, indicating a high level of resolution in most cases (Figure 3.3). Additional inversion runs have been performed by partitioning each cluster according to earthquake magnitude or focal depth, in order to identify (i) eventual local effects of stress recognizable by low-magnitude earthquakes or (ii) stress changes between different tectonic domains distinguishable by depth. No change of stress as function of magnitude or depth has been detected.

3.3 Discussion of Results

In the recent literature different kinds of data and methods have been used in order to depict the present-day crustal stress in southern Italy (Musumeci et al., 2014; Palano, 2015; Montone and Mariucci, 2016).

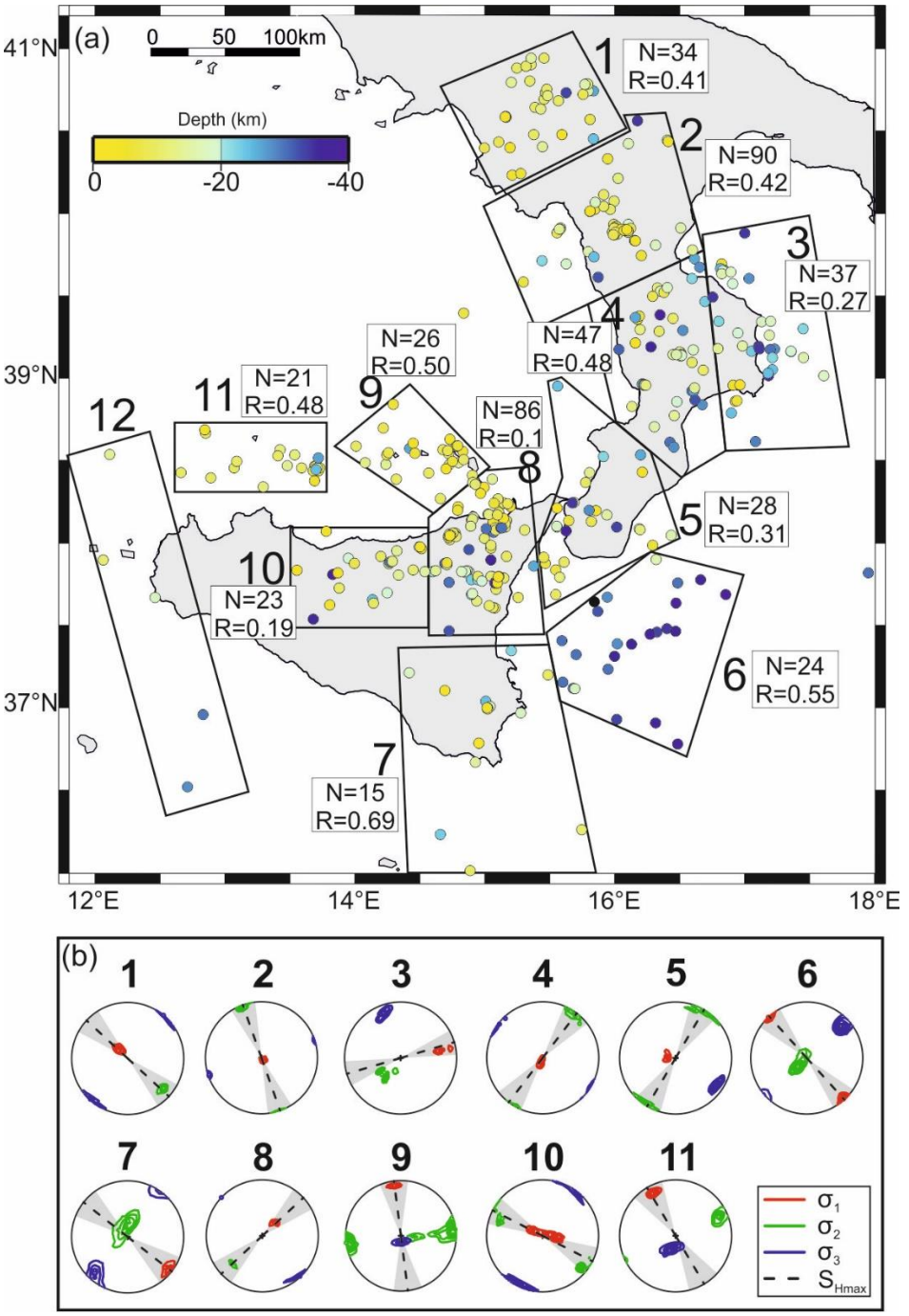

Figure 3.2. (a) Epicenters of the focal mechanisms shown in Figure 3.1 clustered by the k-means algorithm reported with a color code relative to focal depth. Numbers 1 to 12 indicate the clusters, N and R are the number of events and the stress-magnitude ratio relative to each cluster, respectively. **(b)** Stereonets showing the orientations of the principal stress axes estimated for each cluster (lower hemisphere projection; north is up, east is right). Red, green, and blue contours denote the positions of the σ_1, σ_2, and σ_3 axes, respectively, and the corresponding orientation of SH_{max} is marked as a black dashed line with the 90% confidence intervals shaded in gray. The numbers associate each stereonet to the relative cluster. The stereonet of cluster 12 is omitted because the low number of focal solutions available in the cluster (five) has not permitted to constrain the stress tensor.

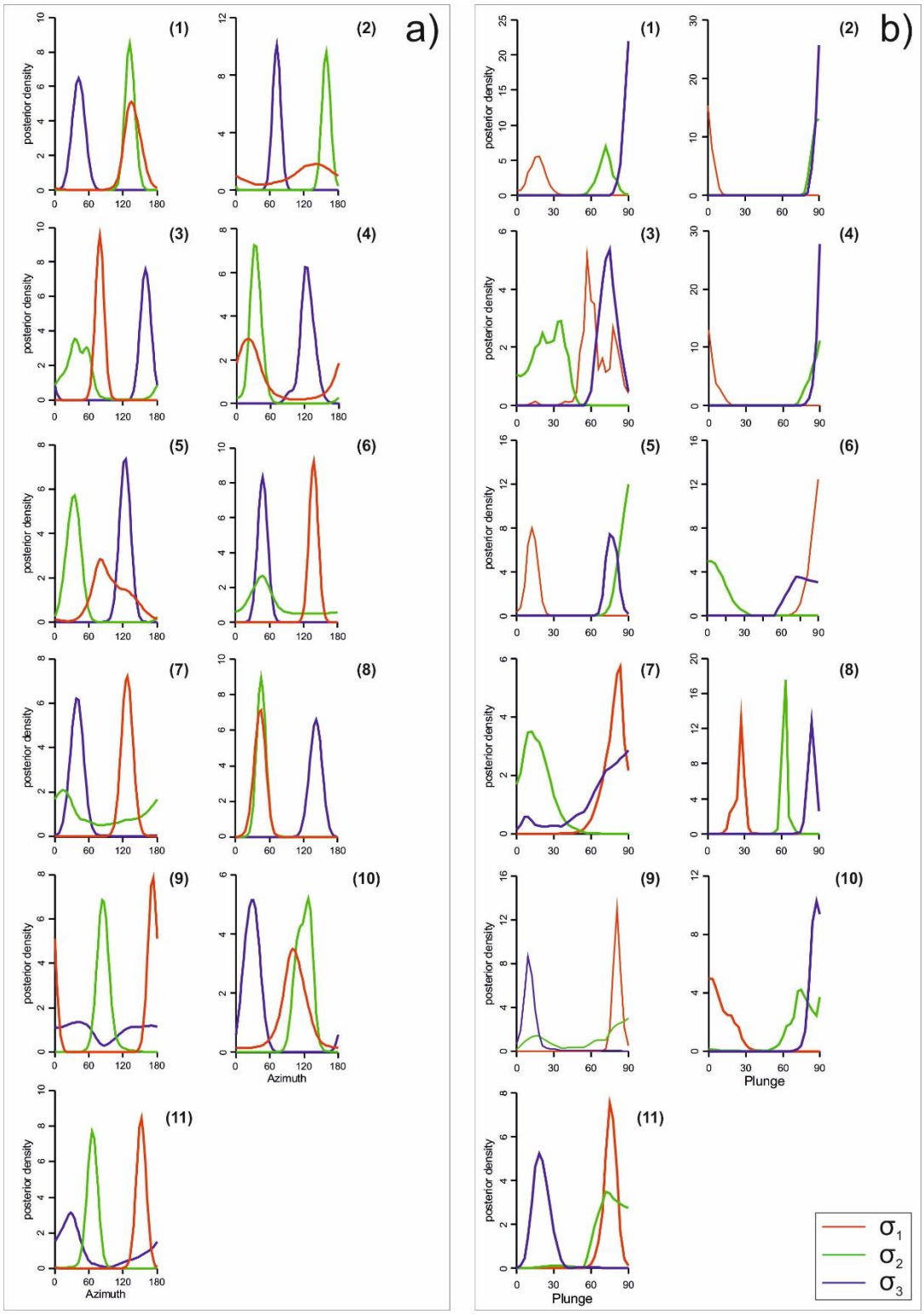

Figure 3.3. Posterior density distributions of azimuth **(a)** and plunge **(b)** of the principal stress axes estimated for clusters 1 to 11 investigated in the present study by application of the method by Arnold and Townend (2007). The numbers associate each plot to the relative cluster. The curves appear in general very peaked, highlighting a good level of resolution of the results. Note that the less peaked azimuth curves are relative to vertical stress axes (see e.g., σ_1 in sectors 2 and 4, σ_3 in sector 9 of Figure 3.2).

Musumeci et al. (2014) and Palano (2015) have focused their attention on specific sectors of our study region and used focal solution data sets where lower quality P onset polarity solutions are dominant with respect to poor numbers of better quality waveform inversion ones. Montone and Mariucci (2016) have used a data set mainly consisting of CMT waveform inversion solutions, but the number of solutions available to them in our study region (slightly more than a hundred) has not permitted to detect more than the gross features of the regional stress, such as extension in the Apennine-Calabria region and compression in the northern offshore of Sicily. More accurate detection of stress tensor variations in the region including the Apennine- Maghrebian chain from south Italy to western Sicily and the Tyrrhenian and Ionian offshores has, conversely, been possible in the present study by means of inversion of a high-quality robust data set including 438 waveform inversion focal solutions. Earthquake focal mechanisms and stress tensor distributions obtained in the present study (Figures 3.1 and 3.2) clearly indicate tectonic domains and suggest geodynamic engines. With their good level of constraint witnessed by posterior density errors as low as 5°–15° (Figures 3.2b and 3.3) our results clarify the stress patterns along the Apennine-Maghrebian chain and also allow improving the knowledge of stress regimes in the forearc area of the Ionian subduction zone, a sector not adequately investigated to date. The extensional dynamics and their changes along the Apennine-Maghrebian arcuate chain, where the Calabrian Arc roughly corresponds to the sector of maximum curvature, are well depicted by our results from the southern Apennines to western Sicily (Figure 3.4). Normal faulting solutions are mainly concentrated along the chain (Figures 3.1 and 1.2) and the opening direction detected by stress inversion is more or less perpendicular to the chain and follows with some approximation its curvature (boxes 1, 2, 4, 5, 8, and 10 in Figures 3.2 and 3.4). The Southern Apennines sector (Figure 3.1 and boxes 1 and 2 in Figure 3.4), which shows a predominance of normal faulting solutions leading to a steep σ_1 together with a horizontal NE trending σ_3,

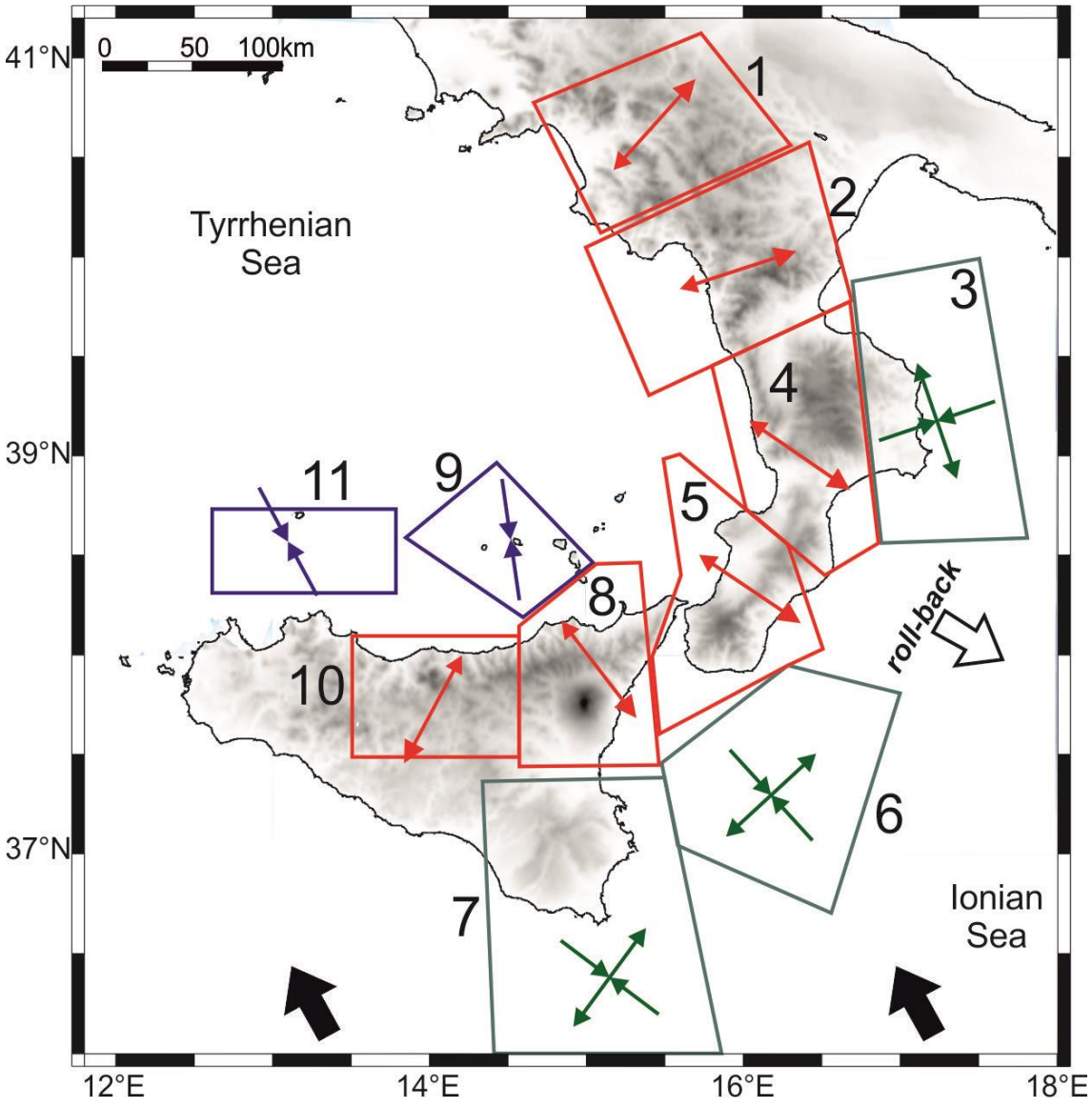

Figure 3.4. Synthesis of the stress orientations estimated in the present study for the southern Italy region. Numbers 1 to 11 indicate the focal mechanism clusters. The main extensional domains are depicted by red boxes reporting the orientation of σ_3 (red arrows). The compressional ones are indicated by blue boxes showing the orientation of σ_1 (blue arrows). Transcurrent domains identified in the Ionian offshore of the study region are indicated by green boxes for which both σ_1 and σ_3 are reported (green arrows). Black arrows indicate the present motion of Africa relative to Europe (Nocquet, 2012, and references therein) and the white one shows the sense of the residual subducting slab rollback.

is presently undergoing extension probably related to postorogenic collapse tectonics (Catalano et al., 2004; Barchi et al., 2007; Li et al., 2007; Reitz and Seeber, 2012; Totaro et al., 2013, 2015). The extensional regime of Calabria and Messina Straits area Figure 3.1 and boxes 4, 5, and 8 in Figure 3.4) highlighted by high concentration of normal faulting solutions and stress patterns showing vertical σ_1 and horizontal SE trending σ_3, can be ascribed to southeastward rollback of the Ionian subducting slab (Neri et al., 2005; D'Agostino et al., 2011; Presti et al., 2013). Looking in detail at the stress pattern of box 8, slight differences can be noted with respect to boxes 4 and 5. Box 8, in fact, is characterized by a σ_1 less steep than those detected for sectors 4 and 5. This reflects a mainly extensional stress pattern with a minor component of dextral strike-slip kinematics possibly due to local transition between collisional domains 9 and 11 and rollback-induced extension of sectors 4 and 5 (Presti et al., 2013; Palano et al., 2015). The compressional tectonics active in the Southern Tyrrhenian Sea offshore Sicily is evidenced by predominance of thrust faulting leading to vertical σ_3 and ~NNW trending horizontal σ_1 (Figure 3.1 and boxes 9–11 in Figure 3.4) referable to Africa-Eurasia convergence in the central Mediterranean (Pondrelli et al., 2004; Billi et al., 2007, 2011; Neri et al., 2014). We also obtained well-constrained stress fields in three large sectors located in the Ionian offshore of the study region (boxes 3, 6, and 7 in Figure 3.4) showing almost pure transcurrent regimes (Figure 3.4). In particular, the Ionian Calabria sector (box 3) is characterized by strike-slip solutions indicating left-lateral kinematics with NNW trending horizontal σ_3 and ENE trending subhorizontal σ_1 implying a minor extensional component. The obtained stress field probably reflects the transition between the area where southeastward rollback of the Ionian subducting slab is still active (south; Figure 3.4) and the area where the subduction slab has already undergone detachment (north) (see also Neri et al., 2012). Strike-slip solutions are also predominant in boxes 6 and 7 in the Ionian offshore. The stress field computed in sector 6 shows horizontal NW trending σ_1 and NE trending σ_3, expression of a

pure transcurrent regime which can be ascribed to Africa-Eurasia convergence that is found oriented NW-SE in this sector of the Mediterranean (Nocquet, 2012). In the Hyblean region and its immediate offshore (box 7) strike-slip solutions are also predominant and the obtained stress field, very similar to the one derived for box 6, reflects again the NW-SE Africa-Eurasia convergence. It seems also reasonable to suppose that relatively low level of seismicity detectable in the Ionian offshore of southern Calabria (Figure 3.1; see also Orecchio et al., 2014) can be an effect of southeastward rollback of the subducting slab active in the same zone (Figure 3.4) which locally reduces the compressional stress due to NW oriented plate convergence. Finally, at the westernmost corner of Sicily (box 12 in Figure 3.4), the five focal mechanisms available for inversion do not guarantee an acceptable estimate of stress tensor orientations and these are therefore omitted in Figure 3.2b and in Figure 3.4.

3.4 Conclusions

The compilation of an updated waveform inversion focal mechanism database and the application of the Bayesian stress inversion algorithm by Arnold and Townend (2007) have permitted us (i) to strongly improve the knowledge of seismotectonic stress regimes in the Calabrian Arc region and (ii) to start exploring seismogenic stress in the Ionian offshore, an area where many investigations have provided other geological and geophysical information. The obtained stress distribution covers with good accuracy the whole arcuate region corresponding to the Apennine-Maghrebian chain from south Italy to western Sicily and the relative Tyrrhenian and Ionian offshores (Figure 3.4). Our analysis highlights, in particular, a more or less perpendicular to - chain extensional process along the chain, compressional effects of Africa-Eurasia slow convergence mainly detected in the Tyrrhenian and Ionian offshores, and NW-SE extension along the Calabrian Arc that jointly

with seismicity distribution in the Ionian offshore of the Arc can be related to southeastward retreat of the Ionian subducting slab. More in detail, the well constrained NNW trending σ_1 in the main east trending seismogenic belt located offshore northern Sicily, and the quite diffused transcurrent regimes in southeastern Sicily and Ionian offshore driven by NW trending σ_1, mark clearly continental plate convergence. At the same time, relatively low level of seismicity in the Ionian offshore of southern Calabria and the extension of Calabrian Arc parallel to southeastward rollback of the Ionian subduction slab, may reflect the superposition of a quite localized residual subduction process onto the continental-scale process of convergence. Our results consisting of a strongly enhanced focal mechanism database and more accurate local-to-regional scale stress distributions throw new light on the kinematics and dynamics of this still widely debated region and furnish useful tools and constraints for future geodynamic investigations.

Id	Data	O.T.	Lat	Lon	Depth	Strike	Dip	Rake	M	Source
1	19770605	13:59:23	37.840	14.460	11.3	61	26	-139	4.6	Italian CMT
2	19780311	19:20:49	38.100	16.030	33.0	270	41	-72	5.6	Italian CMT
3	19780415	23:33:47	38.390	15.070	14.0	135	60	-176	5.5	Italian CMT
4	19790120	13:49:59	38.670	12.860	9.0	72	29	53	5.2	Italian CMT
5	19800220	02:34:03	39.300	16.210	12.0	14	43	-78	4.8	Italian CMT
6	19800309	12:03:40	39.940	16.120	19.0	157	35	-80	4.6	Italian CMT
7	19800514	01:41:04	40.460	15.850	24.0	119	38	-112	4.5	Italian CMT
8	19800528	19:51:19	38.480	14.250	14.0	83	43	99	5.7	Italian CMT
9	19800601	02:32:52	38.390	14.330	10.0	65	39	91	4.9	Italian CMT
10	19801123	18:34:54	40.910	15.370	10.0	135	41	-80	6.9	Italian CMT
11	19801124	00:24:00	40.890	15.260	10.0	131	29	-110	4.9	Italian CMT
12	19801124	03:03:54	40.900	15.330	10.0	115	44	-125	5.1	Italian CMT
13	19801125	17:06:44	40.700	15.470	10.0	122	30	-119	5.1	Italian CMT
14	19801125	18:28:21	40.650	15.400	10.0	129	26	-65	4.9	Italian CMT
15	19801203	23:54:24	40.740	15.480	10.0	148	36	-76	4.9	Italian CMT
16	19810116	00:37:47	40.950	15.370	15.0	115	30	-93	5.0	Italian CMT
17	19810607	13:00:57	37.670	12.470	18.0	48	29	48	4.9	Italian CMT
18	19810622	09:36:18	38.490	14.090	13.0	71	47	116	4.8	Italian CMT
19	19811129	05:06:47	40.740	15.640	33.0	104	41	-138	4.9	Italian CMT
20	19820321	09:44:00	39.700	15.640	18.9	15	39	-127	5.0	Italian CMT
21	19820815	15:09:50	40.810	15.360	10.0	158	48	-45	4.8	Italian CMT
22	19870128	05:33:22	40.950	15.470	10.0	160	45	-79	4.6	Italian CMT
23	19870813	07:22:10	37.900	15.060	35.9	352	42	-10	4.8	Italian CMT
24	19880108	13:05:46	40.080	16.010	10.0	148	30	-86	4.8	Italian CMT
25	19900505	07:21:19	40.750	15.850	26.0	184	73	13	5.3	Italian CMT

26	19900505	07:38:12	40.750	15.810	15.0	282	83	173	5.0	Italian CMT
27	19901029	08:16:14	36.230	14.670	23.0	198	72	-13	4.5	Italian CMT
28	19901213	00:24:24	37.200	15.500	10.0	274	64	174	5.4	Italian CMT
29	19910526	12:26:00	40.730	15.770	8.0	183	71	-9	5.2	Italian CMT
30	19920406	13:08:34	37.830	14.610	21.0	100	37	-97	4.7	Italian CMT
31	19930626	17:47:54	37.920	14.210	10.0	170	53	6	4.4	Italian CMT
32	19950529	06:52:27	37.900	12.070	11.0	82	70	-180	4.8	Italian CMT
33	19960403	13:04:34	40.760	15.490	10.0	123	30	-110	4.9	Italian CMT
34	19961214	00:18:45	37.810	13.840	40.0	123	23	-43	4.7	Italian CMT
35	19970325	00:46:14	36.930	16.030	33.0	104	78	179	4.7	Italian CMT
36	19980117	12:32:51	38.400	12.900	10.0	58	29	71	3.5	Italian CMT
37	19980620	02:25:47	38.460	13.080	10.0	69	22	76	4.9	Italian CMT
38	19980621	08:59:47	38.500	13.100	10.0	69	36	77	4.3	Italian CMT
39	19980621	12:59:04	38.430	12.670	10.0	88	38	102	4.5	Italian CMT
40	19980909	11:27:59	40.030	15.980	10.0	139	29	-83	5.2	Italian CMT
41	19980914	05:24:47	38.460	13.600	10.0	72	30	80	4.4	Italian CMT
42	19990214	11:45:54	38.170	15.060	33.0	18	39	-108	4.5	Italian CMT
43	20010411	00:10:28	40.430	16.120	16.6	130	20	-90	3.0	Orecchio&al.(2014)
44	20010422	13:56:36	37.720	15.100	10.0	316	56	27	5.1	Italian CMT
45	20010526	06:02:20	37.460	16.340	33.0	71	54	134	4.8	Italian CMT
46	20010930	23:44:58	40.220	16.040	12.6	30	70	-80	2.7	Orecchio&al.(2014)
47	20011018	11:02:44	39.100	16.610	10.0	332	44	-88	4.1	Italian CMT
48	20011125	19:34:20	37.910	13.960	20.0	137	31	-57	4.3	Italian CMT
49	20020405	04:52:24	38.480	14.740	10.0	90	41	108	4.1	Italian CMT
50	20020417	06:42:54	39.700	16.840	5.0	121	38	-7	4.7	Italian CMT
51	20020418	20:56:48	40.690	15.580	10.0	340	49	-52	4.4	Italian CMT
52	20020906	01:21:29	38.380	13.700	5.0	26	50	40	5.8	Italian CMT

53	20020906	01:45:30	38.440	13.730	4.0	252	48	126	4.5	Italian CMT
54	20020910	02:32:51	38.470	13.700	5.0	71	29	126	4.0	Italian CMT
55	20020920	23:06:04	38.460	13.740	5.0	46	33	77	4.5	Italian CMT
56	20020927	06:10:45	38.440	13.690	5.0	41	39	70	4.8	Italian CMT
57	20020928	02:46:46	38.470	13.710	5.0	79	39	103	4.6	Italian CMT
58	20021002	22:57:26	38.460	13.720	15.0	33	41	59	4.9	Italian CMT
59	20021027	02:50:26	37.790	15.160	10.0	320	60	171	4.6	Italian CMT
60	20021027	07:32:09	37.920	15.180	10.0	67	54	19	4.4	Italian CMT
61	20021029	10:02:22	37.670	15.270	10.0	316	61	-173	4.4	Italian CMT
62	20021029	16:39:48	37.690	15.560	10.0	207	54	-28	4.1	Italian CMT
63	20030707	15:08:12	36.010	14.900	10.0	350	62	4	4.8	Italian CMT
64	20041011	07:31:41	37.880	15.480	6.6	89	90	-45	3.6	D'Amico&al.(2010)
65	20041022	21:10:13	38.080	15.320	10.7	78	61	-37	3.4	D'Amico&al.(2010)
66	20050131	10:44:50	39.660	16.860	30.0	23	79	-41	4.1	D'Amico&al.(2011)
67	20050419	22:36:23	38.140	15.660	7.1	220	42	-10	3.1	D'Amico&al.(2010)
68	20050423	19:10:48	38.430	15.820	13.6	120	50	-64	2.8	D'Amico&al.(2010)
69	20050423	19:11:43	39.470	16.710	23.0	128	58	14	4.1	D'Amico&al.(2011)
70	20050602	03:05:51	39.590	15.310	7.0	278	73	-172	3.7	Li&al.(2007)
71	20050721	15:41:43	39.400	14.850	7.0	184	68	41	3.8	Li&al.(2007)
72	20050818	22:02:27	37.800	15.120	6.7	82	50	-18	3.1	D'Amico&al.(2010)
73	20050907	12:40:33	38.710	16.320	16.0	80	90	-42	3.6	D'Amico&al.(2011)
74	20050927	22:33:09	38.620	17.100	29.0	38	79	141	3.9	Li&al.(2007)
75	20051030	19:09:47	38.528	15.926	22.0	241	66	-84	3.4	Li&al.(2007)
76	20051118	18:35:25	39.170	17.070	23.0	120	34	3	3.6	D'Amico&al.(2011)
77	20051203	08:33:02	39.200	17.000	15.0	290	64	-18	3.8	Presti&al.(2013)
78	20060107	22:08:44	39.265	17.207	16.0	174	69	61	3.2	Orecchio&al.(2014)
79	20060117	03:33:58	39.198	17.125	34.0	146	62	-21	3.7	Orecchio&al.(2014)

80	20060227	04:34:01	38.100	15.170	10.1	62	50	-71	4.1	D'Amico&al.(2010)
81	20060227	09:11:59	38.140	15.180	10.5	39	48	-90	3.1	D'Amico&al.(2010)
82	20060227	14:16:06	38.140	15.180	9.1	76	48	-58	3.1	D'Amico&al.(2010)
83	20060329	20:20:00	37.730	13.890	10.0	338	80	-42	3.9	TDMT
84	20060417	02:44:06	39.610	17.050	28.0	114	74	-3	4.4	D'Amico&al.(2011)
85	20060423	14:42:38	37.040	15.020	24.0	100	88	147	3.9	TDMT
86	20060520	07:05:56	37.650	14.950	12.0	280	75	47	3.7	TDMT
87	20060619	20:55:35	37.829	14.891	16.0	350	28	11	3.8	Neri&al.(2014)
88	20060619	21:20:13	37.834	14.877	18.0	354	32	2	3.1	present work
89	20060619	21:27:12	37.824	14.868	20.0	0	37	9	3.1	present work
90	20060620	13:16:36	37.832	14.864	18.0	0	26	22	3.3	present work
91	20060621	07:17:50	37.829	14.834	18.0	354	23	11	3.3	present work
92	20060622	19:34:58	39.730	16.630	26.0	110	33	-33	4.4	D'Amico&al.(2011)
93	20060702	17:52:00	38.130	15.100	10.0	70	59	-49	2.6	D'Amico&al.(2010)
94	20060718	07:42:40	38.120	15.170	9.1	90	41	-48	3.1	D'Amico&al.(2010)
95	20060730	09:53:36	37.990	16.306	6.0	292	64	-7	2.7	Orecchio&al.(2014)
96	20060805	20:47:19	38.545	14.732	10.0	40	30	39	3.3	present work
97	20060819	16:29:11	38.577	14.432	26.0	229	78	28	3.3	present work
98	20060830	22:45:03	37.324	15.716	30.0	190	64	-23	3.1	Orecchio&al.(2014)
99	20060907	15:31:43	40.570	16.190	34.0	178	55	35	4.0	Italian CMT
100	20060909	15:45:23	38.702	14.230	8.0	222	68	13	3.3	present work
101	20061006	21:16:23	38.100	15.570	9.6	18	52	-90	3.2	D'Amico&al.(2010)
102	20061022	05:13:10	39.054	16.698	10.0	312	38	-30	3.0	Orecchio&al.(2014)
103	20061104	05:59:22	38.030	15.010	10.6	59	49	-36	3.0	D'Amico&al.(2010)
104	20061118	00:01:56	39.057	17.230	24.0	113	46	-51	3.0	Orecchio&al.(2014)
105	20061124	04:37:40	36.260	15.760	11.0	188	82	0	4.7	Italian CMT
106	20061219	14:58:06	37.780	14.910	23.0	18	16	-40	4.1	Italian CMT

107	20061220	11:38:08	38.539	14.256	6.0	201	64	13	3.6	Neri&al.(2014)
108	20061226	00:49:00	39.220	16.172	2.0	223	38	-12	3.1	Orecchio&al.(2014)
109	20070130	22:18:07	39.914	16.136	8.0	84	90	19	3.6	Orecchio&al.(2014)
110	20070202	06:51:01	39.553	16.345	12.0	31	48	-61	3.2	Totaro&al.(2013)
111	20070326	13:55:26	39.280	16.964	20.0	301	61	8	3.7	Italian CMT
112	20070410	19:17:23	36.960	12.840	29.7	100	75	164	4.1	TDMT
113	20070421	19:41:27	38.571	13.433	12.0	250	52	10	3.9	Neri&al.(2014)
114	20070426	00:49:36	39.535	16.367	16.0	290	8	20	3.8	Orecchio&al.(2014)
115	20070503	18:43:56	39.020	17.627	18.0	92	25	-31	3.5	Orecchio&al.(2014)
116	20070517	05:48:13	38.570	14.690	8.0	22	50	8	3.5	Presti&al.(2013)
117	20070525	09:39:45	39.670	16.830	25.0	91	29	-48	4.2	D'Amico&al.(2011)
118	20070609	05:56:38	39.176	16.619	18.0	71	49	-59	3.1	Orecchio&al.(2014)
119	20070615	22:56:01	36.970	15.290	18.0	12	87	20	3.6	TDMT
120	20070617	12:11:58	38.370	15.790	10.0	262	38	-43	2.9	D'Amico&al.(2010)
121	20070706	23:28:43	39.181	17.247	28.0	118	38	-35	3.5	Orecchio&al.(2014)
122	20070714	18:13:03	38.633	14.745	4.0	30	31	38	3.1	Presti&al.(2013)
123	20070731	06:53:16	37.468	14.738	32.0	142	78	-21	3.4	present work
124	20070801	00:07:54	39.020	17.200	40.0	80	67	-45	4.1	D'Amico&al.(2011)
125	20070818	14:04:07	38.230	15.130	9.4	44	50	-23	3.9	D'Amico&al.(2010)
126	20070818	14:21:11	38.190	15.120	10.0	26	69	18	3.4	D'Amico&al.(2010)
127	20070905	21:24:13	38.559	14.842	6.0	10	54	-2	3.3	present work
128	20070913	15:19:52	38.246	15.157	8.0	246	82	-60	2.9	present work
129	20070923	07:12:46	38.591	14.792	8.0	27	60	28	3.6	Presti&al.(2013)
130	20070930	15:41:20	38.594	14.804	6.0	70	73	16	3.1	Presti&al.(2013)
131	20071213	23:38:24	38.927	16.609	30.0	98	9	-17	3.2	Orecchio&al.(2014)
132	20071214	00:42:55	38.927	16.624	26.0	331	70	-60	3.0	Orecchio&al.(2014)
133	20071217	09:44:39	39.390	16.364	40.0	162	90	-71	3.5	Orecchio&al.(2014)

134	20071220	03:25:32	39.363	16.191	2.0	210	66	-71	3.5	Orecchio&al.(2014)
135	20080115	02:38:31	39.812	16.331	18.0	327	80	39	3.2	Orecchio&al.(2014)
136	20080118	13:01:00	39.140	16.525	14.0	38	60	-72	3.8	TDMT
137	20080209	07:46:36	37.840	15.560	6.9	40	90	-10	3.0	D'Amico&al.(2010)
138	20080221	05:00:09	37.820	17.970	30.0	333	27	134	4.5	Italian CMT
139	20080310	10:33:27	39.658	16.846	20.0	121	39	-7	3.5	Presti&al.(2013)
140	20080408	17:20:01	39.158	16.525	14.0	221	38	-59	4.1	Italian CMT
141	20080413	10:10:02	39.164	16.515	14.0	205	69	-90	3.6	D'Amico&al.(2010)
142	20080413	13:06:57	38.250	15.700	14.3	6	47	-36	2.8	Orecchio&al.(2014)
143	20080414	18:44:34	39.149	16.522	12.0	48	41	-62	3.1	Orecchio&al.(2014)
144	20080419	21:41:11	39.130	17.469	16.0	107	42	-39	3.6	Presti&al.(2013)
145	20080426	22:23:06	39.142	16.530	18.0	256	60	-31	3.2	Orecchio&al.(2014)
146	20080501	21:05:49	37.800	15.070	2.0	97	76	-2	2.8	D'Amico&al.(2010)
147	20080513	21:28:30	37.800	15.060	12.0	76	46	-20	3.5	D'Amico&al.(2010)
148	20080702	17:43:33	38.968	16.228	30.0	266	69	-30	3.2	Orecchio&al.(2014)
149	20080703	20:56:52	38.450	13.710	24.2	182	68	27	3.3	TDMT
150	20080705	17:04:36	38.200	15.870	2.0	311	59	2	2.6	D'Amico&al.(2010)
151	20080709	23:08:27	38.967	16.227	24.0	268	76	-32	3.3	Orecchio&al.(2014)
152	20080710	01:45:45	38.967	16.239	12.0	76	72	-40	3.0	Orecchio&al.(2014)
153	20080710	12:50:20	38.962	16.240	14.0	71	75	-39	3.3	Orecchio&al.(2014)
154	20080711	07:15:00	38.964	16.242	16.0	50	52	-29	3.0	Orecchio&al.(2014)
155	20080711	07:20:21	38.961	16.254	12.0	78	80	-58	2.9	Orecchio&al.(2014)
156	20080813	13:39:30	37.481	16.417	34.0	181	71	11	3.2	Orecchio&al.(2014)
157	20080901	14:45:40	37.970	15.060	8.1	70	31	-80	3.1	D'Amico&al.(2010)
158	20080902	09:16:45	37.990	15.060	10.3	279	64	-44	3.3	D'Amico&al.(2010)
159	20080902	21:57:20	38.246	15.688	34.0	351	72	-65	3.1	Orecchio&al.(2014)
160	20080910	11:30:48	39.183	17.130	34.0	81	69	-90	4.6	Orecchio&al.(2014)

161	20080912	20:12:11	39.166	17.373	34.0	332	85	-2	3.6	Orecchio&al.(2014)
162	20080927	08:28:27	39.179	17.214	30.0	123	71	-8	4.0	TDMT
163	20081024	16:55:37	38.614	16.441	30.0	0	60	70	3.3	Orecchio&al.(2014)
164	20081024	18:47:54	38.586	16.471	28.0	323	38	-24	3.4	Orecchio&al.(2014)
165	20081027	10:55:55	38.110	15.130	2.0	50	28	-71	3.5	D'Amico&al.(2010)
166	20081102	06:46:44	37.636	16.486	40.0	141	67	-79	3.6	Orecchio&al.(2014)
167	20081107	15:00:59	39.149	16.464	14.0	139	72	-65	3.3	Orecchio&al.(2014)
168	20081120	14:09:21	39.169	17.373	20.0	111	30	-26	4.0	Italian CMT
169	20081128	08:04:47	39.886	17.018	34.0	97	50	21	3.6	Orecchio&al.(2014)
170	20081128	23:39:21	37.540	13.690	35.0	337	74	9	4.2	Italian CMT
171	20081209	12:55:27	39.035	17.196	24.0	104	21	-31	3.6	Orecchio&al.(2014)
172	20081225	18:55:58	40.339	15.959	6.0	100	59	-23	2.6	Orecchio&al.(2014)
173	20090205	14:50:14	37.390	16.033	28.0	167	78	18	3.3	Orecchio&al.(2014)
174	20090316	00:28:06	37.674	15.956	28.0	34	60	-24	3.0	Orecchio&al.(2014)
175	20090319	08:27:54	36.520	12.720	28.0	255	48	-180	4.0	Italian CMT
176	20090407	20:24:54	39.185	16.809	14.0	161	70	-33	3.2	Orecchio&al.(2014)
177	20090413	11:39:58	39.525	16.392	8.0	260	40	-7	3.3	Totaro&al.(2013)
178	20090427	09:42:16	38.068	15.079	30.0	69	78	-19	3.6	Presti&al.(2013)
179	20090701	17:58:54	38.342	15.006	2.0	40	90	19	3.1	Presti&al.(2013)
180	20090727	22:15:14	37.119	15.693	30.0	353	48	-13	3.2	Orecchio&al.(2014)
181	20090804	16:17:16	37.116	15.707	18.0	22	73	-13	3.6	Orecchio&al.(2014)
182	20090829	06:55:17	37.915	15.467	8.0	56	80	-47	2.9	Orecchio&al.(2014)
183	20090907	21:26:31	38.590	14.020	10.0	91	59	100	4.9	Italian CMT
184	20091012	20:07:49	37.234	15.964	30.0	204	82	12	3.4	Orecchio&al.(2014)
185	20091108	06:51:16	37.830	14.550	15.0	310	21	-54	4.2	Italian CMT
186	20091125	06:20:07	38.050	16.449	16.0	341	62	-43	3.2	Orecchio&al.(2014)
187	20091215	11:49:07	38.957	15.572	24.0	195	61	-54	3.7	Orecchio&al.(2014)

188	20091219	09:01:19	37.760	15.090	40.0	112	44	176	4.6	Italian CMT
189	20100101	22:01:13	39.196	16.293	36.0	267	58	-60	3.8	Orecchio&al.(2014)
190	20100208	07:23:58	39.498	16.771	34.0	94	73	-31	3.6	Presti&al.(2013)
191	20100317	11:01:11	38.565	14.726	8.0	78	56	81	3.3	Presti&al.(2013)
192	20100325	17:30:18	40.030	15.860	2.0	0	51	-67	3.2	Orecchio&al.(2014)
193	20100402	20:04:47	37.760	15.110	2.0	274	55	10	4.2	Italian CMT
194	20100404	15:40:28	39.349	16.816	22.0	314	76	-18	3.3	Presti&al.(2013)
195	20100413	12:12:14	39.347	17.146	18.0	128	29	-26	3.5	Presti&al.(2013)
196	20100415	20:05:47	39.351	17.216	18.0	137	39	-15	3.6	Presti&al.(2013)
197	20100511	10:28:47	39.750	16.220	6.0	152	56	-90	2.8	Orecchio&al.(2014)
198	20100511	18:09:43	39.306	17.468	22.0	126	40	-28	3.8	Orecchio&al.(2014)
199	20100606	16:49:53	38.271	15.113	10.0	237	82	-34	3.5	Presti&al.(2013)
200	20100616	22:39:41	38.832	16.146	12.0	82	11	-32	3.8	Italian CMT
201	20100801	21:31:53	38.609	14.460	4.0	37	60	78	3.1	Presti&al.(2013)
202	20100816	12:54:46	38.415	14.916	10.0	218	66	42	4.5	Presti&al.(2013)
203	20100910	19:19:48	38.539	16.214	26.0	198	53	-60	3.3	Orecchio&al.(2014)
204	20100910	21:39:20	38.203	15.816	28.0	204	69	-70	3.2	Orecchio&al.(2014)
205	20101008	17:26:58	36.908	16.331	38.0	190	79	17	3.6	Orecchio&al.(2014)
206	20101014	14:18:28	38.844	16.689	28.0	60	60	31	3.2	Orecchio&al.(2014)
207	20101015	05:21:20	38.873	16.633	32.0	18	61	47	4.3	Italian CMT
208	20101109	08:43:20	40.050	15.930	10.0	329	61	-57	3.5	Orecchio&al.(2014)
209	20101127	08:45:49	38.077	15.641	38.0	332	22	-12	3.7	Orecchio&al.(2014)
210	20110325	16:18:12	38.865	16.942	6.0	87	70	-53	3.3	Orecchio&al.(2014)
211	20110325	18:31:31	38.868	16.957	6.0	281	53	-19	3.6	Orecchio&al.(2014)
212	20110426	21:02:30	38.151	15.157	2.0	33	40	-90	3.2	present work
213	20110503	22:24:52	37.779	16.676	36.0	323	49	-41	3.6	Orecchio&al.(2014)
214	20110506	15:12:35	37.780	14.960	22.2	13	57	15	4.0	Italian CMT

215	20110623	22:02:47	38.064	14.784	10.0	315	90	-1	4.7	Neri&al.(2014)
216	20110624	09:00:08	39.611	16.609	22.0	330	21	-20	3.1	Totaro&al.(2013)
217	20110627	05:23:41	38.024	14.744	8.0	313	63	-2	3.2	present work
218	20110627	22:13:45	38.037	14.735	10.0	299	44	-31	3.4	present work
219	20110629	09:04:17	38.046	14.734	8.0	305	90	2	3.2	present work
220	20110629	19:15:15	38.057	14.739	10.0	139	81	-10	3.5	present work
221	20110706	09:08:39	38.051	14.782	10.0	124	42	-41	3.7	Neri&al.(2014)
222	20110707	01:01:15	38.041	14.789	10.0	315	90	10	3.3	present work
223	20110727	04:03:14	38.062	14.766	8.0	113	46	-61	3.2	present work
224	20110817	01:20:32	38.549	14.474	6.0	209	70	38	3.0	present work
225	20110831	16:33:20	37.107	14.702	2.0	7	80	1	3.1	present work
226	20111103	14:37:10	38.427	14.580	10.0	8	90	22	3.5	present work
227	20111109	17:00:48	39.912	16.017	9.0	10	50	-51	2.7	Totaro&al.(2015)
228	20111115	04:59:00	38.274	14.671	10.0	18	74	9	4.1	Neri&al.(2014)
229	20111119	10:19:16	37.807	14.345	14.0	121	70	-25	3.4	present work
230	20111123	14:12:34	39.923	16.013	9.0	7	40	-48	3.5	Totaro&al.(2015)
231	20111201	14:01:20	39.927	16.012	9.8	7	48	-52	3.3	Totaro&al.(2015)
232	20111202	21:25:38	39.921	16.012	9.8	156	49	-90	3.2	Totaro&al.(2015)
233	20111214	17:59:49	39.381	16.202	6.0	178	39	-43	3.1	Orecchio&al.(2014)
234	20111217	23:20:15	39.373	16.175	26.0	345	62	-79	3.6	Orecchio&al.(2014)
235	20111224	20:17:50	39.919	16.024	9.1	348	44	-90	3.2	Totaro&al.(2015)
236	20111227	01:07:45	39.580	16.922	20.0	121	28	-26	3.6	present work
237	20120103	23:47:41	39.640	16.840	16.0	156	29	-29	3.1	Orecchio&al.(2014)
238	20120129	11:14:50	37.876	14.272	10.0	37	61	-23	3.0	present work
239	20120201	14:28:38	37.887	14.279	30.0	119	90	14	3.6	Neri&al.(2014)
240	20120208	16:15:56	37.891	14.299	12.0	200	50	-51	3.1	present work
241	20120225	20:34:35	38.537	13.548	12.0	20	27	19	4.3	Neri&al.(2014)

242	20120226	16:17:23	37.313	16.014	36.0	338	70	-40	3.7	Polonia&al.(2016)
243	20120324	20:34:59	37.588	15.884	32.0	158	84	-9	3.1	Polonia&al.(2016)
244	20120405	03:01:06	39.556	16.420	18.0	275	42	-53	3.0	Totaro&al.(2013)
245	20120409	23:29:02	40.413	15.457	14.0	165	58	-77	3.1	Totaro&al.(2013)
246	20120412	13:20:28	37.887	15.624	10.0	319	90	81	3.1	Polonia&al.(2016)
247	20120413	06:21:33	38.345	13.304	12.0	319	29	-71	4.4	Neri&al.(2014)
248	20120528	01:06:27	39.891	16.117	7.0	146	49	-90	4.3	Totaro&al.(2015)
249	20120528	01:32:10	39.904	16.099	9.3	236	51	-27	3.1	Totaro&al.(2015)
250	20120531	03:16:22	39.890	15.570	8.0	211	45	2	3.0	Orecchio&al.(2014)
251	20120531	20:18:23	38.962	16.925	4.0	258	82	-74	2.9	present work
252	20120615	06:27:25	37.449	16.286	38.0	190	80	7	3.8	Polonia&al.(2016)
253	20120618	03:17:12	39.903	16.106	9.5	162	29	-90	2.7	Totaro&al.(2015)
254	20120625	10:52:51	37.008	15.054	18.0	164	77	-16	3.2	present work
255	20120627	01:14:20	37.001	15.034	4.0	182	90	3	3.5	present work
256	20120627	01:20:59	36.994	15.032	4.0	10	81	-3	2.9	present work
257	20120627	02:48:02	37.001	15.031	4.0	172	90	-6	2.9	present work
258	20120704	11:12:12	37.69	16.87	40	186	74	3	4.6	Regional CMT
259	20120715	11:51:55	39.650	16.910	18.0	118	27	-17	3.0	Orecchio&al.(2014)
260	20120726	14:20:03	37.903	16.335	16.0	134	83	-19	3.1	Polonia&al.(2016)
261	20120813	07:30:51	38.52	13.73	26.5	19	24	63	4.2	Regional CMT
262	20120819	17:45:08	39.893	16.023	8.8	154	46	-90	3.5	Totaro&al.(2015)
263	20120819	21:28:29	39.894	16.026	8.3	341	37	-62	2.7	Totaro&al.(2015)
264	20120901	14:02:45	39.889	16.028	8.4	178	60	-69	3.4	Totaro&al.(2015)
265	20120904	03:48:03	39.896	16.027	8.3	161	55	-81	2.8	Totaro&al.(2015)
266	20120907	12:40:51	39.887	16.028	7.9	177	52	-70	3.3	Totaro&al.(2015)
267	20120907	15:10:07	39.886	16.020	6.0	176	61	-62	2.8	present work
268	20120914	03:50:11	39.899	16.031	7.9	156	57	-90	3.6	Totaro&al.(2015)

269	20120922	01:45:02	39.908	16.024	8.0	139	58	-84	2.7	Totaro&al.(2015)
270	20120922	05:10:35	39.783	16.614	14.0	128	90	71	3.5	present work
271	20120923	06:13:56	39.908	16.018	8.4	331	32	-90	2.7	Totaro&al.(2015)
272	20120924	20:48:36	39.917	16.033	6.4	231	59	-42	2.7	Totaro&al.(2015)
273	20120928	05:56:46	39.908	16.097	7.3	22	41	-80	2.8	Totaro&al.(2015)
274	20121001	20:28:28	39.905	16.029	7.7	343	39	-82	3.5	Totaro&al.(2015)
275	20121001	21:27:51	39.908	16.024	7.8	13	40	-43	3.3	Totaro&al.(2015)
276	20121002	00:08:57	39.908	16.029	8.6	331	40	-80	3.3	Totaro&al.(2015)
277	20121002	04:35:18	39.911	16.028	8.2	140	58	-78	2.8	Totaro&al.(2015)
278	20121004	09:32:33	39.900	16.024	8.0	159	52	-84	2.9	Totaro&al.(2015)
279	20121005	11:12:28	39.896	16.030	7.6	0	40	-73	3.0	Totaro&al.(2015)
280	20121014	14:49:24	39.913	16.018	8.7	20	42	-40	2.7	Totaro&al.(2015)
281	20121018	02:51:57	39.901	16.034	7.8	350	34	-90	3.3	Totaro&al.(2015)
282	20121023	10:40:24	39.909	16.026	8.4	324	30	-82	3.1	Totaro&al.(2015)
283	20121025	23:05:25	39.889	16.033	8.8	166	50	-77	5.0	Totaro&al.(2015)
284	20121026	00:31:53	39.893	15.997	10.0	349	29	-49	3.0	present work
285	20121026	02:25:09	39.919	16.032	6.6	352	40	-81	2.9	Totaro&al.(2015)
286	20121026	02:40:08	39.884	16.015	8.1	73	50	-50	2.8	Totaro&al.(2015)
287	20121026	16:08:58	39.887	16.030	8.9	11	56	-23	2.7	Totaro&al.(2015)
288	20121028	13:52:18	39.926	16.016	8.5	12	75	27	3.1	Totaro&al.(2015)
289	20121102	01:59:34	38.778	16.473	14.0	69	22	-50	3.1	Orecchio&al.(2014)
290	20121102	17:50:44	39.914	16.030	7.9	244	58	-66	3.0	Totaro&al.(2015)
291	20121102	17:58:47	39.918	16.028	7.8	39	52	-56	2.7	Totaro&al.(2015)
292	20121105	12:06:32	39.939	16.006	8.8	21	71	-11	3.4	Totaro&al.(2015)
293	20121108	11:11:57	39.908	16.104	8.4	158	16	-79	3.1	Totaro&al.(2015)
294	20121112	03:03:53	39.919	16.012	8.7	229	42	20	3.0	Totaro&al.(2015)
295	20121121	06:43:25	39.921	16.016	8.2	63	60	-39	2.9	Totaro&al.(2015)

296	20121122	01:59:52	39.921	16.024	9.0	0	41	-78	3.2	Totaro&al.(2015)
297	20121122	09:10:41	37.8	14.96	10	258	65	154	4.1	Regional CMT
298	20121122	11:25:52	37.77	14.99	20	6	57	23	4.2	Regional CMT
299	20121124	22:24:26	39.915	16.019	7.9	0	47	-79	2.8	Totaro&al.(2015)
300	20121125	08:28:39	39.917	16.015	9.4	360	42	-72	3.5	Totaro&al.(2015)
301	20121125	08:42:25	39.927	16.028	5.5	0	41	-74	2.9	Totaro&al.(2015)
302	20121125	08:53:33	39.894	16.012	7.6	168	45	-90	3.0	Totaro&al.(2015)
303	20121125	17:48:02	39.920	16.014	9.5	7	43	-69	3.1	Totaro&al.(2015)
304	20121128	02:43:46	39.916	16.011	9.1	45	86	2	2.9	Totaro&al.(2015)
305	20121211	14:28:43	39.878	16.011	9.4	339	29	-70	3.3	Totaro&al.(2015)
306	20121213	04:44:03	39.881	16.034	8.8	20	70	-31	3.2	Totaro&al.(2015)
307	20121218	11:03:18	39.841	16.167	2.0	130	49	-90	3.3	present work
308	20121218	11:05:43	39.838	16.172	4.0	158	62	-30	3.0	present work
309	20121226	08:22:48	39.503	16.308	8.0	41	29	-41	3.2	present work
310	20130104	07:50:06	37.879	14.720	12.0	318	43	41	4.4	Neri&al.(2014)
311	20130104	10:50:21	37.879	14.704	31.0	301	81	-14	3.2	present work
312	20130106	07:50:19	37.870	14.719	18.0	118	63	-22	3.2	present work
313	20130109	16:10:34	37.881	14.719	6.0	312	78	-11	3.0	present work
314	20130205	22:08:04	40.072	15.862	18.0	176	71	-66	3.1	present work
315	20130223	19:14:18	38.305	14.981	4.0	220	79	-7	3.4	present work
316	20130303	23:39:13	38.133	15.832	8.0	237	57	-82	3.3	present work
317	20130307	22:36:59	37.968	14.524	2.0	0	50	-31	3.6	Neri&al.(2014)
318	20130317	14:22:15	39.619	15.887	32.0	31	79	48	3.3	present work
319	20130319	07:50:06	37.979	14.507	4.0	164	78	-43	3.4	present work
320	20130319	08:37:04	37.978	14.512	4.0	159	69	-39	3.3	present work
321	20130319	08:38:45	37.838	13.564	2.0	183	69	-8	2.8	present work
322	20130324	15:47:22	37.76	16.5	30	257	87	178	4.6	Regional CMT

323	20130401	03:07:13	39.678	16.670	28.0	127	68	90	3.4	present work
324	20130402	01:10:52	37.794	15.590	12.0	219	85	-10	2.9	present work
325	20130406	04:14:11	40.407	15.206	2.0	249	47	22	2.9	present work
326	20130412	17:50:00	38.160	14.924	16.0	0	67	15	3.1	present work
327	20130509	20:41:22	39.1805	16.0475	31	344	82	-110	3.8	TDMT
328	20130704	13:56:06	40.486	15.607	4.0	211	41	-42	2.9	present work
329	20130717	04:26:36	40.017	15.825	10.0	149	90	-72	2.9	present work
330	20130804	02:47:47	38.692	12.852	4.0	12	72	-11	3.3	present work
331	20130815	23:04:58	38.142	14.910	12.0	78	82	57	4.5	Neri&al.(2014)
332	20130815	23:06:51	38.148	14.917	12.0	77	82	55	4.6	Neri&al.(2014)
333	20130819	05:48:23	37.699	14.261	20.0	23	59	-14	3.0	present work
334	20130828	09:07:00	38.846	14.308	6.0	210	72	12	3.6	present work
335	20130917	22:56:38	40.793	15.795	8.0	339	69	1	3.3	present work
336	20130917	23:38:49	40.793	15.806	10.0	133	72	-83	3.4	present work
337	20130921	13:18:02	40.791	15.782	16.0	342	57	-34	3.2	present work
338	20130926	12:19:59	39.130	17.229	22.0	188	12	52	3.1	present work
339	20131003	18:22:25	38.473	13.490	14.0	20	51	0	3.4	present work
340	20131007	04:44:05	38.128	15.076	6.0	84	63	-29	2.8	present work
341	20131008	10:33:20	40.019	15.823	2.0	55	60	-10	2.7	present work
342	20131009	08:14:49	37.608	15.090	4.0	33	81	8	2.9	present work
343	20131009	08:33:22	37.610	15.072	10.0	258	90	1	3.2	present work
344	20131018	08:03:44	38.105	14.903	14.0	258	79	-61	3.0	present work
345	20131018	11:05:21	36.785	14.966	2.0	173	82	3	2.9	present work
346	20131018	20:50:52	40.802	15.218	14.0	319	41	-76	3.1	present work
347	20131019	11:08:03	40.590	15.177	14.0	112	30	58	3.0	present work
348	20131103	14:33:41	40.596	15.175	2.0	87	58	-80	2.7	present work
349	20131105	05:06:39	37.690	14.911	22.0	84	57	-11	3.1	present work

350	20131105	05:29:58	37.696	14.917	18.0	99	72	-14	3.0	present work
351	20131105	17:25:23	39.879	16.007	8.0	80	51	-45	3.0	present work
352	20131105	17:26:45	39.876	16.010	10.0	328	32	-79	3.4	present work
353	20131210	20:39:39	39.717	15.454	22.0	172	19	69	3.1	present work
354	20131214	21:49:05	37.764	14.738	30.0	53	67	-27	3.4	present work
355	20131215	03:57:33	36.67	14.94	15	83	47	143	4.1	Regional CMT
356	20131223	04:20:39	38.215	15.569	2.0	31	61	-60	3.5	Neri&al.(2014)
357	20131223	16:17:11	38.179	15.037	16.0	113	63	-33	3.1	present work
358	20140102	06:13:18	38.175	15.044	12.0	103	38	8	3.0	present work
359	20140114	03:43:42	38.37	14.92	12	315	78	171	4.1	Regional CMT
360	20140114	04:35:00	38.36	14.94	11	308	47	159	4.2	Regional CMT
361	20140122	19:35:01	40.441	15.119	8.0	61	32	-61	3.6	present work
362	20140127	21:39:32	40.121	15.931	10.0	38	58	-19	3.0	present work
363	20140218	21:44:19	37.626	13.816	4.0	250	79	33	3.3	present work
364	20140219	06:58:05	38.174	15.109	8.0	34	62	17	3.0	present work
365	20140301	01:48:50	40.238	15.222	4.0	19	27	40	2.9	present work
366	20140301	11:51:25	40.248	15.289	6.0	305	68	8	2.7	present work
367	20140303	06:26:04	40.403	15.009	8.0	287	47	-64	3.0	present work
368	20140308	14:19:05	39.772	15.809	16.0	280	79	46	3.0	present work
369	20140308	20:52:51	37.962	14.890	32.0	13	47	-40	3.8	Neri&al.(2014)
370	20140314	03:32:24	38.222	14.808	2.0	19	90	-1	3.0	present work
371	20140314	03:37:16	38.202	14.803	6.0	331	62	4	2.8	present work
372	20140323	18:31:52	37.466	16.484	38.0	177	61	21	3.6	present work
373	20140325	07:56:52	39.294	16.540	28.0	276	59	-50	3.6	present work
374	20140412	06:53:05	37.820	13.879	2.0	360	81	-1	3.1	present work
375	20140417	21:52:26	38.225	15.210	2.0	12	90	2	2.8	present work
376	20140503	20:04:06	39.902	16.109	4.0	232	31	-70	3.0	present work

377	20140506	08:24:42	39.909	16.067	4.0	241	51	-90	3.0	present work
378	20140507	17:08:35	39.892	16.020	8.0	160	49	-58	2.9	present work
379	20140517	22:38:44	37.408	15.605	30.0	191	78	-38	3.1	present work
380	20140604	21:20:41	39.876	16.002	8.0	159	58	-90	3.6	present work
381	20140606	13:41:38	39.901	16.088	4.0	155	31	-90	3.9	present work
382	20140607	15:00:49	38.093	15.095	10.0	285	73	7	3.7	Neri&al.(2014)
383	20140607	15:13:20	38.080	15.097	10.0	238	39	-49	2.6	present work
384	20140617	12:25:02	38.963	16.979	2.0	239	40	-90	2.7	present work
385	20140627	02:56:49	37.834	14.635	14.0	360	37	-26	3.3	present work
386	20140629	04:24:28	39.917	15.597	14.0	248	22	1	3.8	present work
387	20140629	05:32:22	39.909	15.595	6.0	47	65	-47	2.6	present work
388	20140629	05:42:56	39.910	15.585	14.0	240	21	-21	3.3	present work
389	20140702	18:49:46	40.593	15.170	2.0	71	49	-70	3.1	present work
390	20140707	17:44:15	40.722	15.496	12.0	32	64	30	3.3	present work
391	20140708	05:02:43	39.899	16.118	2.0	347	51	-83	2.7	present work
392	20140711	21:57:58	40.485	15.390	10.0	344	82	-49	3.5	present work
393	20140724	01:12:51	38.088	15.022	30.0	100	90	-16	3.2	present work
394	20140731	03:29:29	39.907	16.106	4.0	349	58	-82	3.4	present work
395	20140806	08:16:21	40.577	15.825	8.0	323	83	-9	3.0	present work
396	20140812	20:15:34	40.45	16.42	16	330	44	54	3.9	Regional CMT
397	20140813	10:08:09	40.443	16.425	4.0	160	63	-25	3.0	present work
398	20140816	05:00:12	38.532	13.4182	10	161	86	59	3.4	TDMT
399	20140826	01:19:46	37.954	14.334	14.0	298	20	-90	3.5	present work
400	20140919	05:32:38	38.490	14.810	14.0	66	78	25	3.2	present work
401	20140924	15:39:09	39.743	15.854	24.0	51	80	-39	3.2	present work
402	20140926	23:38:11	36.78	16.5	40	267	75	170	4.2	Regional CMT
403	20141009	22:58:28	38.51	14.85	10	76	40	80	4.1	Regional CMT

404	20141010	16:16:18	38.094	15.136	34.0	60	90	-76	3.1	present work
405	20141010	16:27:13	38.093	15.143	30.0	349	72	-31	2.8	present work
406	20141013	03:34:47	39.368	16.464	10.0	18	77	-73	2.8	present work
407	20141014	00:50:55	38.946	16.629	14.0	150	74	-1	2.9	present work
408	20141025	20:09:48	38.1735	15.9548	15	275	68	-79	3.3	TDMT
409	20141116	12:38:42	38.243	15.084	6.0	276	84	1	2.8	present work
410	20141127	09:09:44	38.862	16.492	20.0	28	39	-81	3.2	present work
411	20141228	21:43:38	39.289	16.358	10.0	179	49	-69	4.2	present work
412	20150110	03:40:38	38.074	13.79	4.0	327	81	1	2.9	present work
413	20150120	07:17:22	38.105	15.566	18.0	199	38	32	3.3	present work
414	20150208	19:39:22	37.348	15.218	22.0	87	52	-50	3.1	present work
415	20150211	01:42:09	38.049	14.749	4.0	127	37	-57	3.0	present work
416	20150211	03:57:01	38.046	14.744	4.0	272	70	-37	3.1	present work
417	20150312	15:29:04	38.433	16.226	2.0	230	59	-78	3.3	present work
418	20150328	22:07:51	38.088	16.205	20.0	233	79	79	3.1	present work
419	20150329	10:48:46	38.085	16.209	12.0	52	76	-83	3.5	present work
420	20150420	01:07:43	37.797	15.116	3	178	83	-164	3.5	TDMT
421	20150430	05:35:21	37.863	15.39	26.0	160	61	44	2.9	present work
422	20150521	22:13:22	38.454	14.715	2.0	281	53	-10	2.9	present work
423	20150611	04:31:45	37.88	14.005	8.0	148	60	-54	2.7	present work
424	20150617	09:44:07	37.657	14.146	24.0	332	82	8	3.4	present work
425	20150703	01:07:24	39.918	16.522	16.0	188	60	62	3.2	present work
426	20150715	04:19:11	37.215	14.43	18.0	164	79	11	3.1	present work
427	20150715	16:29:49	37.62	15.048	10.0	214	90	-11	3.0	present work
428	20150726	13:39:38	38.5	14.762	6.0	204	84	48	2.9	present work
429	20150801	02:46:51	37.644	15.858	42.0	195	90	9	3.4	present work
430	20150803	07:27:49	39.148	16.49	16.0	242	19	-33	3.9	present work

431	20150803	13:52:37	37.388	16.144	38.0	205	59	1	3.6	present work
432	20150804	23:36:31	37.637	14.153	10.0	168	84	14	3.2	present work
433	20150806	01:59:43	38.242	15.189	8.0	214	76	-61	3.1	present work
434	20150808	22:46:24	38.551	14.27	8.0	173	90	14	3.8	present work
435	20150818	05:59:15	40.64	15.445	12.0	326	70	-45	3.0	present work
436	20150826	04:28:36	38.792	16.914	24.0	10	90	-33	3.3	present work
437	20150829	20:25:13	38.541	12.12	14.0	332	81	8	4.0	present work
438	20150920	22:27:58	37.156	15.614	30.0	226	58	-2	3.8	present work

Table3.1. Database of focal mechanisms of the Calabrian Arc region. ID is the order number; Strike, dip, and rake are fault parameters of the focal solution; M is earthquake magnitude; Source is the bibliographic source.

Analyses and results reported in this chapter have been also published by Totaro, C., Orecchio, B., Presti, D., Scolaro, S., & Neri, G. (2016). *Seismogenic stress field estimation in the Calabrian Arc region (south Italy) from a Bayesian approach*. Geophysical Research Letters, 43(17), 8960-8969.

CHAPTER 4

THE 1905 CALABRIA, SOUTHERN ITALY, EARTHQUAKE: HYPOCENTER LOCATION, CAUSATIVE PROCESS, AND STRESS CHANGES INDUCED IN THE AREA OF THE 1908 MESSINA STRAITS EARTHQUAKE

4.1 Introduction

At the beginning of the past century, two earthquakes with magnitudes over 7 occurred in the Calabrian arc area at a space–time distance of a few tens of kilometers and only three years (Fig. 4.1). To date, the location, magnitude, and causative process of the first of these earthquakes (8 September 1905) are quite controversial, with several investigators reporting shallow along-coast or onshore macroseismic locations and magnitude values close to 7 (see, Rovida et al., 2016; among others) while others suggest offshore and possibly deeper locations (see, e.g., Galli and Molin, 2009) with magnitude values as large as 7.5 (Margottini et al., 1993) or even 7.9 (Dunbar et al., 1992). These differences imply basic differences in the earthquake generation process and environment, ranging from shallow, normal faulting in the Tyrrhenian overriding plate to intraslab rupture of the Ionian subducting lithosphere. The scientific debate is quite intense also concerning the causative fault of the second earthquake (28 December 1908), even if in this case all the investigators share the location of the source in the normal fault environment of upper crust of the Messina Straits area (Fig. 4.1). In addition, no investigation has, to date, been performed on the possible relationship between the two events, a subject that has a certain appeal considering their top values of magnitude for the central Mediterranean region and the very short

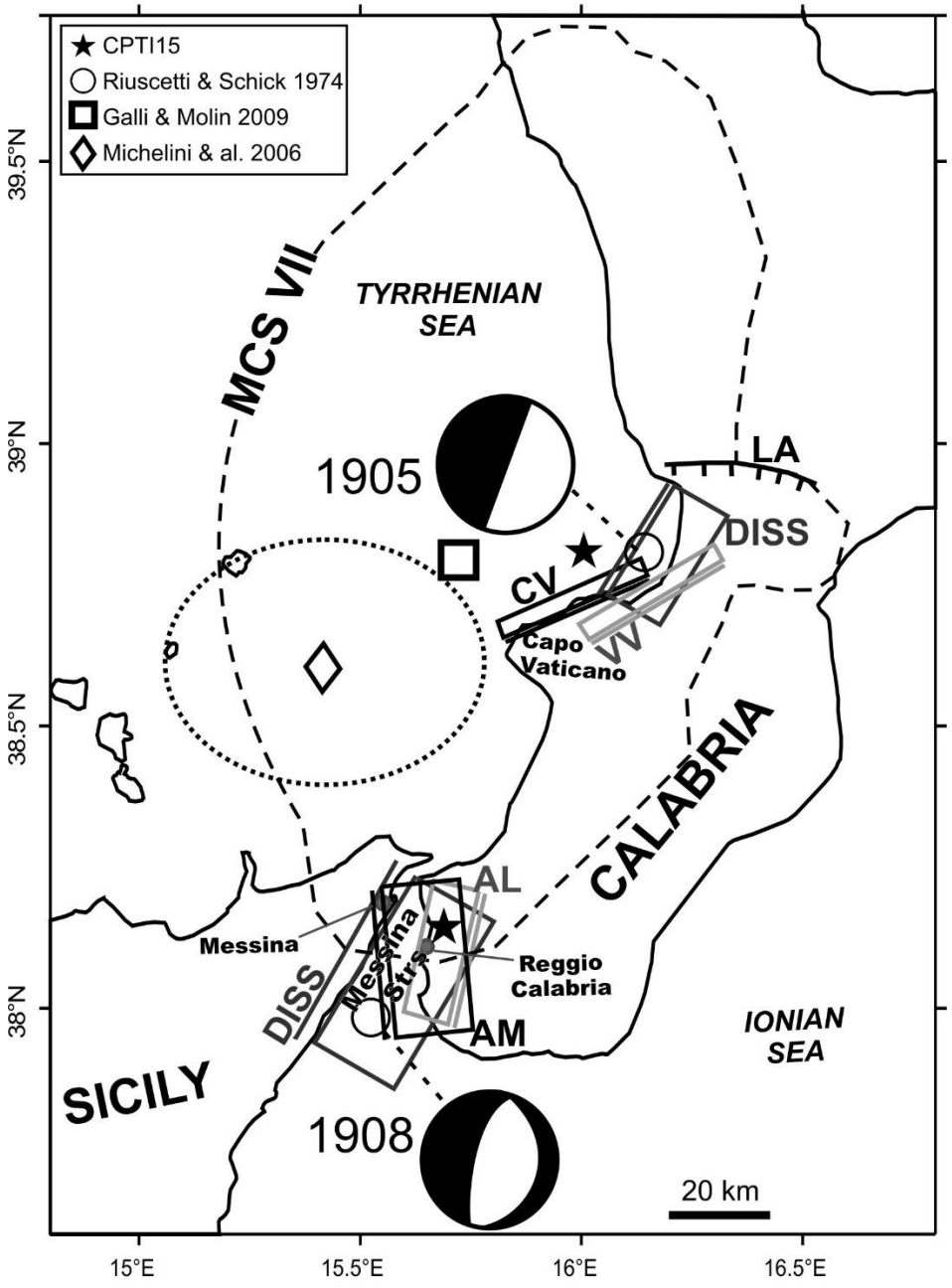

Figure 4.1. Map of the study area reporting literature information concerning locations, sources, and focal mechanisms of the 1905 and 1908 earthquakes. The bibliographic sources of the epicenters are indicated in the legend, top left. The dotted ellipse around the diamond represents the contour of non-nil epicenter probability of the 1905 earthquake location of Michelini et al. (2006). Rectangles and nearby segments represent, respectively, the surface projection of proposed sources and the intersection of the source plane with the earth surface (CV, Capo Vaticano; VV, Vibo Valentia; DISS, 1905 and 1908 sources reported by DISS Working Group, 2015; AM, 1908 source by Amoruso et al., 2002; AL, 1908 source by Aloisi et al., 2013; LA, Lamezia fault). The focal mechanisms of both earthquakes are from Riuscetti and Schick (1975), the intensity VII Mercalli–Cancani–Sieberg (MCS) isoseismal of 1905 earthquake (dashed curve) is from Galli and Molin (2009).

space–time distance they exhibit (Fig. 4.1). On the basis of macroseismic effects, several investigators proposed that the source of the 8 September 1905 earthquake may have been located in the proximity of the Tyrrhenian coast of Calabria in the area of Capo Vaticano (Fig. 4.1; Rovida et al., 2016). Other investigators suggested that the earthquake may have occurred a few tens of kilometers offshore (Michelini et al., 2006; Galli and Molin, 2009). No analytical estimate of the focal depth is reported in the literature, this parameter being inferred sometimes on the basis of the distribution of effects (e.g., Galli and Molin, 2009). Piatanesi and Tinti (2002) attempted to model the data of the weak tsunami wave associated with the event and concluded that no shallow fault known in the Capo Vaticano area (e.g., the Capo Vaticano, Vibo Valentia, and Lamezia faults; Fig. 4.1) furnishes an acceptable explanation of the tsunami data. The same authors report that an offshore source located 10–20 km west of Capo Vaticano could eventually reduce the misfits between the expected and observed tsunami data, but the lack of structural information in the identified marine area has not allowed them to proceed further with tsunami modeling. Riuscetti and Schick (1975) computed the focal mechanism of the earthquake using the low number of *P*-onset polarities available and reported a quite poorly constrained solution showing a horizontal and a N20°E-striking vertical nodal plane (Fig. 4.1). This eventual north-northeast (NNE) orientation of the source would match well with the shape of the very large area of damage and environmental effects (see, Galli and Molin, 2009 among many others).

The magnitude of the 1905 earthquake is also quite controversial, ranging between values slightly smaller than 7.0 (DISS Working Group, 2015) and values as large as M_s 7.5 (Margottini et al., 1993) or even M_L 7.9 (Dunbar et al., 1992) in papers in which this earthquake is indicated as the most powerful earthquake ever to occur in Italy. The 28 December 1908 earthquake has been imputed to east-dipping faults with the top located beneath the western side of Messina Straits (e.g., Amoruso et al., 2002; DISS Working Group, 2015), or to west-dipping

faults with the top located beneath the eastern side (e.g., Tortorici et al., 1995; Aloisi et al., 2013). In particular, by joint inversion of leveling and seismic data associated with this earthquake, Amoruso et al. (2002, 2006) obtained a nearly north-trending, eastdipping source plane passing through Messina (Fig. 4.1), whereas Aloisi et al. (2013) proposed a northeast (NE)-striking, northwest (NW)-dipping fault located east of Reggio Calabria (Fig. 4.1) on the grounds of geologic evidence of Holocene activity, geodetic strain, and seismic activity recorded in the last decades. For the same earthquake, the DISS Working Group (2015) reports a NE-trending southeast SE-dipping fault with the top located a couple of kilometers beneath the Sicilian coast of the Straits (Fig. 4.1). Despite the fact that different opinions still exist in the scientific community concerning the causative fault of this event, there is a general consensus concerning the depth of the source which is assumed to be confined to the upper 15 km of crust. Magnitude M_s values between 6.9 and 7. 2 are reported for this event in the literature (Pino et al., 2009), a value of 7.1 is given in the Parametric Catalog of Italian Earthquakes (CPTI15; Rovida et al., 2016). In the present study, we first use the Bayesian earthquake location method by Presti et al. (2004, 2008) for nonlinear hypocenter location of the 1905 earthquake. This method, named Bayloc, allows generally more accurate estimates of hypocenter parameters and location uncertainties with respect to the more commonly used linearized location methods (Presti et al., 2008). Even considering the limitations of the seismometric network existing at the beginning of the past century, the hypocenter location obtained by Bayloc for the 1905 earthquake (see Paragraph 4.2) results in being of a quality suitable for investigation of the process that generated the earthquake itself. We compare the obtained hypocenter location with the information taken from the literature (such as the crustal and mantle structure of the study region, the earthquake focal mechanism, and damage area), then we suggest a possible generation process for the earthquake and estimate the stress perturbation that it may have

induced in the area of the forthcoming 1908 earthquake. The results are framed in the geodynamic context of the Calabrian arc region.

4.2 Earthquake Locations: Analysis of Data and Results

In the present study, we performed hypocenter locations and location error estimates by Bayloc, the Bayesian nonlinear location method proposed by Presti et al. (2004, 2008). Starting from seismic phase arrival times at the recording stations, Bayloc computes for an individual earthquake a probability cloud marking the hypocenter location uncertainty. Also, Bayloc estimates the spatial distribution of probability relative to a set of earthquakes by summing the probability densities of the individual events. This method has been shown to help detection of the seismogenic structures through better hypocenter location and estimation of location errors compared with linearized methods (Presti et al., 2004, 2008). The details on methodological aspects of Bayloc can be found in the above cited papers. For hypocenter location of the 1905 earthquake, we used the seismic-wave arrival times recorded at seismic observatories existing at that epoch (Rizzo, 1906), which were recently checked and analyzed for re-association of phase types and outlier removal by Michelini et al. (2006).

A map of the observatories which recorded the earthquake in Italy and the nearby countries is given in Figure 4.2a. We decided to use seismic-wave arrival times at observatory stations located at distances from the epicentral area not greater than ~900 km. At these distances, the flat earth model can still be adopted (see, e.g., Lay and Wallace, 1995; Snoke and Lahr, 2001). This large value of epicentral distance upper bound was also suggested by the geometry of the recording network (Fig. 4.2a) showing only a few stations relatively close to the epicenter zone and an increasing density of stations when moving to northern Italy and central Europe; the number of stations available in

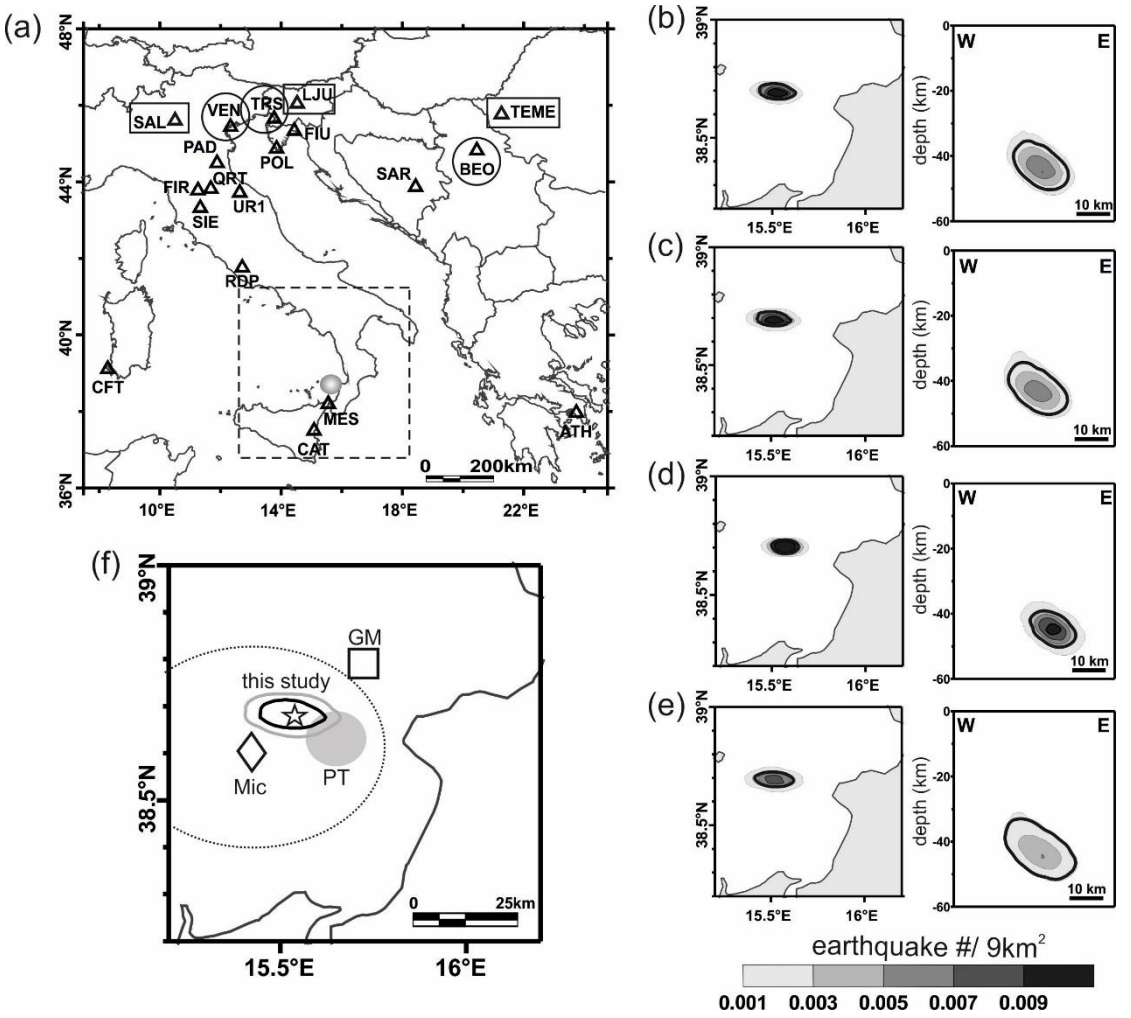

Figure 4.2. **(a)** Map of the seismic stations used in the present study to locate the 1905 earthquake. The epicentral area of the earthquake is indicated by shadowing closely north of MES station. For hypocenter location, we adopted the local velocity structure of Neri et al. (2012) inside the dashed rectangular area and the ak135 standard velocity model of Kennett et al. (1995) outside. **(b–e)** Results of our Bayesian nonlinear hypocenter location are reported both in map and in vertical section in terms of location probability per surface unit (9 km2), with the 68% probability contour evidenced by a black continuous line. In particular, we report in the different plots the 1905 earthquake location obtained (b) using all the recording stations available in a radius of 900 km from the epicentral area, that is, all the stations given in plot (a); (c) using all the recording stations available in a radius of 800 km from the epicentral area, that is, excluding the stations enclosed by rectangles in plot (a); (d) using the same recording network as in case (b) but considering only P-wave arrivals; (e) excluding from computation all the stations enclosed by rectangles and circles in (a). (f) Comparison of our 1905 earthquake location of (b) with other offshore locations by Michelini et al. (2006) and Galli and Molin (2009). The location obtained in the present study is given through the 95% and 68% probability contours and the point of maximum probability (star). The dotted ellipse represents the contour of non-nil epicenter probability of Michelini et al.'s location. Finally, the shadowed circle indicates the approximate location of a source capable to fit the tsunami-observed data according to Piatanesi and Tinti (2002) (see Paragraph 4.1 for details).

the 900 km radius was 19, furnishing 19 *P* and 3 *S* readings, respectively. For the earthquake zone and up to epicentral distances of a few hundred kilometers (dashed rectangle in Fig. 4.2a), we used the seismic-velocity model obtained by Neri et al. (2012) by integration of the crustal (Orecchio et al., 2011) and subcrustal (Neri et al., 2009) seismotomographic models of the Tyrrhenian region. We used the ak135 model (Kennett et al., 1995) for the surrounding zones involved by seismic ray traveling to farther stations (Fig. 4.2a). Several hypocenter location attempts have been performed for the 1905 earthquake by varying the network configuration to check the stability of the results. Figure 4.2b–e shows some examples of these tests, performed considering all the data available in the 900 km radius (Fig. 4.2b), the stations in a radius of 800 km (Fig. 4.2c), only *P* readings at all stations (Fig. 4.2d), and a selection of 13 stations (Fig. 4.2e). Considering that the dataset used comes from recordings of the early instrumental epoch (i.e., the station distribution was quite sparse and the quality of recordings clearly not comparable to today's standards), the hypocentral solution of Figure 4.2b–e appears relatively stable and constrained enough for further analysis in the present work. Finally, we applied Bayloc for hypocenter location of local earthquakes recorded in the study area during 1981–2012 with a minimum of 8 *P*+*S* readings. We used the same velocity model already used for the 1905 earthquake location. Figure 4.3a displays the map of stations used for locations. Figure 4.3b and 4.3c shows the Bayloc epicenter map (cumulative map of the individual earthquake probability distributions) obtained, respectively, for the 630 events shallower than 30 km and for the 156 events located between 30 and 70 km depth. A Bayloc hypocenter vertical section along the dip direction of the subducting slab is given in Figure 4.3d. Epicenter and focal depth errors of the order of 2 and 3 km have, on average, been estimated by Bayloc for the events of plate (b) (0–30 km depth), quite similar estimates of 3 and 3 km have been obtained for slightly deeper events of plate (c) (30–70 km depth).

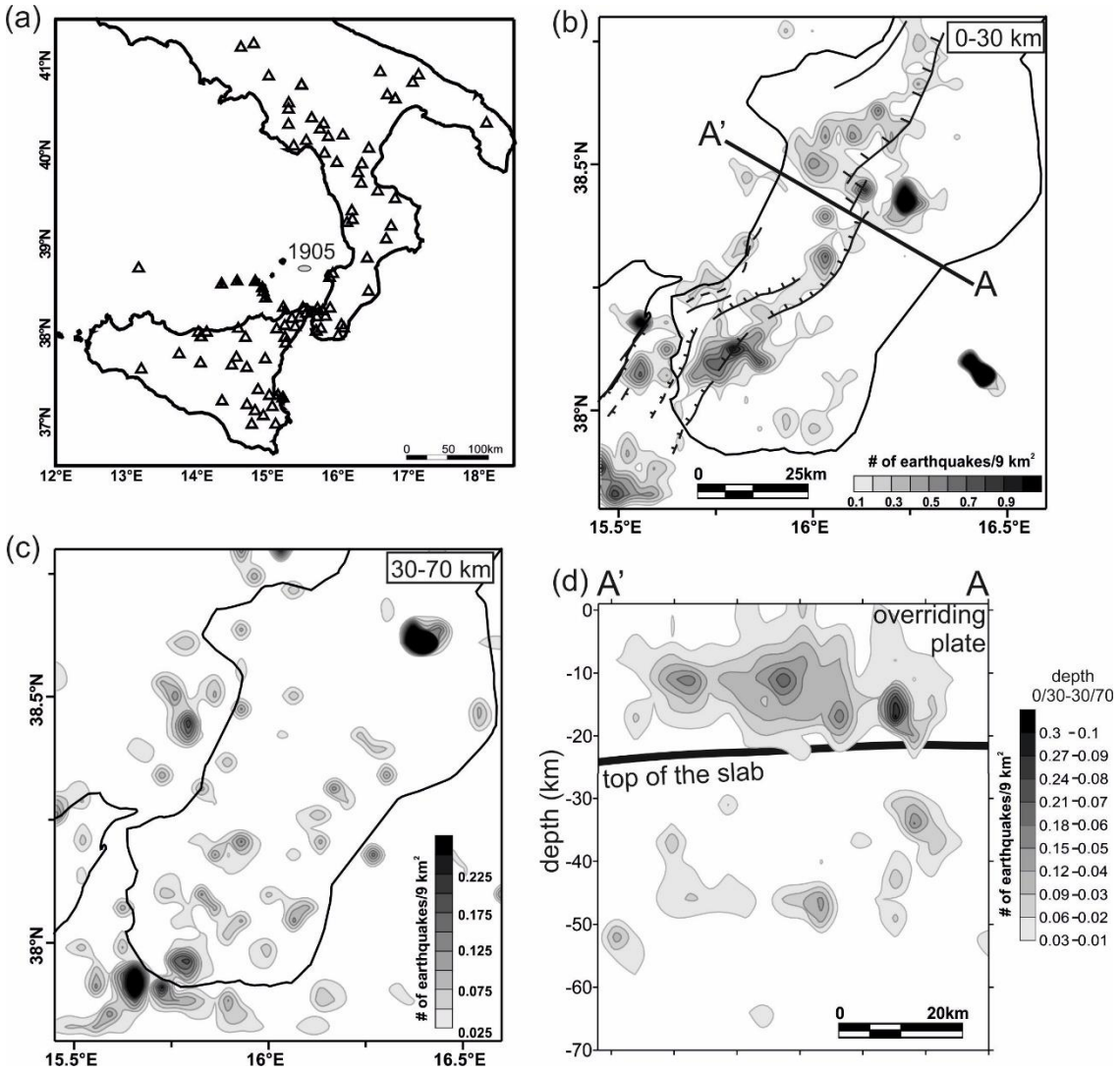

Figure 4.3. **(a)** The map of the stations used for Bayloc hypocenter location of the earthquakes occurred in the study area during 1981– 2012. Here, the 68% probability contour of our location of the 1905 earthquake is also shown. **(b,c)** The epicenter density maps obtained by Bayloc for the earthquakes occurring in the depth ranges 0–30 and 30–70 km, respectively. **(d)** Avertical section of hypocenter density along the dip direction AA′ of the Ionian subducting slab. The structural information reported in (b) is taken from Tortorici et al. (1995) and Monaco et al. (1996). The location of the top of the Ionian slab in (d) is reconstructed on the basis of results from deep seismic sounding (DSS; Cassinis et al., 2005), seismotomographic (Barberi et al., 2004), and receiver function (Piana Agostinetti et al., 2009) analyses, see Paragraph 4.3 and the caption of Figure 4.4 for more details.

4.3 Discussion

Our results highlight that the 1905 earthquake occurred in the Tyrrhenian offshore of Calabria, a few tens of kilometers west of Capo Vaticano, at a depth between 35 and 55 km with a maximum probability at 47 km depth beneath the point of coordinates 38.64° N–15.54° E (Fig. 4.2). In previous works, offshore locations of the event were proposed by Michelini et al. (2006) and Galli and Molin (2009), whereas other investigators (e.g., Rovida et al., 2016) suggested onshore or along-to-coast locations of the earthquake (Fig. 4.1). With the exception of Michelini et al. (2006), who applied the NonLinLoc probabilistic algorithm for analytical location of the event and reported only its epicenter location, all previous investigators reported epicenter estimates made using macroseismic intensity data. We report in the present study the first analytical location of the 1905 earthquake including hypocenter depth. Using the constraints furnished by previous deep seismic sounding (DSS), seismotomographic, and receiver function analyses made in the study area (e.g., Lucente et al., 1999; Barberi et al., 2004; Cassinis et al., 2005; Montuori et al., 2007; Neri et al., 2009; Piana Agostinetti et al., 2009), we may attempt a comparison between our 1905 earthquake hypocenter location and the location of the Ionian subduction slab descending beneath the southern Tyrrhenian tectonic unit. Figure 4.4 displays the top of the Ionian subducting slab constrained between 20 and 30 km depth beneath Calabria according to several authors (Barberi et al., 2004; Cassinis et al., 2005; Piana Agostinetti et al., 2009). Also, the figure shows the nearly vertical northwestern boundary of the descending slab highlighted by sudden transition from high to low velocity resulting from both local earthquake tomography (Neri et al., 2009) and teleseismic data inversion (Lucente et al., 1999; Montuori et al., 2007). Our hypocenter location of the 1905 earthquake falls into the slab, in the upper part of its bending zone. The map view given in the inset of the same figure shows that the earthquake has been located in the

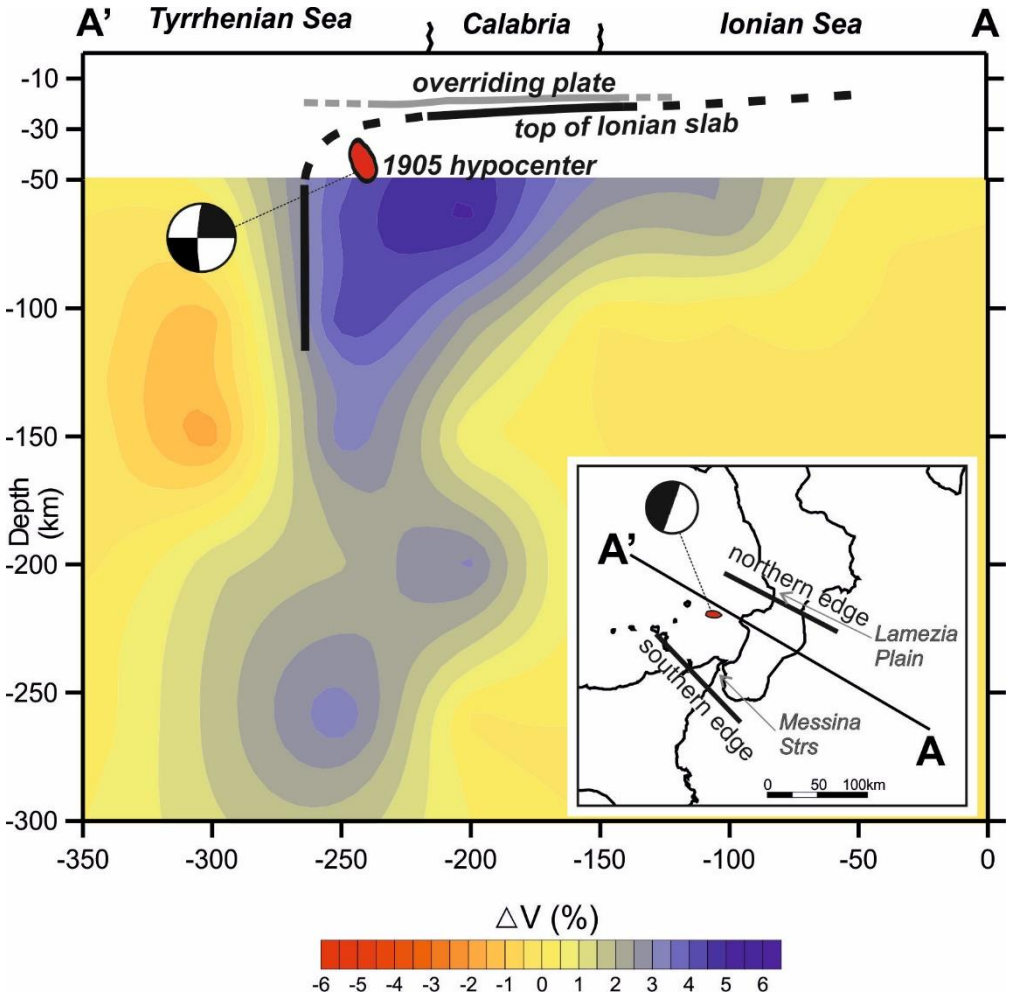

Figure 4.4. Cross-section view of the main tectonic units in the area of the 1905 earthquake. The P-wave velocity structure taken from Neri et al. (2009) is reported in terms of percentage deviation of P velocity from ak135 model (Kennett et al., 1995). The top of the Ionian slab underneath Calabria and the northwestern boundary of it beneath the Tyrrhenian Sea are constrained according to the literature information (Lucente et al., 1999; Barberi et al., 2004, Cassinis et al., 2005; Montuori et al., 2007; Neri et al., 2009; Piana Agostinetti et al., 2009). Also, the gray line indicates the Moho discontinuity along the profile as reported by Cassinis et al. (2005) who also stated that beneath Calabria it represents the bottom of the Tyrrhenian thinned crust overriding the Ionian subduction slab. The 68% probability contour of our Bayloc hypocenter location of 1905 is also displayed. **(Inset)** Map view of the study area with the location of the edges of the Ionian subducting slab (Orecchio et al., 2014; Polonia et al., 2016).

central part of the residual subducting slab, which extends from Messina Straits to Lamezia plain, approximately. Orecchio et al. (2014) proposed a sketch model of the subducting Ionian slab interacting with the overriding Tyrrhenian plate, according to which major normal-faulting earthquake activity occurring in the overriding plate is closely related to shallow deformation of the subducting slab pulled down by gravity in a weak-coupling regime. Coherently with this model, the rupture of the upper part of the bending zone of the slab—if it occurs along a vertical plane oriented parallel to strike of the descending slab (NNE– SSW), with the western side of the descending slab slipping down with respect to the eastern side, may explain our hypocenter location of the 1905 earthquake and other information available in the literature for the same event (Fig. 4.4). In particular, such a rupturing process would agree with the NNE–SSW orientation of the damage area (intensity VII Mercalli–Cancani–Sieberg [MCS] and larger) reported by Galli and Molin (2009), and with the 1905 earthquake focal mechanism computed by Riuscetti and Schick (1975), which appears quite uncertain, however. Also, as explained below, hypocenter location and rupturing process are compatible with the weak tsunami effects observed in correspondence with the earthquake. In their analysis of the earthquake-related tsunami data, Piatanesi and Tinti (2002) found remarkable discrepancies between observations and values expected from sources like the Capo Vaticano (CV), Vibo Valentia (VV) and Lamezia (LA) faults (Fig. 4.1) documented by previous investigators in the earthquake area. Piatanesi and Tinti (2002) concluded their analysis by stating that an eventual subvertical shallow normal-fault striking NE and located 10–20 km west of Capo Vaticano could fit the tsunami data better than the initially tested along-coast known faults. In their source modeling attempts, Piatanesi and Tinti (2002) assumed a magnitude value of 7.0 for the earthquake. It is worth noting that the location of the offshore source hypothesized by these authors is close to the epicenter cloud of our location (Fig. 4.2) while clear difference exists between the source shallow depth assumed by Piatanesi and Tinti

(2002), (between seafloor and 20 km depth), and our hypocenter location between 35 and 55 km depth. Considering that magnitude values around 7.0 have been assigned to the 1905 event on the basis of macroseismic data and assuming its along-coast shallow origin (see, Rovida et al., 2016, among others), and that the event actually occurred at 35–55 km depth about 20 km west of the Capo Vaticano shoreline in the Tyrrhenian offshore of Calabria, higher values of magnitude of the order of 7.5 estimated by instrumental data (see, e.g., Margottini et al., 1993) appear quite more realistic for the 1905 earthquake. An earthquake of this size, occurring at that location with the mechanism described above, may justify the weak tsunami effects observed in correspondence with the earthquake. In fact, by application of the Okada analytical model (Okada, 1992) to the seismic-faulting process and relative location proposed here for the 1905 earthquake, we estimated seafloor coseismic displacements between 20 and −20 cm in the epicentral area. Previous investigators (see, e.g., Tanioka et al., 1995) stated that seafloor coseismic displacements of this order can generate tsunami waves of height of the order of few tens of centimeters (just the values observed for the 1905 tsunami). Therefore, our location and source mechanism of the 1905 earthquake appear to be compatible with the weak tsunami effects observed and documented by Platania (1907). Other eventual hypotheses concerning the earthquake generation mechanism, based on other processes known to occur in subduction zones at the depth we estimated for the 1905 earthquake, appear less convincing. In particular, we refer to (1) overthrusting of the Tyrrhenian overriding plate onto the Ionian subducting lithosphere and (2) perpendiculartо- trench tear imputable to STEP (Subduction-Transform Edge Propagator) fault in the sense introduced by Govers and Wortel (2005). With reference to the overthrusting hypothesis, we have to consider that locally low coupling of plates does not represent the proper environment for that mechanism. Also, the depth of the earthquake should be smaller than estimated in the present work to fit the shallow location of the contact plane between overriding and

subducting plates in the specific area (Fig. 4.4). The STEP hypothesis, too, does not seem appropriate because it contrasts with our analytical location of the earthquake close to the center of the subducting slab front rather than to the slab's lateral edges (Fig. 4.4). Figure 4.3b,c shows the Bayloc epicenter distribution of the recent seismicity (1981–2012) which occurred in the depth ranges 0–30 km (plot b) and 30–70 km (plot c) in the area SE of the 1905 earthquake, including the Messina Straits. For the same events, Figure 4.3d displays a Bayloc hypocenter vertical section along the dip direction of the subducting slab. Plot (c) shows some diffused activity that can be associated with the dynamics of the upper part of the subducting slab; the vertical section of plot (d) reveals that this activity occurs mainly in the 35–55 km depth range where we located the source of the 1905 earthquake. Plot (b) shows the shallow seismicity occurring in Tyrrhenian overriding plate (see also the vertical section of plot d). This seismicity appears to be mainly concentrated in correspondence with the NE-trending normal-fault systems accommodating the motion of the basins (west) with respect to the chain (east) (Monaco et al., 1996). An extensional stress with σ_3 oriented NW–SE was detected in these fault systems by geostructural analyses (Tortorici et al., 1995) and by inversion of earthquake focal mechanisms (Presti et al., 2013; Totaro et al., 2016), as seen in Chapter 3. The seismic activity detected in the upper part of the subducting slab and the shallow one occurring in the NE-trending normal faults of the overriding plate (Fig. 4.3b–d) delineate a picture of recent seismicity compatible with the already mentioned scheme by Orecchio et al. (2014). As reported in Paragraph 4.1, different sources have been hypothesized in the literature for the 1908 earthquake of Messina Straits (e.g., Amoruso et al., 2002; Aloisi et al., 2013; DISS Working Group, 2015). A common feature of these sources is, however, that all of them are characterized by normal faulting according to the main extensional stress regime affecting the shallow internal structure of the Calabrian arc. We computed the coulomb stress change (CSC) produced by the 1905 earthquake on the sources of the 1908

earthquake proposed by Amoruso et al. (2002; AM in Fig. 4.1), Aloisi et al. (2013; AL), and DISS Working Group (2015; DISS). We used the CSC modeling algorithm by Troise et al. (1998), in which the normal and shear stresses are obtained from stress tensor components estimated on a 3D grid through spatial derivatives of displacements associated with the fault dislocation. The analytical formulation introduced by Okada (1992) for rectangular faults embedded within a homogeneous elastic half-space has been used. We parameterized the 1905 source using the above presented model of a NNE-trending vertical plane of rupture with the western side slipping down with respect to the eastern side. For quantification of fault dimensions and mean coseismic slip, we applied the empirical relationships proposed by Wells and Coppersmith (1994) for normal-faulting earthquakes. Figure 4.5a,b shows the CSC values estimated on the three respective 1908 sources by assigning the magnitude values 7.0 (Rovida et al., 2016) and 7.5 (Margottini et al., 1993), respectively, to the 1905 earthquake. The parameterizations of the 1905 and 1908 earthquakes are indicated in the figure caption. The results show positive values of CSC in all cases. Values between 0.01 and 0.04 MPa are found when the magnitude of the 1905 earthquake is fixed to 7.0, and they rise to 0.1–0.4 MPa when the magnitude is put to 7.5. As explained above, magnitude values as large as 7.5 estimated by instrumental data appear more realistic than the value of 7.0 assigned to the event on the basis of macroseismic data and assuming an incorrect onshore or along-coast shallow origin of it (see, e.g., Rovida et al., 2016). Considering that CSC positive values of the order of 0.01 MPa are commonly believed to be able to produce significant effects in promoting seismic source activation (e.g., Toda et al., 1998), we infer that the 1905 earthquake has played a significant role in promoting the Messina Straits earthquake on 28 December 1908.

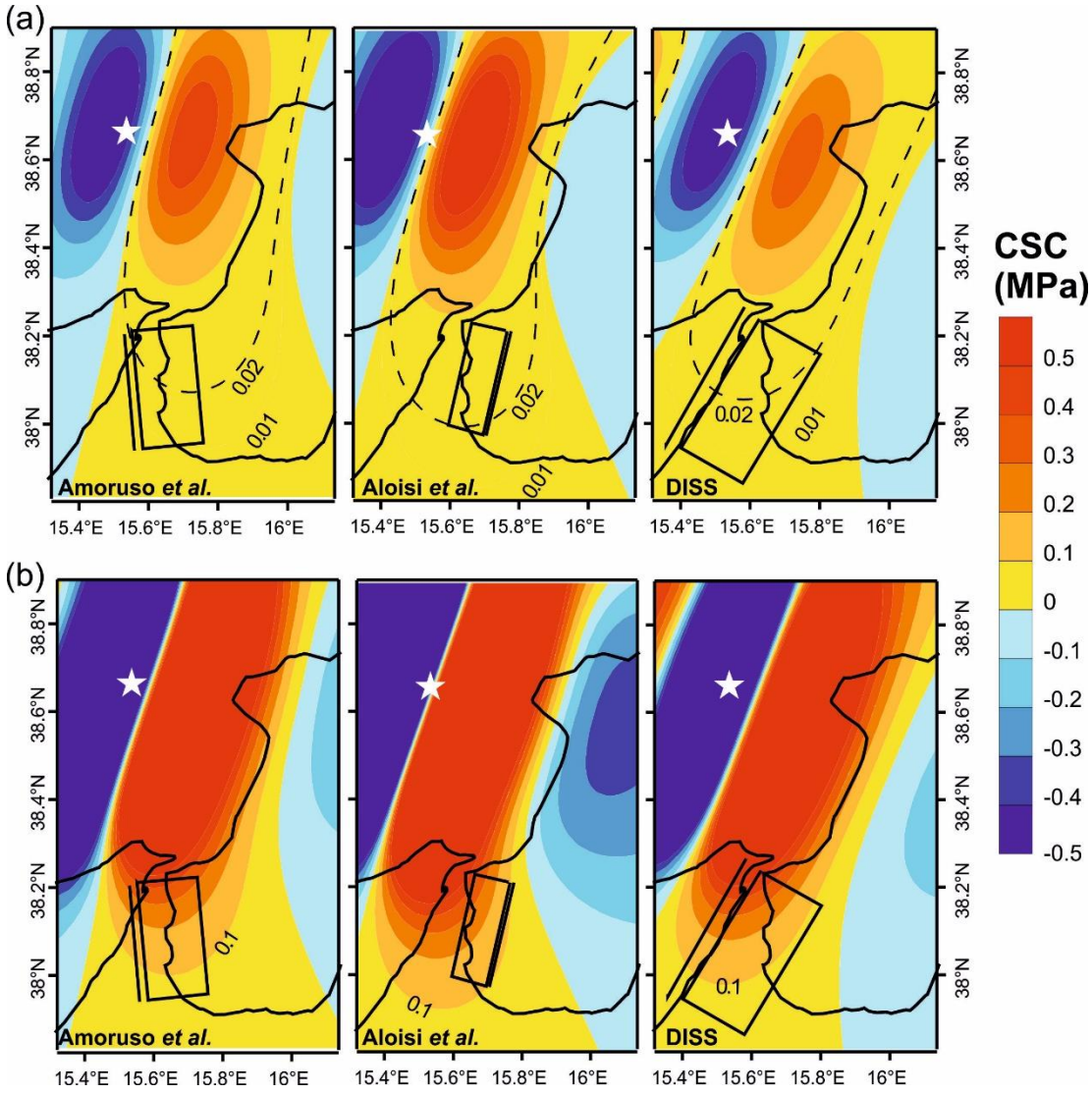

Figure 4.5. Coulomb stress change (CSC) at 10 km depth produced by the 1905 earthquake on three seismogenic sources proposed for the 1908 Messina Straits earthquake (Amoruso et al., 2002; Aloisi et al., 2013; DISS Working Group, 2015). **(a, b)** The results obtained by assigning to the 1905 earthquake magnitude values of 7.0 and 7.5, respectively. The star indicates the Bayloc location of the 1905 earthquake obtained in the present study. According to our reconstruction of the earthquake process described in the text, we assume that the 1905 seismic dislocation occurred on a vertical plane oriented N20°E, that is, parallel to the strike of descending slab. Rectangles and nearby segments represent, respectively, the surface projection of the 1908 sources and the intersection of the source plane with the earth surface. Strike and dip of the respective 1908 sources are −5.5° and 42.4° (Amoruso et al., 2002), −172° and 60° (Aloisi et al., 2013), and 30° and 30° (DISS Working Group, 2015).

4.4 Conclusion

Comparison of our Bayesian hypocentral location of the southern Calabria 1905 earthquake with data from literature concerning the same earthquake and the local structure of crust and upper mantle allows us to intervene in the current debate on location, magnitude, and generation process of this major earthquake by stating that it had a magnitude of the order of 7.5 and originated at 35–55 km depth in the Tyrrhenian offshore of Calabria from rupture of the bending zone of the Ionian subduction slab (Fig. 4.6). According to our reconstruction, rupture may have occurred on a vertical plane parallel to the SSW–NNE-subduction trench orientation, with the most advanced western part of the slab slipping down with respect to the eastern part (Fig. 4.6a). This process can be framed in the widely shared geodynamic model of the study region assuming slow east-southeastward rollback of the Ionian subducting slab pulled by gravity (Malinverno and Ryan, 1986; Faccenna et al., 1996; Wortel and Spakman, 2000; among many others). Gravity pull of the Ionian subducting slab, concurring to the extensional stress detected in the overriding plate where seismogenic fault systems are highlighted by our Bayesian location of recent seismicity, is believed to be the primary factor in the generation of the 1905 earthquake. This earthquake is also shown to have caused CSC positive values on the hypothesized sources of the 1908 earthquake in the Messina Straits area, of the order of 0.01–0.04 or 0.1–0.4 MPa if the 1905 earthquake is assigned a magnitude value of 7.0 (probably incorrect macroseismic estimate) or 7.5 (more realistic instrumental estimate), respectively. Considering that CSC positive values of the order of 0.01 MPa are commonly believed to play a significant role in regard to the activation of seismic sources (see, e.g., Toda et al., 1998), we conclude that the 1905 earthquake has played a significant role in promoting the magnitude 7.1 Messina Straits earthquake on 28 December 1908. In other words, gravity pull of the Ionian subducting slab may have determined the 1905 earthquake rupture at a depth of

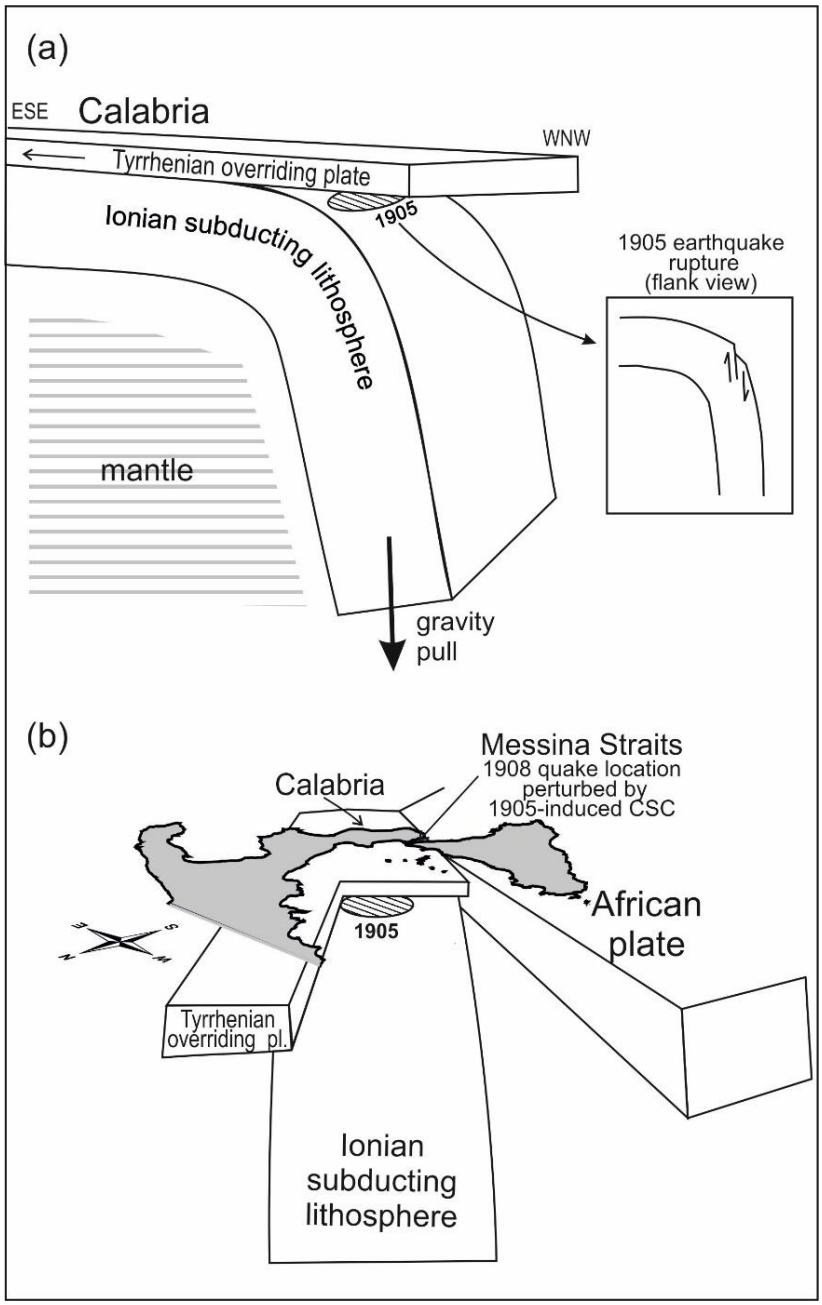

Figure 4.6. Sketch views of the Calabrian arc subduction zone, with location and presumed dislocation process of the 1905 major earthquake. In particular, seismic rupture of the upper subduction slab on a vertical plane perpendicular to the east-southeast–westnorthwest (ESE–WNW) dip direction of the slab **(a)** is proposed to have occurred in a geodynamic scenario controlled by gravity pull of the Ionian subducting slab (Malinverno and Ryan 1986; Faccenna et al., 1996; Wortel and Spakman, 2000; among many others). This 1905 seismic rupture is also proposed to have played a significant role in promoting the other major earthquake occurred a few tens of kilometers south, only three years later, in the Messina Straits compartment of the Tyrrhenian overriding plate **(b)**.

35–55 km in the bending zone of the slab and this rupture has likely perturbed the shallow normal faults of the Tyrrhenian overriding plate in the Messina Straits area (Figs. 4.5 and 4.6) favoring the occurrence of the other major earthquake at very short distance only three years later.

Analyses and results reported in this chapter have been also published by Presti, D., Neri, G., Orecchio, B., Scolaro, S., & Totaro, C. (2017). *The 1905 Calabria, Southern Italy, Earthquake: Hypocenter Location, Causative Process, and Stress Changes Induced in the Area of the 1908 Messina Straits Earthquake*. Bulletin of the Seismological Society of America, 107(6), 2613-2623.

CHAPTER 5

MOMENT TENSOR INVERSION OF THE 1978 FERRUZZANO EARTHQUAKE (SOUTHERN CALABRIA)

5.1 Introduction

As already discussed in the previous chapters, the Calabrian Arc is a high seismic risk area struck by several destructive earthquakes (up to 7-7.5 magnitude) mainly occurred in historical times (Fig. 1.3. Rovida et al., 2016; Tiberti et al., 2017). Despite the large amount of geological and geophysical studies carried out in this area, both the fault geometry of the strongest earthquakes and the relationship between large-scale geodynamics and more localized seismogenic processes is still largely debated (Neri et al., 2004; Galli et al., 2008; Billi et al., 2010; Palano, 2015; Presti et al., 2017; Tiberti et al., 2017).

In this context, the study of moderate-to-major earthquakes (e.g., $M_w \geq 5$), directly related to the regional-scale processes, may be crucial to better characterize regional seismotectonics and seismic hazard. Only a small number of moderate-to-major earthquakes occurred in the Calabrian Arc region in the last ca. thirty years while several $M_w \geq 5$ earthquakes were recorded in the early seismic instrumental periods (see e.g. 1900-1980). This makes very precious every effort aimed to accurately investigate these past earthquakes. In the last decades, the scientific community has become increasingly aware of the importance of recovering historical data and many authors have proven the effectiveness of the use of these kind of data in combination with modern techniques of analysis (Batlló et al., 2008, 2010; Okal and Reymond, 2003; Pino et al., 2008; Stich et al., 2003b, 2005, 2018;

Vannoli et al., 2015, 2016). On this regards, specific projects have been implemented with the aim to collect, recover and store historical seismograms. In particular for the Italian region we may refer to the SISMOS and EuroSeismos Projects (Ferrari and Pino, 2003; Michelini et al., 2005) focused on the digitization of seismogram records and seismic bulletins relative to the period 1895-1984, i.e., from the early age of seismometry to the advent of the digital era (Michelini et al., 2005). The availability of these data furnishes the opportunity to investigate not fully resolved earthquakes of the past by using modern technique of analysis.

In this framework we studied the most recent M_w>5 earthquake included in the SISMOS catalogue for the Calabrian Arc region that is the so called *Ferruzzano* earthquake (Bottari, 1981) occurred in southern Calabria on 1978, March 11th (M_w=5.2, Dziewonski et al., 1987). Contrasting and poorly constrained results have been reported in the literature both concerning hypocenter location and focal mechanism solution of this earthquake (Dziewonski et al., 1987; Gasparini et al.; 1985; Rovida et al., 2016). Moreover, framing of the proposed focal mechanisms in the regional seismotectonic scenario appears quite problematic. For this study we performed a new hypocenter location by means of Bayloc non-linear probabilistic algorithm (Presti et al., 2004 and 2008) and we estimated the focal mechanism solution by using original seismograms mainly obtained from the SISMOS Project and by applying a time-domain waveform inversion analysis properly calibrated for analog seismic data (Stich et al., 2005).

5.2 Seismotectonic framework

The seismic activity of southern Calabria has been characterized by several destructive earthquakes, as clearly shown in Figure 5.1 reporting M_w>5 events occurred from 1000 to 2014 (Rovida et al., 2016). The latest moderate-to-major earthquake is the *Ferruzzano* one

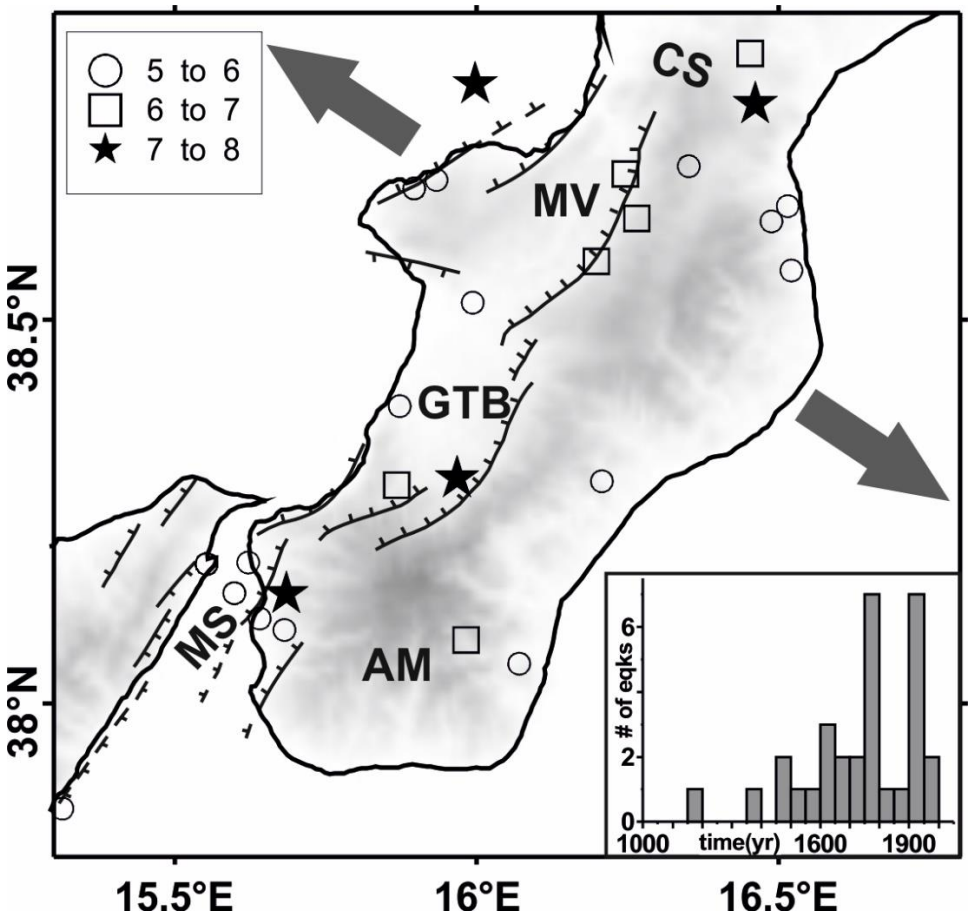

Figure 5.1. Enlarged view of the southern Calabria area showing the main fault system (Monaco and Tortorici, 2000) and the earthquakes of magnitude 5.0 and larger that have occurred after 1000 A.D., according to the CPTI15 catalog (Rovida et al., 2016). MS=Messina Straits, AM=Aspromonte Massif, GTB= Gioia Tauro Basin, MV=Mesima Valley and CS=Catanzaro Straits. The gray divergent arrows indicate the direction of extension according to seismogenic stress field estimation shown in Chapter 3. The **inset** shows the time distribution of earthquakes reported in map (i.e., M≥5 earthquakes occurred after 1000 A.D., from the CPTI15 catalog).

occurred on March 11th, 1978 in the southeasternmost sector of Calabria, while the strongest events (i.e. $M_w \geq 7$) are (i) two events occurred during the seismic sequence of February-March 1783 (Jacques et al., 2001; Tiberti et al., 2017), (ii) the 1905 earthquake (Riuscetti and Shick, 1975; Galli and Molin, 2009; Presti et al., 2017; also see Chapter 4) and (iii) the 1908 Messina Straits earthquake, among the most catastrophic events in Italian history (Billi et al., 2008;

Pino et al., 2009). Despite years of seismotectonic studies, the causative faults of these major earthquakes are still unknown or debated (e.g., Galli et al., 2008; Billi et al., 2010; Tiberti et al., 2017), and this is also due to the lack of coseismic surface faulting (Valensise and Pantosti, 2001; Tiberti et al., 2017). The dominant faulting mechanism, instead is widely shared and indicated as normal faulting (see, e.g., Ghisetti, 1984; Tortorici et al., 1995; Neri et al., 2006; DISS Working Group 2015;); in particular, only normal faulting mechanisms have been proposed for M7 earthquakes in the belt. Normal faults located closely west of the chain are considered to be major seismogenic faults, with particular reference to the NE-trending fault systems of the Messina Straits, Gioia Tauro Basin and Mesima Valley (Fig. 5.1). The structural setting of the central-eastern portion of southern Calabria is less constrained with respect to the eastern one where major earthquakes have been occurred and main structural systems have been deeply investigated. On overall, geostructural data (Tortorici et al., 1995) provided evidence that the fault systems of southern Calabria are mainly subjected to a ca. SE-NW trending extensional regime.

In spite of the strong historical seismicity, a light to moderate seismic activity has been recorded in the southern Calabria region in recent times with no M_w>5 earthquakes in the last thirty years. As already shown in Chapters 2 and 3, a huge effort has been devoted to investigate the kinematics of the region by estimating stable and reliable focal mechanism solutions also for such moderate energy seismicity and the results indicate a dominant normal faulting mechanism in Southern Calabria (D'Amico et al., 2010, 2011; Presti et al., 2013; Totaro et al,. 2016). Moreover, the derived seismogenic stress field (Neri et al., 2005; Presti et al., 2013; Totaro et al,. 2016) clearly shows a relatively uniform extension with a nearly NW-SE orientation of the minimum compressive stress axis (see Chapter 3). An extensive regime has been revealed in southern Calabria also by geodetic data, in particular the strain-rate pattern estimated from the GPS-based velocity field clearly shows a positive areal change with maximum extension in the WNW–ESE

direction (Serpelloni et al., 2010; Palano, 2015; Chiarabba and Palano, 2017).

5.3 The *Ferruzzano* earthquake: previous knowledge

The *Ferruzzano* earthquake occurred in the Aspromonte area on March 11th 1978, 19:20 GMT (Fig. 5.2). According to the Parametric Catalogue of Italian Earthquakes (CPTI15; Rovida et al., 2016) the earthquake has been felt in southern Calabria and northeastern Sicily and it has produced a maximum intensity I_{max}=VIII MCS in the villages of *Ferruzzano*, *Bova*, *Palizzi* and *Roccaforte del Greco* (Fig. 5.2). Studying the macroseismic field, Bottari et al. (1981 and 1990) evidenced that unfavorable geomorphological and/or hydrogeological conditions in the maximum Intensity area have probably caused an increase in intensity from ca. VII to VIII at the four I_{max} sites. Similar conclusions have been also proposed for the 1907 earthquake (October 23th, M_w=6). occurred approximately in the same epicentral area (Baratta, 1907; Sabatini, 1908; Murphy, 1993).

Macroseismic and instrumental location indicates the epicentral area of the 1978 earthquake in the central-eastern portion of the Aspromonte region (Fig. 5.2). The International Seismological Center catalogue (ISC hereafter) reports a focal depth of 26 km and magnitude values of M_s=5 and m_b=5.5. Two quite different focal mechanism solutions are available from the literature. The first one has been obtained by Gasparini et al. (1985) by using ISC location and *P*-onset polarities inversion and it indicates a ca. transpressive mechanism with nodal planes about N-S and E-W oriented (Fig. 5.2). It is widely known that focal mechanisms elaborated by using *P*-wave first motions may be strongly biased by data distribution and uncertainty (e.g., Lay and Wallace, 1995; Pondrelli et al., 2006; Scognamiglio et al., 2009; Presti et al., 2013). Moreover, the hypocenter location

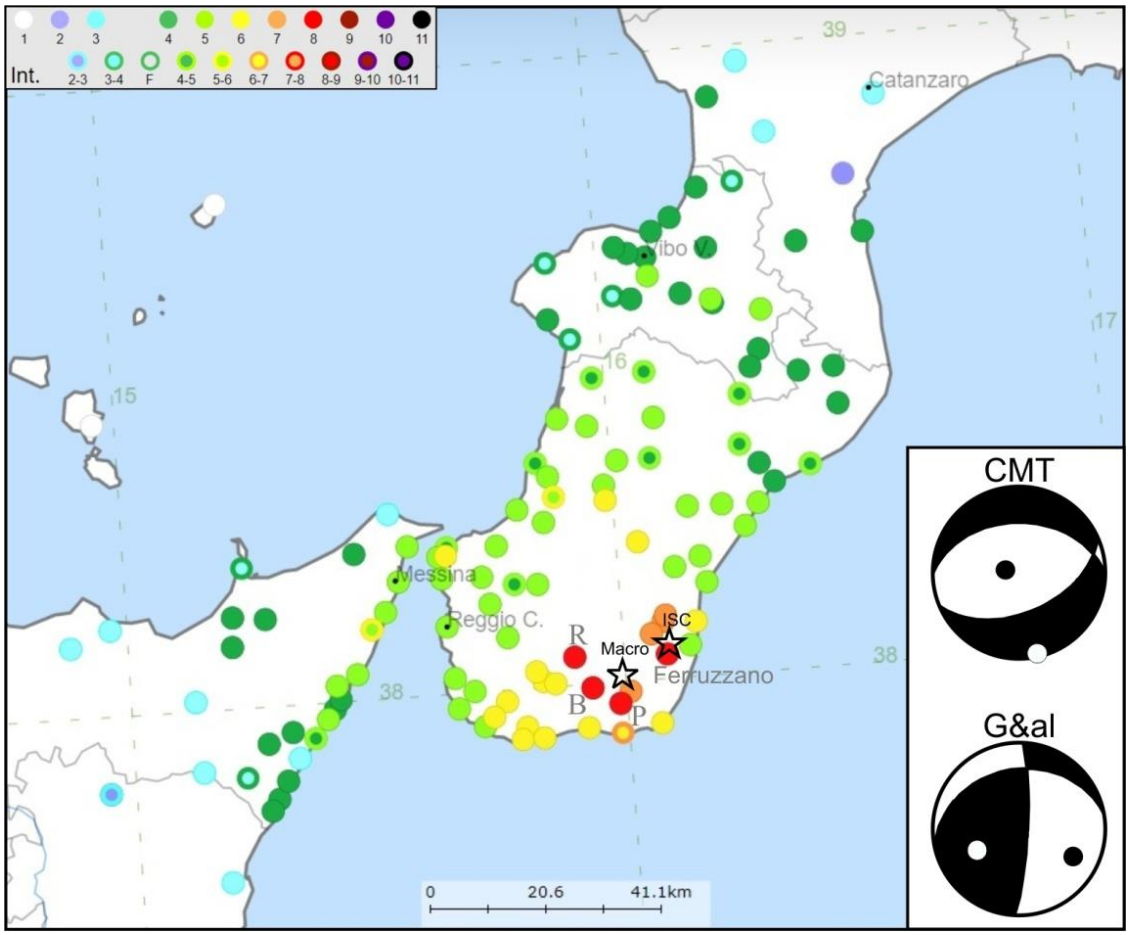

Figure 5.2. Macroseismic intensity map of the 1978 earthquake (taken from the Italian Archive of Historical Earthquake Data) also reporting literature information concerning locations and focal mechanisms of the event. R, B and P stand for *Roccaforte del Greco*, *Bova* and *Palizzi*, respectively. Macro and ISC indicate the macroseismic location of CPTI15 and the instrumental location of the International Seismological Center, respectively. The inset shows the focal mechanism solutions furnished by the Centroid Moment Tensor catalogue, CMT in figure (strike/dip/rake 270°/41°/-72°) and by Gasparini et al.(1985), G&al in figure (strike/dip/rake 259°/31°/164°). In the beach-balls we also displayed the P and T axes (black and white circle, respectively).

uncertainty, with particular reference to the focal depth, may influence the estimation of take-off angles and thus the polarity distribution. Concerning Gasparini et al. (1985) solution the authors have not discussed the reliability of the result but the polarity distribution suggests a quite poorly resolved solution characterized by several discrepancies between observed and predicted polarities. The latter is

the Centroid Moment Tensor solution (Dziewonski et al., 1987) indicating normal faulting on a ca. E-W trending fault plane (Fig. 5.2) and furnishing moment magnitude M_w=5.2 and depth=15 km. CMT computes the moment tensors by inverting mantle waves in the band 125–350 s and body waves in the band 40–125 s recorded at teleseismic distances and, only after 2003, even teleseismic surface waves with period 50–150 s (Hjorleifsdottir and Ekström, 2010). For magnitude less of about 5.5 the amplitudes of mantle waves may be comparable with the noise level for most stations and the CMT solutions of earthquake occurred before 2003 could be constrained only by the body waves. This is the case of the *Ferruzzano* earthquake being the CMT solution obtained by using only body waves from 8 stations.

5.4 Non-linear hypocenter location

Hypocenter location for the 11 March 1978 and relative location error estimate have been performed by the Bayesian non-linear location method Bayloc (Presti et al., 2004 and 2008). Starting from seismic phase arrival times at the recording stations, Bayloc computes for an individual earthquake a probability cloud marking the hypocenter location uncertainty. Also, Bayloc estimates the spatial distribution of probability relative to a set of earthquakes by summing the probability densities of the individual events. This method uses a 3D velocity model and it has shown to furnish more reliable locations and hypocentral errors with respect to standard linearized algorithms, especially in suboptimal network conditions (Presti et al., 2004 and 2008). Moreover, the continuous character of the output quantities is particularly indicated for seismic-network-testing purposes. Further details on methodological aspects of Bayloc can be found in the above quoted papers.

For hypocenter location of the 1978 earthquake the seismic wave arrival times collected from the ISC and from the seismic networks of

Istituto Nazionale di Geofisica e Vulcanologia and Messina and Catania universities (see Neri et al., 2003) have been used. We selected seismic wave arrival times at observatory stations located at distances from the epicentral area not greater than 700 km, approximately (Fig.5.3a). At these distances the flat earth model can still be adopted (see e.g. Lay and Wallace, 1995; Snoke and Lahr, 2001). For the earthquake zone and up to epicentral distances of a few hundred kilometers (gray rectangle in Fig. 5.3a) the 3D seismic velocity model obtained by Neri et al. (2012) through the integration of crustal (Orecchio et al., 2011) and sub-crustal (Neri et al., 2009) seismotomographic models of the Tyrrhenian region has been used. For surrounding zones including seismic ray travelling to farther stations (Fig. 5.3a) the ak-135 model (Kennet et al., 1995) was considered.

The obtained solution indicates that the 1978 earthquake occurred in the Aspromonte area, more than 10 km West of the ISC epicenter location and in better agreement with the macroseismic location, with a maximum probability at depth of 11 km beneath the point of coordinates 38.04° N–15.91° E (Fig.5.3b). Epicenter and focal depth errors of the order of 4 and 5 km, respectively have been estimated.

Several hypocenter location attempts have been performed for earthquake location by varying the network configuration. The hypocentral solutions so obtained appear relatively stable always reporting the epicenter westward with respect to that computed by ISC and with hypocenter depths approximately in the range 10-14 km. To further check the dependence of earthquake location from seismic network geometry, we examine the retrieval of simulated seismic-event distribution with the real seismic network already used (Fig. 5.3a). The synthetic events were positioned at 10 km depth (i.e. approximately the depth of obtained event location) on a two-dimensional grid with spacing of 5 km (Fig. 5.4). For each synthetic event, the arrival times of *P* and *S* waves were estimated at the stations used for locating the 11 March 1978 event. A Gaussian noise with standard deviation of 0.1 and

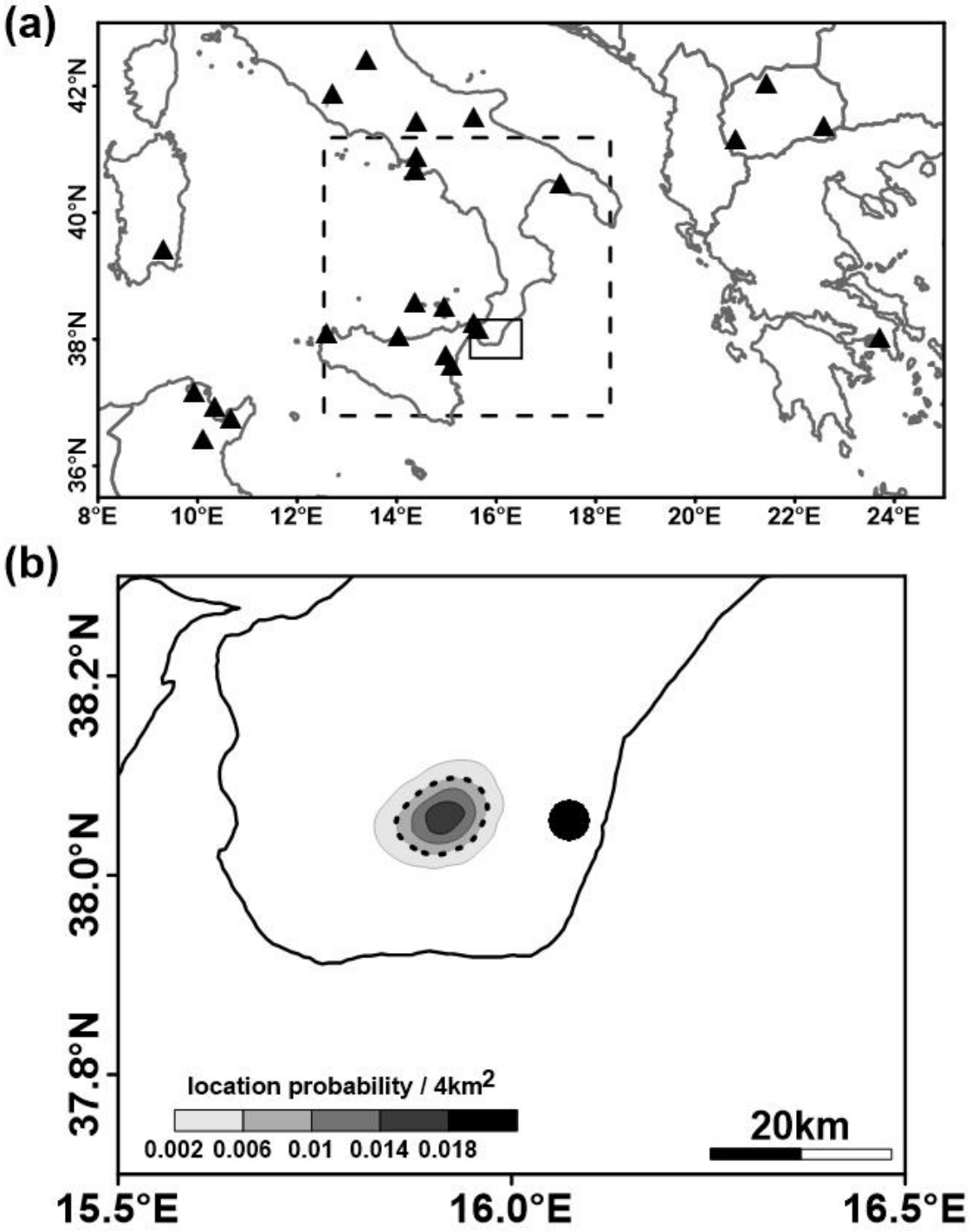

Figure 5.3. (a) Map of the seismic stations used in the present study to locate the 1978 earthquake. For hypocenter location, we adopted the local velocity structure of Neri et al. (2012) inside the dashed rectangular area and the ak135 standard velocity model of Kennett et al. (1995) outside. The black contoured rectangle indicates the epicentral area reported in plot b. **(b)** Results of our Bayesian non-linear hypocenter location reported in terms of location probability per surface unit (4 km^2), with the 68% probability contour evidenced by a black dashed line. The dot indicates the epicentral location reported by the ISC catalogue.

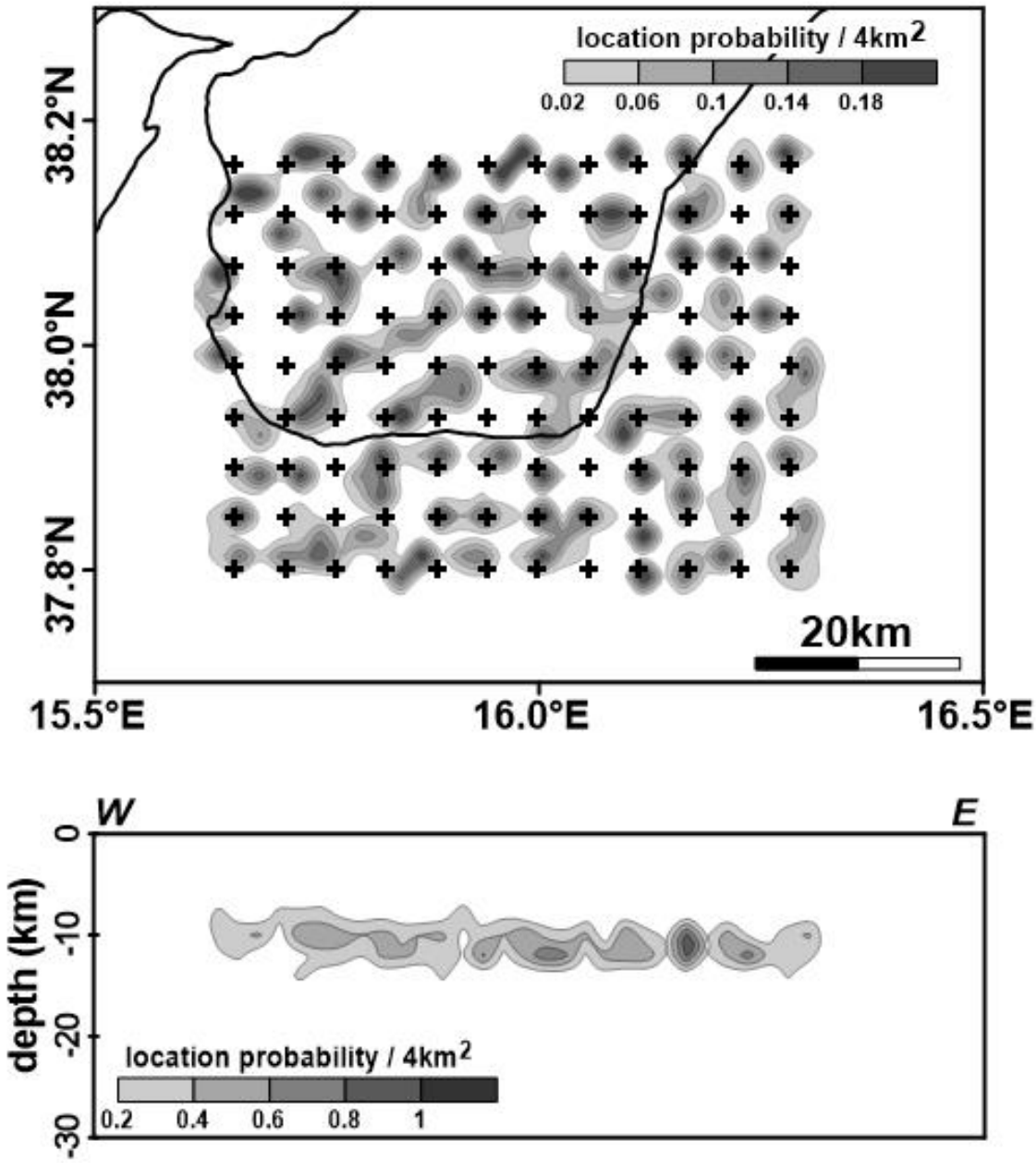

Figure 5.4. Bayloc relocations of synthetic events generated over a two-dimensional grid in the area of 1978 earthquake (see Paragraph 5.4 for details). Crosses in the map **(top)** indicate the starting position of synthetic earthquakes. **Bottom**, W-E vertical section of the relocated hypocenters originally generated at a fixed depth of 10 km.

0.4 s was adopted for perturbation of *P* and *S* wave readings, respectively. In Figure 5.4, we show the results obtained by relocating the simulated earthquakes. The Bayloc relocations of the synthetic events (Fig. 5.4) provided a faithful reproduction of the two-dimensional grid, both in map and in depth so proving that the network configuration does not produce systematic biases in the hypocenter location.

5.5 Moment tensor inversion of digitized seismograms

5.5.1 Data collection

To perform the moment tensor inversion of the 1978 *Ferruzzano* earthquake we collected the original seismograms available from the digital archives of the SISMOS and EuroSeismos Projects. In 2001 the INGV started the SISMOS Project focused on digitization and diffusion of seismogram records and bulletins of the Italian seismic observatories relative to the period 1895-1984, that is approximately from the early age of seismometry to the advent of the digital era (Michelini et al., 2005). The Project was extended, in 2002, to seismograms and bulletins from observatories in 28 countries of the Euro-Mediterranean area in the frame of the EuroSeismos project (Ferrari and Pino, 2003). The use of these kind of data needs of particular care being, for example, necessary to properly know the instrumental characteristics of the recording system in order to reconstruct the analytical form of the transfer function (Kanamori, 1988). In the period covered by the SISMOS and EuroSeismos Projects the seismic observatories could be equipped by different type of seismographs and, often, even a same type of instrument could have a different configuration from one observatory to another, thus implying a different transfer function. The instrument information necessary to process the recordings, that were documented

manually, sometimes are uncertain or missing and this may preclude the use of the related seismic records. Moreover, the main features of old seismographs could lead to low quality data and/or to data affected by intrinsic uncertainties, such as gaps in the waveform due to time-marks and distortions produced by instrumental limit (Crouse and Matuschka, 1983; Cadek, 1987; Herrmann, 1987; Grabrovec and Allegretti, 1994; Schlupp, 1996). Even if since the sixties the development of the Worldwide Standardized Seismograph Network (WWSSN) has led to a progressive improvement of data quality and availability, the recording systems of the Euro-Mediterranean area in 1978 was still affected by some of the above discussed problems. Therefore, the analysis of the 1978 *Ferruzzano* earthquake has required an accurate data selection based on carefully evaluations of each seismogram and of the related instrumental parameters.

To perform moment tensor inversion by using the time-domain technique of Stich et al. (2005) we selected only the original seismograms recorded by long-period seismographs. The period-band used for waveform modeling (20 – 50 s) is above the free period of the sensor where the instrumental amplification quickly decrease (Stich et al., 2003b and 2005). We selected the original seismograms characterized by good quality of the recordings and we recovered instrument response parameters from the original station bulletins and from the literature; only in few cases we used the instrument constants reported for the same station in a close time period. Following this approach we selected 16 seismograms from 10 seismic stations (see Table 5.1 for details on instrumental parameters); in addition to data available from SISMOS and EuroSeismos catalog we also used seismograms of MAL and TOL stations provided by Instituto Geográfico Nacional – Observatorio Geofísico de Toledo. Our dataset mainly consists of waveforms recorded by electromagnetic Sprengnether and Press-Ewing long-period seismographs. For the stations TRI, MAL and TOL the three components of motion are available, for EBR only a single horizontal (N-S) trace and for the remnant stations just the vertical

	Lat (°)	Lon (°)	Instrument	Comp	T_0 S (s)	T_0 G (s)	V	ε	Zeroes	Poles
COP	55.68	12.45	Sprengnether	Z	15	100	1500 *	1.0*	0.0 triple	0.4188±j0.0000 0.0628±j0.0000
EBR	40.82	0.48	Sprengnether	N-S	15	90	1470	0.75	0.0 triple	0.3142±j0.2771 0.0524±j0.0462
IST	41.05	29.00	Sprengnether	Z	15	100	1500	1.0	0.0 triple	0.4188±j0.0000 0.0628±j0.0000
LJU	46.04	14.53	Sprengnether	Z	15*	85*	1300 *	1.0*	0.0 triple	0.4188±j0.0000 0.0739±j0.0000
MAL	36.73	-4.41	Sprengnether	E-W, N-S, Z	15	100	1500	1.0	0.0 triple	0.4188±j0.0000 0.0628±j0.0000
RMP	41.81	12.70	Press-Ewing	Z	15	90	1400	1*	0.0 triple	0.4188±j0.0000 0.0698±j0.0000
SKO	41.97	21.44	Press-Ewing	Z	15*	100*	1500 *	1*	0.0 triple	0.4188±j0.0000 0.0628±j0.0000
TIM	45.75	21.23	Kirnos system	Z	25	1.20	500	0.5 (*sensor*) 8.0 (*galvan.*)	0.0 triple	0.1257±j0.2177 0.3286+j0.0000 83.4474+j0.0000
TOL	39.88	-4.05	Sprengnether	E-W, N-S, Z	15	100	1500	1.0	0.0 triple	0.4188±j0.0000 0.0628±j0.0000
TRI	45.42	13.46	Press-Ewing	E-W, N-S, Z	15	100	3000	1*	0.0 triple	0.4188±j0.0000 0.0628±j0.0000

Table 5.1. Main parameters of the recording stations used in the present study. Columns report: station code, coordinates, type of instrument, recording component (Comp), free period of the electromagnetic sensor (T_0 S) and of the recording galvanometer (T_0 G), magnification (V), damping constant (ε) and the poles and zeroes of the instrument response function we estimated according to Batlló (2004). The asterisk indicates the instrumental parameters we extrapolated from data reported for the same station in a close time period.

traces. Each seismogram has been digitized manually with the software GIMP (GNU Image Manipulation Program) by redrawing the whole traces. Then it has been interpolated and converted to modern seismological format (i.e., SAC) by TESEO2 (Turn the Eldest Seismograms into the Electronic Original ones) a GIMP plug-in made up by INGV (Pintore et al., 2005). Finally, all waveforms have been corrected for geometrical distortions and first arrivals have been accurately verified (see example of Fig. 5.5). Figure 5.6(a) shows the earthquake epicenter location and the network geometry characterized by an azimuthal coverage of about 180° and epicentral distances ranging from ca. 500 to 1970 km.

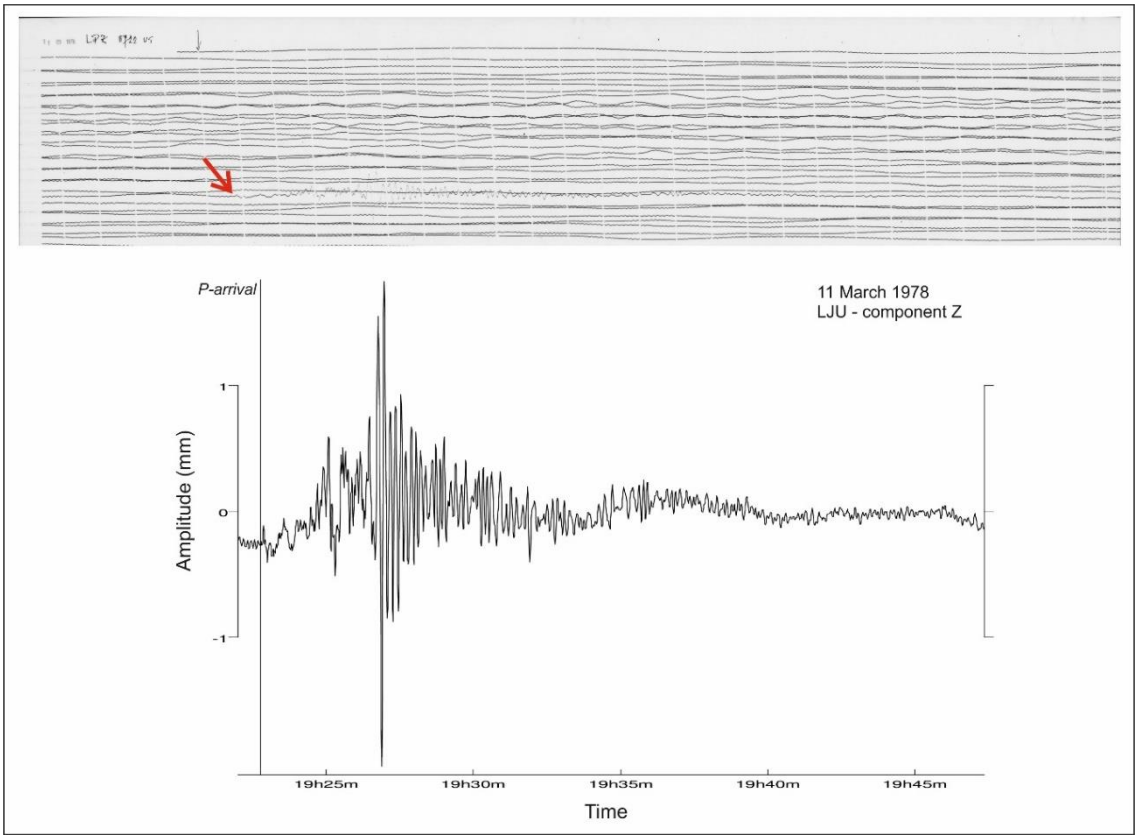

Figure 5.5. (Top) Scanned image of the record of the Z component of the Spregnether seismograph at LJU seismic station for the 11 March 1978 earthquake. The red arrow show the start of the earthquake trace. **(Bottom)** The same trace digitized and corrected for geometrical distorsions.

5.5.2 Waveform inversion

The time-domain waveform inversion technique we used to analyze the *Ferruzzano* earthquake, has been properly calibrated to work with data collected before the advent of the digital era (Stich et al., 2005). In particular this technique processes directly the original historical recording without previous rotation of the horizontal seismograms into radial and transverse components. This approach allows preserving all the available waveforms also including those stations where only one horizontal single-component can be recovered, which is the case of station EBR here. Moreover, by using separately each recording it is possible to reduce the errors due to the misalignment of time signals from component to component, wrong polarities and uncertainty of instrumental parameters. The use of historical seismograms processed in the original sensor orientations requires the appropriate treatment of the theoretical Green's functions. The synthetic waveforms are rotated to match the coordinate reference frames of unrotated recordings and then, processed by convolution to apply the corresponding instrumental response, modelled with poles & zeroes (Scherbaum, 1996; Batlló and Bormann, 2000; Stich et al., 2005; Batlló et al., 2010). To compute the Green's Functions we used a specific 1D velocity model for each ray-path hypocenter-station as derived from the 1-D global model CRUST 2.0 (Bassin et al., 2000). Green's Functions calculated from 2 to 30 km depths (every 2 km) were tried successively to find the best combination of focal mechanism and depth. A band-pass filter from 20 s to 50 s has been applied to both the original digitized and synthetic waveforms. During the inversion procedure we assigned different weight factors to the individual waveforms with the aim to take into account data quality, signal amplitudes and waveform fits and also to evaluate the solution stability.

We report in figure 5.6 the final focal mechanism solution and the observed-versus-synthetic waveform fits. The best solution for the *Ferruzzano* earthquake indicates normal faulting on a ca. N-trending

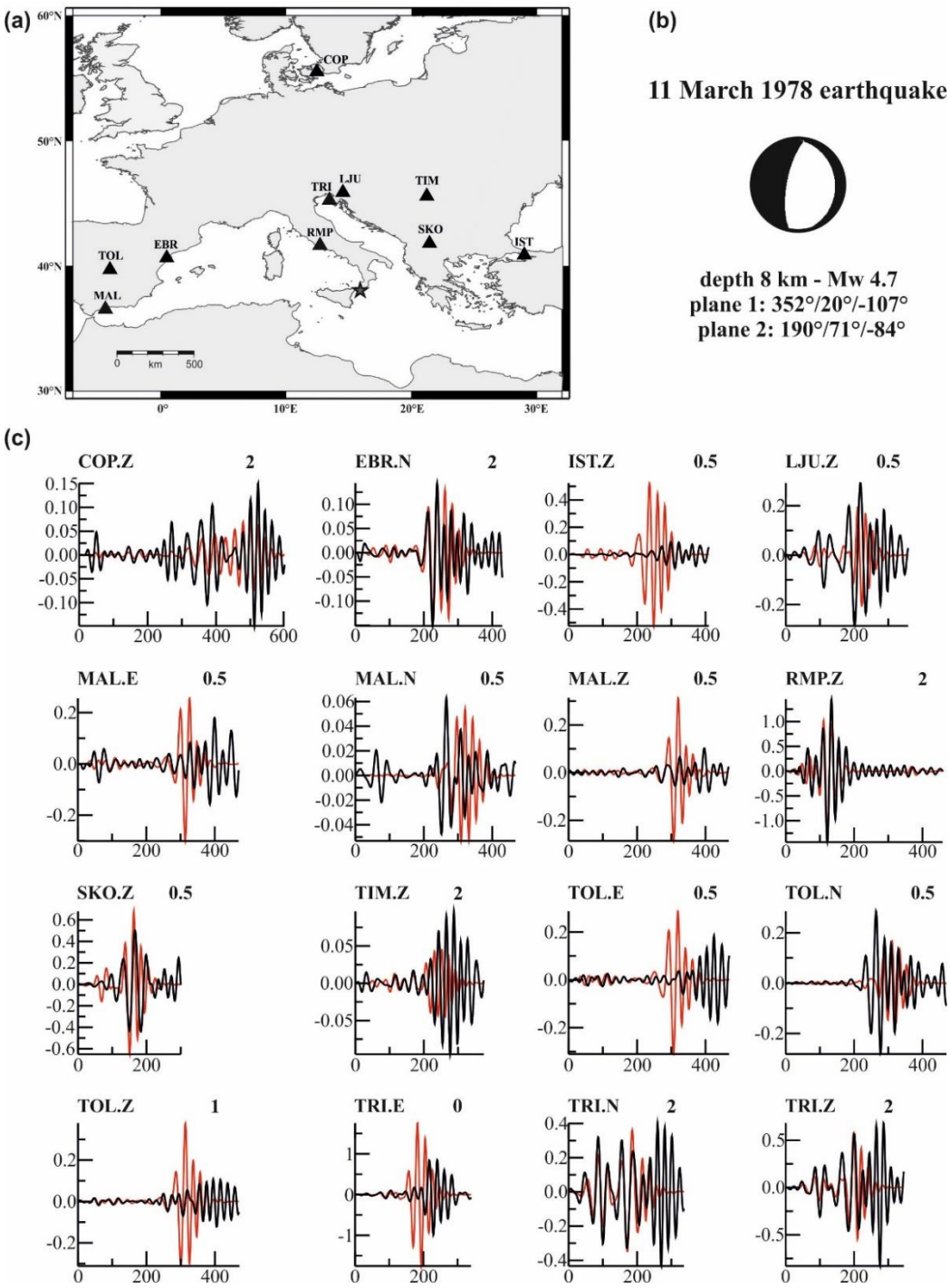

Figure 5.6. **(a)** Map showing epicenter location of the 11 March 1978 earthquake as obtained in this study (grey star) and the seismic stations used for the moment tensor inversion (black triangles). Data relative to MAL and TOL have been furnished by Instituto Geográfico Nacional - Observatorio Geofisico de Toledo the others by the SISMOS database of Istituto Nazionale di Geofisica e Vulcanologia. **(b)** Best focal mechanism solution estimated for 1978 earthquake. **(c)** Waveform fits obtained from the moment tensor inversion, the observed waveforms are indicated by black lines and predicted by red ones. Displacement (y-axis) is in mm and time (x-axis) in s. Above each trace the station code and the weighting factor for inversion are reported. All traces start at the P waves arrival.

plane, strike/dip/rake of 352°/20°/-107° and 190°/71°/-84° for the two nodal planes, with an almost horizontal ESE-trending T-axis (Fig. 5.6b). The best solution is obtained at a depth of 8 km and the resulting moment magnitude is M_w=4.7 (M_0=0.110x1024 Nm). The observed-versus-synthetic fits are quite good being the waveforms reproduced adequately at most stations (Fig. 5.6c). Slightly mismatched phases or small differences in wave amplitudes can be due to crustal structure heterogeneities along the propagation wave paths and to local site effects, respectively. The differences observed at TOL and MAL (components E and Z) seem to indicate a low capability of the sensors to properly recover long wavelength Rayleigh waves, probably as a consequence of the limitations of the instrument sensitivity. The overall level of mismodeling is comparable to other examples of small-magnitude earthquakes recorded at far-regional analog instruments (e.g. Batlló et al., 2010; Stich et al., 2018). The best solution is obtained at a depth of 8 km and the misfit error as function of depth (Fig. 5.7a) shows that the solution is stable around the minimum. By trial and error, several tests have been performed to evaluate the stability of the focal parameters obtained during the inversion procedure. In particular, we slightly changed the weighting factors of the seismograms, the velocity models used for Green's Functions estimate and we tested both different station configurations and epicenter locations. We found that the obtained moment tensor solution, moment magnitude and focal depth are very stable (see few examples reported in Fig. 5.7b). The CLVD component seems more sensitive to variations (values of 8%-20%) suggesting, however, that at long periods the earthquake can be still modeled as a simple faulting source. The use of an average velocity model, instead of a specific model for each ray-path, has furnished a slightly different focal mechanism solution and the greatest misfit value, so showing the relevance of using an accurate input model in the waveform inversion.

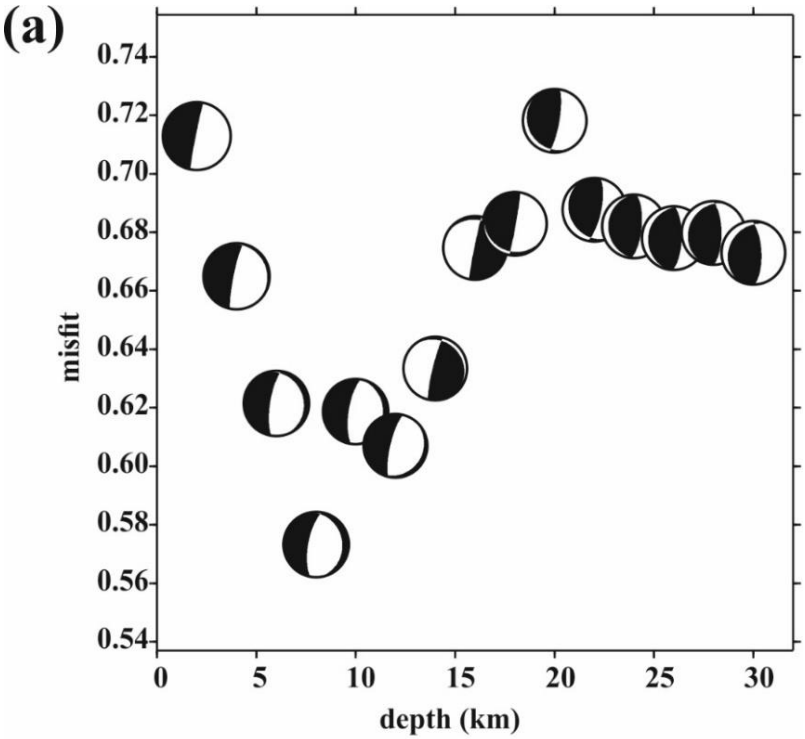

(b)

	**Focal mechanism solution** CLVD 19.8% - misfit 0.57 - depth 8 km 352°/20°/ -107° 190°/71°/ -84°
	**Epicenter location ISC** CLVD 13.5% - misfit 0.61- depth 8 km 356°/ 19°/ 256° 190°/ 71°/ -85°
	**Stations used** **RMP-TRI-LJU-COP-TIM-SKO-IST** CLVD 12.3% - misfit 0.57 - depth 8 km 350°/23°/-106° 188°/68°/-83°
	**Stations used** **TOL-MAL-EBR-RMP-TRI-LJU-COP** CLVD 10.9% - misfit 0.55 - depth 8 km 358°/17°/-98° 187°/73°/-87°
	**Stations used** **EBR-RMP-TRI-LJU-COP-TIM** CLVD 8.6% - misfit 0.50 - depth 8 km 358°/18°/-98° 186°/72°/-87°
	**Average velocity model** CLVD 10.1% - misfit 0.76 - depth 4 km 342°/48°/-106° 185°/44°/-73°

Figure 5.7. (a) Misfit error as function of depth. The distribution shows the stability of the solution around the minimum. **(b)** Results of tests performed by changing the epicenter location, the station configurations (also using unfavorable conditions) and the velocity model used for Green's Function computation.

5.6 Results and discussion

The hypocenter location we obtained by using the probabilistic non-linear algorithm Bayloc, indicates that the 1978 *Ferruzzano* earthquake occurred approximately in the central-eastern area of the Aspromonte massif. The epicenter is located more than 10 km west of ISC instrumental location and closer to the macroseismic one, the hypocenter is about 11 km deep, significantly shallower than previous ISC location (i.e., 26 km depth). The tests we performed indicate that the obtained solution is well constrained without showing relevant biases due to network geometry. Epicentral and focal depth errors are of the order of 4 and 5 km, respectively.

The moment tensor solution for the 1978 earthquake has been obtained by using a time domain algorithm (Stich et al., 2005) already successfully applied to seismic events occurred before the recording period of modern digital seismometers (see e.g., Batlló et al., 2008 and 2010; Stich et al., 2018). The estimated focal mechanism solution indicates normal faulting on a ca. N-S oriented fault plane and it is characterized by an almost horizontal ESE-trending T-axis. We highlight that, in contrast with the focal mechanism solutions previously proposed in the literature (Gasparini et al., 1985; Dziewonski et al., 1987), our result is better framed in the local extensional domain. This is clearly shown by the comparison of T-axis orientations with the extensional directions proposed for southern Calabria by seismologic, geodetic and geologic data (see Fig. 5.8a). The local geology of the central-eastern portion of southern Calabria is quite debated and different structural settings have been proposed in the literature (see e.g., Ciaranfi et al., 1983; Ghisetti, 1984; Ghisetti and Vezzani, 1981; Van Dijk, 1992). In this framework we cannot uniquely identify a causative fault system but also taking into account these limitations, we highlight the good agreement between our solutions and the structural settings proposed by Ghisetti and Vezzani (1981). In particular the fault plane orientation depicted by our moment tensor

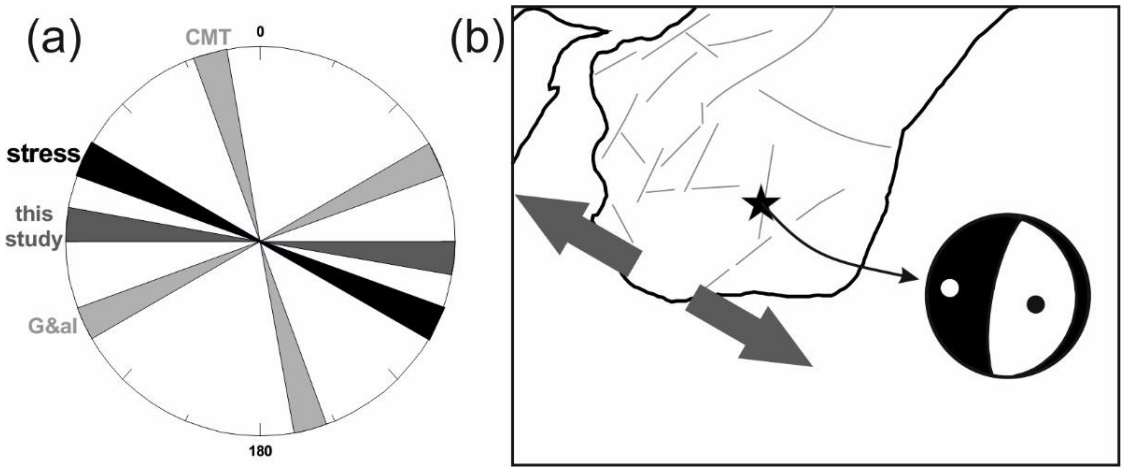

Figure 5.8. (a) Rose diagram reporting: in black the σ_3 orientation of the local seismogenic stress field (from Totaro et al., 2016), in dark-gray the T-axis orientations relative to our moment tensor solution (this study), and in light-gray the T-axis orientations relative to the Centroid Moment Tensor (CMT) and Gasparini et al.'s (G&al) solutions. It clearly appears that the result obtained in this study is more coherent with the local seismogenic stress field with respect to the previous available solutions. **(b)** Hypocenter location and focal mechanism solution (with P and T axes) obtained in this study have been reported on the map view of principal structures proposed by Ghisetti and Vezzani (1981). The gray divergent arrows indicate the direction of extension according to seismogenic stress field estimation shown in Chapter.

solution matches very well with the N- to NE-trending lineaments reported by Ghisetti and Vezzani (1981) near the Bayloc epicenter location of the 1978 earthquake (see Fig. 5.8b).

The best focal mechanism solution also indicates a focal depth of 8 km, compatible with the Bayloc hypocenter depth (11 km), and a moment magnitude M_w=4.7, lower than M_w=5.2 reported by the CMT catalogue. The waveform fits obtained by the CMT inversion are not available (Dziewonski et al. 1987, CMT website) and then it is not possible to compare the quality of solution. We suggest that this difference could be mainly related to the characteristics of the algorithms, the local structure complexities and the different station distributions. In the last years several studies have been performed to compare CMT source parameters with data coming from other moment tensor catalogs (Gasperini et al., 2012; Hjörleifsdóttir and Ekström,

2010; Konstantinou and Rontogianni, 2011). These authors highlighted, in particular, that the CMT algorithm tends to overestimate seismic moment for earthquakes with M_w<5.0-5.5 occurred before 2003, that is when only the body waves were used for the CMT inversion. Moreover, Hjörleifsdóttir and Ekström (2010) have shown that such overestimate is influenced by local structural setting being more relevant for earthquakes located in a crust thicker than average. This is just the case of the 1978 earthquake located in a region where crustal doubling due to presence of the Ionian subducting slab is testified by seismic tomography results (Di Stefano et al., 2011; Orecchio et al., 2011). These observations may explain the greater magnitude estimate furnished by the CMT analysis with respect to our estimate of M_w 4.7. On this regards, we remark that the *Ferruzzano* earthquake represents one of the smallest earthquakes analyzed through moment tensor inversion of digitized seismograms (Batlló et al., 2010).

5.7 Conclusions

We studied the 1978 *Ferruzzano* earthquake, that is the most recent moderate-to-major earthquake occurred in the southern Calabria area, by using old analog data and modern inversion techniques. Non-linear earthquake location and waveform inversion of digitized data have allowed us to define new hypocenter location and focal mechanism solution and also to re-assess moment magnitude estimate of the 1978 earthquake. In particular we located the *Ferruzzano* earthquake in the central-eastern portion of the Aspromonte Massif and at shallower depth with respect to previous instrumental location. Normal faulting on ca. N-S oriented fault plane obtained by the time-domain moment tensor inversion well agrees both with the extensional domain defined by seismogenic stress and geodetic strain and with the structural settings proposed by Ghisetti and Vezzani (1981). Waveform inversion

have also furnished a moment magnitude of 4.7 quite lower than the previously available estimate of 5.2 coming from the CMT catalog. According to recent studies (Gasperini et al., 2012; Hjörleifsdóttir and Ekström, 2010; Konstantinou and Rontogianni, 2011) we ascribed this overestimate to technical limits of the old CMT approach combined with local structural complexity.

In addition to the intrinsic interest in this earthquake, the 1978 event can be considered a test-case to proof that digitized seismograms may be successfully used to study also relatively small earthquakes (i.e., M_w<5) of the past. We have shown as the use of modern algorithms in combination with data collected from relatively old instruments may allow to re-evaluate moderate-to-strong earthquakes occurred before the diffusion of modern digital broadband instruments. The good results obtained encourage the use of this approach also to more ancient earthquakes aiming to improve seismotectonics and seismic hazard evaluations in regions of minor recent seismicity.

Analyses and results reported in this chapter have been also reported in the paper by Orecchio, B., Scolaro, S., Batlló J., Ferrari G., Presti D. & D. Stich. *Moment tensor inversion of the 1978 Ferruzzano earthquake (southern Calabria, Italy)*. Submitted to Physics of the Earth and Planetary Interiors

CONCLUSIONS

The results shown in this thesis have furnished a more detailed picture of the kinematics and deformation processes occurring in the Calabrian Arc region and have also contributed to the improvement of knowledge concerning the main geodynamic engines acting in this very complex area. These goals have been reached by increasing the number and quality of focal mechanism solutions available for the Calabrian Arc region, by using them to evaluate the seismogenic stress fields and by studying with high-quality modern algorithms two moderate-to-strong events of the past. In addition to the intrinsic interest in the results concerning local and regional seismotectonics, this analysis have also provided some relevant methodological results: (i) a careful evaluation of the waveform inversion algorithm *Cut And Paste*, capable to estimate high-quality focal mechanism solutions also for relatively low-magnitude earthquakes (i.e., Mw>2.5) and (ii) a first application in Italy of the time-domain inversion algorithm of Stich et al. (2005), properly calibrated to analyze the waveforms of earthquakes occurred before the advent of the digital era (i.e., ca. 1900-1980).

The capability of *Cut And Paste* to furnish high-quality and reliable focal mechanism solutions even for earthquakes over a wide range of magnitude (down to a minimum of ca. 2.5) and not included in official catalogs has been proven by several analyses and tests. In addition, a new procedure for estimating fault parameter errors has been proposed and its application has allowed to evaluate an error range of the order of 8°-10° for the CAP solutions. Thanks to these estimates we were able to compile a new focal mechanism database of earthquakes occurred in Southern Italy between 1977 and 2015; in particular, it was built by integrating 292 mechanisms selected from literature and catalogs with 146 newly computed high-quality solutions.

The new database has been used for computation of posterior density distributions of stress tensor components by the Bayesian method of Arnold and Townend (2007). The application of this method to the enhanced database has allowed to well constrain tectonic domains of Calabrian Arc and to depict the stress patterns along the Appennine-Maghrebian chain and in Ionian offshore area, a sector not adequately investigate to date. The analysis highlighted a complex stress pattern mainly characterized by perpendicular-to-chain extensional processes along the whole chain and compressional effects of Africa-Eurasia convergence in the Tyrrhenian and Ionian offshores. The NW-SE extension along the Calabrian Arc jointly with earthquake spatial distribution in the Ionian offshore of the Arc has been related to southeastward retreat of the Ionian subducting slab.

The complex description of the regional geodynamics of the Calabrian Arc is affected by the low number, in recent times, of moderate-to-strong earthquakes (i.e., magnitude greater than 5) able to provide direct information on regional tectonic processes. On the other hand, the seismic activity shows the presence throughout the Italian territory of a considerable number of magnitude greater than 5 earthquakes occurred in the early stages of the seismological instrument era (e.g. 1900-1980); quantitative investigations of these events can provide invaluable data useful to obtain information actually not available from recent seismicity. On this regards, the studies carried out in this thesis have also focused on the re-evaluation of two events occurred in the Calabrian Arc area: the 8 September 1905 southern Calabrian earthquake, one of the most energetic event (M_w=7.0) occurred in Italy and the 11 March 1978 *Ferruzzano* earthquake, the most recent M_w>5 event of southern Calabria according to the official catalogs (Rovida et al., 2016).

The Bayloc seismic location method, by Presti et al. (2004, 2008), has been applied for the nonlinear hypocenter location of the 1905 earthquake for which very different views exist concerning location, magnitude, and causative process. The obtained offshore, 35–55 km

deep location of the event, jointly with an accurate evaluation of literature information about the same earthquake and the local structure of crust and upper mantle, led us to suggest that the earthquake may have been generated by rupture of the bending zone of the Ionian subduction slab with a seismic event magnitude as large as 7.5. By computation of the Coulomb Stress Change produced around the source by this earthquake, we found that it may have played a significant role in the generation of the magnitude 7.1 earthquake which struck the Messina Straits area, a few tens of kilometers south, only three years later (December 1908). The 1905 seismic dislocation occurring in the most arcuate part of the pulled-by-gravity descending slab has been then proposed to have caused the 1908 earthquake by inducing positive changes of Coulomb Stress of the order of 0.1–0.4 MPa on the shallow normal faults of the overriding plate in the Messina Straits area.

The few information available from the literature on the 1978 *Ferruzzano* earthquake is quite contrasting and not well framed in the regional seismotectonic scenario. We then decided to better study it by means of modern algorithms and original analog data. The original bulletin data and Bayloc location technique have been used to estimate a new hypocentral location. For focal mechanism evaluation the analog seismograms coming from several stations distributed in the Euro-Mediterranean region have been digitized and processed, and for the first time in Italy the time-domain waveform inversion method of Stich et al. (2005) has been applied. Several inversion tests have been performed to verify the quality and stability of both hypocenter location and moment tensor solution. Obtained results are quite different with respect to previous available knowledge furnished by official catalogs. More specifically, the resulting hypocenter is located at about 11 km depth in the central-eastern portion of the Aspromonte Massif and the waveform inversion have furnished a very stable focal mechanism solution indicating normal faulting on ca. N-S trending fault plane, in good agreement with seismic and geologic data available for the region.

The estimated moment magnitude is 4.7, thus suggesting an overestimate of the previous solutions probably due to algorithm and data limits, as already discussed in Chapter 5. This study casts new light on the 1978 Ferruzzano earthquake allowing to better frame it in the local seismotectonic scenario. Moreover, it has been proven that the time-domain waveform inversion algorithm applied to digitized old seismograms is capable to successfully invert also light-to-moderate earthquakes (i.e., Mw<5) of the past. The obtained results pave the way for new analyses of the early instrumental seismicity, not yet fully known and potentially capable to furnish very precious constraints to local and regional seismotectonic modeling.

In conclusion, the analyses here presented have significantly improved the number and the quality of seismological data available for the study region, allowing to highlight new features of the present-day kinematics and to furnish new constraints to current investigations of seismotectonics and seismic hazard in Southern Italy. The application of CAP algorithm allowed to expand the focal mechanism database of the Calabrian area down to a minimum of magnitude 2.6, so improving the kinematic reconstruction of the area and also the detection of stress field variations. The resulting dataset represents an important deliverable for the scientific community because it will furnish basic information for better understanding local and regional tectonic processes. In addition, the new results obtained from the study of historical earthquakes have proven the value of the preservation of historical seismic data and the capability of modern techniques to properly analyze them. On these grounds, several investigations should be carried out to analyze other Italian earthquakes of the early XX century and to complete the dataset of the moment tensors also including the strongest earthquakes (M_w>5) occurred in southern Italy in the early instrumental ages.

REFERENCES

Aloisi, M., V. Bruno, F. Cannavò, L. Ferranti, M. Mattia, C. Monaco, M. Palano (2013). Are the source models of the M 7.1 1908 Messin Straits earthquake reliable? Insights from a novel inversion and sensitivity analysis of levelling data. *Geophys. J. Int.* 192, no. 3, 1025–1041, doi: 10.1093/gji/ggs062.

Amoruso, A., L. Crescentini, R. Scarpa (2002). Source parameters of th 1908 Messina Straits, Italy, earthquake from geodetic and seismic data. *J. Geophys. Res.* 107, no. B4, doi: 10.1029/2001JB000434.

Amoruso, A., Crescentini, L., Neri, G., Orecchio, B., Scarpa, R. (2006). Spatial relation between the 1908 Messina Straits earthquake slip and recent earthquake distribution. *Geophys. Res. Lett.* 33. http://dx.doi.org/10.1029/2006GL027227.

Anderson, H., T. Webb, J. Jackson (1993), Focal mechanisms of large earthquakes in the south-island of New Zealand—Implications for the accommodation of Pacific-Australia plate motion. *Geophys. J. Int.* 115, 1032–1054, doi:10.1111/j.1365-246X.1993.tb01508.x.

Argnani, A. (2000). The Southern Tyrrhenian subduction system: recent evolution and neotectonic implications. *Ann. Geophys.*, 43, 3.

Argnani A. (2009) - Evolution of the southern Tyrrhenian slab tear and active tectonics along the western edge of the Tyrrhenian subducted slab. In: "Collision and collapse at the Africa-Arabia-Eurasia subduction zone" Edited by: Van Hinsbergen D.J.J., Edwards M. A., Grovers R., *Geol. Soc. Spec. Publ.*, 311, Pages: 193-212.

Arnold, R., and J. Townend (2007). A Bayesian approach to estimating tectonic stress from seismological data. *Geophys. J. Int.*, 170, 1336–1356.

Baratta, M. (1907). Il nuovo massimo sismico calabrese (23 ottobre 1907), *Boll. Soc. Geol. It.*, XIII, 1259-1264.

Baratta, M. (1910). La catastrofe sismica Calabro messinese (28 dicembre 1908). Società geografica italiana.

Barberi, G., Cosentino, M.T., Gervasi, A., Guerra, I., Neri, G., Orecchio, B. (2004). Crustal seismic tomography in the Calabrian Arc region, south Italy. *Phys. Earth Planet. In.* 147, 297–314.

Barchi, M., A. Amato, G. Cippitelli, S. Merlini, and P. Montone (2007). Extensional tectonics and seismicity in the axial zone of the Southern Apennines, in Results of the CROP Project, Sub-Project CROP 04 Southern Apeninnes, Ital. J. Geosci., vol. 7, edited by A. Mazzotti, E. Patacca, and P. Scandone, pp. 47–56, *Boll. Soc. Geol. It.*, Italy.

Bassin, C., G. Laske, and G. Masters (2000). The current limits of resolution for surface wave tomography in North America, *Eos Trans.*, AGU, F897, 81.

Batlló, J. and P. Bormann (2000). A catalog of old Spanish seismographs, *Seismol. Res. Lett.*, 71: 570–582.

Batlló, J. (2004). Catálogo – Inventario de Sismógrafos Antiguos Españoles, pp. 414, Instituto Geográfico Nacional, Madrid.

Batlló, J., D., Stich B., Palombo R., Macia, Morales, J. (2008). The 1951 Mw 5.2 and Mw 5.3 Jaén, Southern Spain, earthquake doublet revisited, *B. Seismol. Soc. Am.*, 98(3), 1535-1545.

Batlló, J., D. Stich, R. Macià, Morales, J. (2010). Moment tensor inversion for the 5 July 1930 Montilla earthquake (southern Spain). *Seismol. Res. Lett.*, 81(5), 724-731.

Bevington, P. R., and Robinson, D. K. (2003). Chapter 3, Error analysis. Data reduction and error analysis for the physical sciences, 36-49.

Billi, A., Presti, D., Faccenna, C., Neri, G., Orecchio, B. (2007), Seismotectonics of the Nubia plate compressive margin in the south-Tyrrhenian region, Italy: Clues for subduction inception, *J. Geophys. Res.*, 112, B08302, doi:10.1029/2006JB004837.

Billi, A., Funiciello, R., Minelli, L., Faccenna, C., Neri, G., Orecchio, B., Presti, D. (2008). On the cause of the 1908 Messina tsunami, southern Italy. *Geophys. Res. Lett.*, 35(6)

Billi, A., Minelli, L., Orecchio, B., Presti, D. (2010). Constraints to the cause of three historica tsunamis (1908, 1783, and 1693) in the Messina Straits region, Sicily, souther Italy. *Seismol. Res. Lett.* 81, 907–915.

Billi, A., C. Faccenna, O. Bellier, L. Minelli, G. Neri, C. Piromallo, D. Presti, D. Scrocca, Serpelloni, E. (2011). Recent tectonic reorganization of the Nubia–Eurasia convergent boundary heading for the closure of the western Mediterranean. *Bull. Soc. Géol. Fr.*, 182, 279–303.

Bottari, A., Lo Giudice, E., Nicoletti, P.G., Sorriso Valvo, M. (1981). The Ferruzzano earthquake of 1978: macroseismic effects and slope stability conditions in southern Calabria (Italy). *Rev. Geol. Dyn. Geogr.*, 23 (1), 7384.

Bottari, A., Pietrafesa, M., and E. Stillitani (1990). Sull'attenuazione dell'intensità macrosismica nella regione dell'Arco Calabro-Peloritano, Atti del Convegno del GNDT, 1, 1-13.

Brandmayr, E., Romanelli, F., Panza, G.F. (2013). Stability of fault plane solutions for the major N Italy seismic events in 2012. *Tectonophysics* 608:525–529

Burrato, P. and G. Valensise (2008). Rise and Fall of a Hypothesized Seismic Gap: Source Complexity in the M w 7.0 16 December 1857 Southern Italy Earthquake. *B. Seismol. Soc. Am.*, 98(1), 139-148.

Cadek, O. (1987). Studying earthquake ground motion in Prague from Wiechert seismograph records. *Gerl. Beitr. Geoph.*, 96, 438–447.

Carminati, E.,Wortel, R., Spakman,W., Sabadini, R. (1998). The role of slab-detachment processes in the opening of the western-central Mediterranean basins: some geological and geophysical evidence. *Earth Planet. Sc. Lett.* 160, 651–665.

Cassinis, R., Scarascia, S., and A. Lozej (2005). Review of seismic wideangl reflection-refraction (WARR) results in the Italian region (1956–1987), in *CROP PROJECT*: Deep Seismic Exploration of the Central Mediterranean and Italy, , 31–55.

Catalano, R., Di Stefano, P., Sulli, A., Vitale, F.P. (1996). Paleogeography and structure of the central Mediterranean: Sicily and its offshore area. *Tectonophysics* 260, 291–323. http://dx.doi.org/10.1016/0040-1951(95)00196-4.

Catalano, S., Monaco, C., Tortorici, L., Paltrinieri, W., Steel, N. (2004). Neogene-Quaternary tectonic evolution of the southern Apennines. *Tectonic*s, 23, TC2003, doi:10.1029/2003TC001512.

Cello, G., Tondi, E., Micarelli, L., Mattioni, L. (2003). Active tectonics and earthquake sources in the epicentral area of the 1857 Basilicata earthquake (southern Italy). *J. Geodyn.*, 36(1-2), 37-50.

Chen, W., Wang, D., Wei, S. (2013). A study on the uncertainties of the centroid depth of the 2013 Lushan earthquake from teleseimic body wave data. *Earthq. Sci.* 26(3–4):161–168

Chiarabba, C., De Gori, P., Speranza, F. (2008). The Southern Tyrrhenian subduction zone: deep geometry, magmatism and Plio-Pleistocene evolution. *Earth Planet. Sc. Lett.* 268, 408–423. http://dx.doi.org/10.1016/j.epsl.2008.01.036.

Chiarabba, C., and M. Palano (2017). Progressive migration of slab break-off along the southern Tyrrhenian plate boundary: Constraints for the present day kinematics. *J. Geodyn.*, 105, 51-61.

Ciaranfi, N., Ghisetti, F., Guida, M., Iaccarino, G., Lambiase, S., Pieri, P., Rapisardi ,L., Ricchetti, G., Torre, M., Tortorici, L., Vezzani, L. (1983). Carta neotettonica dell'Italia meridionale, Prog. Fin. Geod. Pub., 515, 1-62.

Crouse, CB, and T. Matuschka (1983). Digitialization noise and accelerograph pen offset associated with Japanese accelerograms. *Bull. Seism. Soc. Am.*, 73, 1187–1196.

D'Agostino, N., D'Anastasio, E., Gervasi, A., Guerra, I., Nedimović, M.R., Seeber, L., Steckler, M. (2011). Forearc extension and slow rollback of the Calabria Arc from GPS measurements. *Geophys. Res. Lett.* 38, L17304. http://dx.doi.org/ 10.1029/2011GL048270.

D'Amico, S., Orecchio, B., Presti, D., Zhu, L., Herrmann, R.B., Neri, G. (2010). Broadband waveform inversion of moderate earthquakes in the Messina Straits, southern Italy. *Phys. Earth Planet. In.*, 179, 97–106.

D'Amico, S., Orecchio, B., Presti, D., Gervasi, A., Zhu, L., Guerra, I., Neri, G., Herrmann, R.B. (2011). Testing the stability of moment tensor solutions for small earthquakes in the Calabro-Peloritan Arc region (southern Italy). *B. Geofis. Teor. Appl.*, 52 (2), 283–298.

Devoti, R., Riguzzi, F., Cuffaro, M., Doglioni, C. (2008). New GPS constraints on the kinematics of the Apennines subduction. *Earth Planet. Sc. Lett.* 273, 163–174.

DISS Working Group (2015). Database of Individual Seismogenic Sources (DISS), version 3.2.0: A compilation of potential sources for earthquakes larger than M 5.5 in Italy and surrounding areas, Istituto Nazionale di Geofisica e Vulcanologia, available at http://diss.rm.ingv.it/diss/, doi: 10.6092/INGV.IT-DISS3.2.0.

Dreger D.S., Helmberger D.V. (1993). Determination of source parameters at regional distances with three-component sparse network data. *J Geophys. Res. Solid Earth* 98(B5):8107–8125

Dreger D. (2003). TDMT_INV: time domain seismic moment tensor INVersion. In: *International handbook of earthquake and engineering seismology*, vol 81B, p 1627

Dunbar, P. K., Lockridge, P. A., and L. S. Whiteside (1992). Catalog of Significant Earthquakes, 2150 BC-1991 AD: Including Quantitative Casualties and Damage, U.S. Department of Commerce, National Oceanic and Atmospheric Administration, Environmental Data and Information Service, National Geophysical Data Center, Boulder, Colorado.

Di Stefano, R., Bianchi, I., Ciaccio, M. G., Carrara, G., Kissling, E. (2011). Three-dimensional Moho topography in Italy: New constraints from receiver functions and controlled source seismology. *Geochem. Geophy. Geosys.*, 12(9).

Dziewonski, A. M., Chou, T. A., and J. H. Woodhouse (1981). Determination of earthquake source parameters from waveform data for studies of global and regional seismicity. *J. Geophys. Res.*, 86, 2825–2852, doi:10.1029/JB086iB04p02825.

Dziewonski, A. M., Ekström, G., Franzen, J. E., Woodhouse. J. H. (1987). Global seismicity of 1978: centroid-moment tensor solutions for 512 earthquakes. *Phys. Earth Planet. In.*, 46(4), 316-342.

Ekström, G., Nettles, M., Dziewonski, A.M. (2012). The global CMT project 2004–2010: Centroidmoment tensors for 13,017 earthquakes. *Phys. Earth Planet Inter.* 200–201. https://doi.org/10.1016/j.pepi.2012.04.002

Faccenna, C., Davy, P., Brun, J. P., Funiciello, R., Giardini, D., Mattei, M., Nalpas, T. (1996). The dynamics of back-arc extension: An experimental approach to the opening of the Tyrrhenian Sea. *Geophys. J. Int.* 126, no. 3, 781–795, doi: 10.1111/j.1365-246X.1996.tb04702.x.

Faccenna, C., Becker, T.W., Lucente, F.P., Jolivet, L., Rossetti, F. (2001). History of subduction and back-arc extension in the central Mediterranean. *Geophys. J. Int.* 145, 809–820. http://dx.doi.org/10.1046/j.0956-540x.2001.01435.x.

Faccenna, C., Piromallo, C., Crespo-Blanc, A., Jolivet, L. (2004). Lateral slab deformation and the origin of the western Mediterranean arcs. *Tectonics* 23, TC1012. http:// dx.doi.org/10.1029/2002TC001488.

Faccenna, C., Molin, P., Orecchio, B., Olivetti, V., Bellier, O., Funiciello, F., Minelli, L., Piromallo, C., Billi, A. (2011). Topography of the Calabria subduction zone (southern Italy): Clues for the origin of Mt. Etna. *Tectonics*, 30, TC1003, doi:10.1029/2010TC002694.

Ferrari, G., and N. A. Pino (2003). EuroSeismos 2002–2003 a project for saving and studying historical seismograms in the Euro-Mediterranean area. *Geophys. Res. Abs.* 5, EAE03-A-05274.

Gallais, F., Graindorge, D., Gutscher, M.A., Klaeschen, D. (2013). Propagation of a lithospheric tear fault (STEP) through the western boundary of the Calabrian accretionary wedge offshore eastern Sicily (Southern Italy). *Tectonophysics*, 602, 141–152.

Galli, P., and Bosi, V. (2003). Catastrophic 1638 earthquakes in Calabria (southern Italy): New insights from paleoseismological investigation. *J. Geophys. Res.-Sol. Ea*, 108(B1).

Galli, P., Galadini, F., Pantosti, D. (2008). Twenty years of paleoseismology in Italy. *Earth Sci. Rev*, 88, 89–117.

Galli, P., and D. Molin (2009). Il terremoto del 1905 in Calabria: Revisione della distribuzione degli effetti e delle ipotesi sismogenetiche. *Il Quaternario Italian J. Quaternary Sci.,* 22, no. 2, 207–234.

Gasparini, C., Iannaccone, G., and R., Scarpa (1985). Fault-plane solutions and seismicity of the Italian peninsula. *Tectonophysics*, 117(1-2), 59-78.

Gasperini, P., Lolli, B., Vannucci, G., and E., Boschi (2012). A comparison of moment magnitude estimates for the European—Mediterranean and Italian regions. *Geophys. J. Int.*, 190(3), 1733-1745.

Gephart, J., and W., Forsyth (1984), An improved method for determining the regional stress tensor using earthquake focal mechanism data: Application to the San Fernando earthquake sequence, *J. Geophys. Res.*, 89, 9305–9320, doi:10.1029/JB089iB11p09305.

Ghisetti, F., and L., Vezzani (1981). Contribution of structural analysis to understanding the geodynamic evolution of the Calabrian Arc (Southern Italy), *J. Struct. Geol.*, 3, 371-381

Ghisetti, F. (1984). Recent deformations and the seismogenic source in the Messina Strait (southern Italy). *Tectonophysics*, 109(3-4), 191-208.

Govers, R., and M. J. R., Wortel (2005). Lithosphere tearing at STEP faults: Response to edges of subduction zones. *Earth Planet Sci. Lett.* 236, 505–523.

Grabrovec, D., and I., Allegretti (1994). On the digitizing of historical seismograms. *Geofizika*, 11, 27-31.

Guarnieri, P. (2006). Plio-Quaternary segmentation of the south Tyrrhenian forearc basin. *Int. J. Earth Sci.*, 95.1, 107–118.

Gueguen, E., Doglioni, C., Fernandez, M., (1998). On the post-25 Ma geodynamic evolution of the western Mediterranean. *Tectonophysics* 298, 259–269.

Guidoboni, E., Ferrari, G., Mariotti, D., Comastri, A., Tarabusi, G., Valensise, G. (2007). Catalogue of Strong Earthquakes in Italy (461 BC-1997) and Mediterranean Area (760 BC-1500).

Hardebeck, J. L., and A. J., Michael (2004). Stress orientations at intermediate angles to the San Andreas fault, California. *J. Geophys. Res.*, 109, B11303, doi:10.1029/2004JB003239.

Hardebeck, J. (2006). Homogeneity of small-scale earthquake faulting, stress, and fault strength. *Bull. Seismol. Soc. Am.*, 96, 1675–1688, doi:10.1785/0120050257.

Hartigan, J. A. (1975), Clustering Algorithms, Wiley, New York.

Heidbach, O., Tingay, M., Barth, A., Reinecker, J., Kurfeß, D., Muller, B. (2010). Global crustal stress pattern based on the World Stress Map database release 2008. *Tectonophysics*, 482(1–4), 3–15.

Herrmann, R.B. (1987). Computer Programs in Seismology, Vol. 2, Saint Louis University, St. Louis.

Hjörleifsdóttir, V., and G., Ekström (2010). Effects of three-dimensional Earth structure on CMT earthquake parameters. *Phys. Earth Planet. In.*, 179 (3-4), 178-190.

Hollenstein, C.H., Kahle, H.-G., Geiger, A., Jenny, S., Goes, S., Giardini, D. (2003). New GPS constraints on the Africa–Eurasia plate boundary zone in southern Italy. *Geophys. Res. Lett.* 30, 1935. http://dx.doi.org/10.1029/2003GL017554.

Holt, R. A., Savage, M. K., Townend, J., Syracuse, E. M., Thurber, C. H. (2013). Crustal stress and fault strength in the Canterbury Plains, New Zealand. *Earth Planet. Sci. Lett.*, 383, 173–181.

Jacques, E., Monaco, C., Tapponier, P., Tortorici, L., Winter, T. (2001). Faulting and earthquake triggering during the 1783 Calabria seismic sequence. *Geophys. J. Int.* 147, 499–516.

Kanamori, H. (1988). Importance of Historical Seismograms for Geophysical Research, in Historical Seismograms and Earthquakes of the World, pp 16–33.

Kennett, B. L. N., Engdahl, E. R., and R., Buland (1995). Constraints on seismic velocities in the Earth from traveltimes. *Geophys. J. Int.* 122, no. 1, 108–124, doi: 10.1111/j.1365-246X.1995.tb03540.x.

Konstantinou, K. I. and S., Rontogianni (2011). A comparison of teleseismic and regional seismic moment estimates in the European-Mediterranean region. *Seismol. Res. Lett.*, 82(2), 188-200.

Lay, T., and T. C., Wallace (1995). Modern Global Seismology, Academic Press, San Diego, California.

Li, H., Michelini, A., Zhu, L., Bernardi, F., Spada, M. (2007). Crustal velocity structure in Italy from analysis of regional seismic waveforms. *Bull. Seismol. Soc. Am.*, 97, 2024–2039, doi:10.1785/0120070071.

Lucente, F. P., Chiarabba, C., Cimini, G. B., Giardini, D. (1999). Tomographic constraints on the geodynamic evolution of the Italian region. *J. Geophys. Res.* 104, no. B9, 20,307–20,327, doi: 10.1029/1999JB900147.

Malinverno, A., and W., Ryan (1986). Extension in the Tyrrhenian Sea and shortening in the Apennines as result of arc migration driven by sinking of the lithosphere. *Tectonics*, 5, 227–245, doi:10.1029/TC005i002p00227.

Margottini, C., Ambraseys, N. N., and A., Screpanti (1993). La magnitudo dei terremoti italiani del XX secolo, ENEA, rapporto interno, Roma, Italy, 57 (in Italian).

Mazzotti, S., and J., Townend (2010). State of stress in central and eastern North American seismic zones. *Lithosphere*, 2(2), 776–83.

McKenzie, D. (1969). The relationship between fault plane solutions for earthquakes and the directions of the principal stresses. *Bull. Seismol. Soc. Am.*, 59, 591–601.

Michelini, A., De Simoni, B., Amato, A., Boschi, E. (2005). Collecting, digitizing, and distributing historical seismological data. Eos, *Transactions*, Am. Geophys. Un. 86 (28), 261; doi:10.1029/2005EO280002.

Michelini, A., Lomax, A., Nardi, A., Rossi, A. (2006). La localizzazione del terremoto della Calabria dell'8 settembre 1905 da dati strumentali, in 8 settembre 1905: terremoto in Calabria, I. Guerra and A. Savaglio (Editors), Vol. 8, Regione Calabria Assessorato alla Cultura, Castrovillari, Italy, 225–240 (in Italian).

Monaco, C., Tortorici, L., Nicolich, R., Cernobori, L., Costa, M. (1996). From collisional to rifted basins: An example from the southern Calabrian arc (Italy). *Tectonophysics* 266, nos. 1/4), 233–249, doi:10.1016/S0040-1951(96)00192-8.

Monaco, C., and L., Tortorici (2000). Active faulting in the Calabrian arc and eastern Sicily. *J. Geodyn.* 29, 407–424.

Monna, S. and T., Dahm (2009). Three-dimensional P wave attenuation and velocity upper mantle tomography of the southern Apennines-Calabrian Arc subduction zone. *J. geophys. Res.*, 114, B06304, doi:10.1029/2008JB005677

Montone, P., and M. T., Mariucci (2016). The new release of the Italian contemporary stress map. *Geophys. J. Int.*, 205, 1525–1531.

Montuori, C., Cimini, G. B., and P., Favali (2007). Teleseismic tomography of the southern Tyrrhenian subduction zone: New results from seafloor and land recordings. *J. Geophys. Res.* 112, no. B3, doi: 10.1029/2005JB004114.

Murphy, W. (1993). Mechanisms of slope failure during strong ground motion in Southern Italy-some historical evidence. WIT Transactions on The Built Environment, 3

Musumeci, C., Scarfì, L., Palano, M., and D., Patanè (2014). Foreland segmentation along an active convergent margin: New constraints in southeastern Sicily (Italy) from seismic and geodetic observations. *Tectonophysics*, 630, 137–149, doi:10.1016/j.tecto.2014.05.017.

Neri, G., Barberi, G., Orecchio, B., and A., Mostaccio (2003). Seismic strain and seismogenic stress regimes in the crust of the southern Tyrrhenian region. *Earth Planet. Sci. Lett.*, 213, 97–112.

Neri, G., Barberi, G., Oliva, G., Orecchio, B. (2004). Tectonic stress and seismogenic faulting in the area of the 1908 Messina earthquake, south Italy. *Geophys. Res. Lett.*, 31(10), doi:10.1029/2004GL019742.

Neri, G., Barberi, G., Oliva, G., Orecchio, B. (2005). Spatial variations of seismogenic stress orientations in Sicily, south Italy. *Phys. Earth Planet. In.*, 148(2-4), 175-191.

Neri, G., Oliva, G., Orecchio, B., Presti, D. (2006). A possible seismic gap within a highly seismogenic belt crossing Calabria and eastern Sicily, Italy. *Bull. Seismol. Soc. Am.*, 96(4A), 1321–1331, doi:10.1785/0120050170.

Neri, G., Orecchio, B., Totaro, C., Falcone, G., Presti, D. (2009). Seismic tomography says that lithospheric subduction beneath south Italy is close to die. *Seismol. Res. Lett.* 80, 63–70. http://dx.doi.org/10.1785/gssrl.80.1.63.

Neri, G., Marotta, A. M., Orecchio, B., Presti, D., Totaro, C., Barzaghi, R., Borghi, A. (2012). How lithospheric subduction changes along the Calabrian Arc in southern Italy: Geophysical evidences. *Int. J. Earth Sci.*, 101, 1949–1969.

Neri, G., Aloisi, M., Cannavò, F., Orecchio, B., Palano, M., Presti, D., Siligato, G., Totaro, C. (2014). Crustal stress and strain distribution in Sicily (Southern Italy) from joint analysis of seismicity and geodetic data. AGU Fall Meeting, Abstract-ID: T33B-4691.

Nocquet, J.-M., Calais, E. (2004). Geodetic measurements of crustal deformation in the Western Mediterranean and Europe. *Pure Appl. Geophys.,* 161, 661–681. http://dx.doi.org/10.1007/s00024-003-2468-z.

Nocquet, J. (2012). Present-day kinematics of the Mediterranean: A comprehensive overview of GPS results. *Tectonophysics*, 579, 220–242.

Okada, Y. (1992). Internal deformation due to shear and tensile faults in a half-space. *Bull. Seismol. Soc. Am.* 82, no. 2, 1018–1040.

Okal, E.A., and D., Reymond (2003). The mechanism of great Banda Sea earthquake of 1 February1938: Applying the method of preliminary determination of focal mechanism to a historical event. *Earth Planet. Sci. Lett.*, 216: 1–15.

Orecchio, B., Presti, D., Totaro, C., Guerra, I., Neri, G. (2011). Imaging the velocity structure of the Calabrian Arc region (South Italy) through the integration of different seismological data. *Boll. Geofis. Teor. Appl.*, 52, 625–638.

Orecchio, B., Presti, D., Totaro, C., Neri, G. (2014). What earthquakes say concerning residual subduction and STEP dynamics in the

Calabrian Arc region, south Italy. *Geophys. J. Int.*, 199, 1929–1942, doi:10.1093/gji/ggu373.

Orecchio, B., Presti, D., Totaro, C., D'Amico, S., Neri, G. (2015). Investigating slab edge kinematics through seismological data: The northern boundary of the Ionian subduction system (south Italy). *J. Geodyn.*, 88, 23–25, doi:10.1016/j.jog.2015.04.003.

Orecchio B., Aloisi, M., Cannavò, F., Palano, M., Presti, D, Pulvirenti, F., Totaro, C., Siligato, G., Neri, G. (2017). Present-day kinematics and deformation processes in the southern Tyrrhenian region: new insights on the northern Sicily extensional belt. *Ital. J. Geosci.*, 136(3), 418-433.

Palano, M., Ferranti, L., Monaco, C., Mattia, M., Aloisi, M., Bruno, V., Cannavò, F., Siligato,G. (2012). GPS velocity and strain fields in Sicily and southern Calabria, Italy: updated geodetic constraints on tectonic block interaction in the central Mediterranean. *J Geophys. Res.* 117, B07401. http://dx.doi.org/10.1029/2012JB009254.

Palano, M. (2015). On the present-day crustal stress, strain-rate fields and mantle anisotropy pattern of Italy. *Geophys. J. Int.*, 200, 969–985, doi:10.1093/gji/ggu451.

Palano, M., Schiavone, D., Loddo, M., Neri, M., Presti, D., Quarto, R., Totaro, C., Neri G. (2015). Active upper crust deformation pattern along the southern edge of the Tyrrhenian subduction zone (NE Sicily): Insights from a multidisciplinary approach. *Tectonophysics*, 657, 205–218.

Palano, M., Piromallo, C., Chiarabba, C. (2017). Surface imprint of toroidal flow at retreating slab edges: The first geodetic evidence in the Calabrian subduction system. *Geophys. Res. Lett.*, 44(2), 845-853.

Pepe, F., Sulli, A., Bertotti, G., Catalano, R. (2005). Structural highs formation and their relationship to sedimentary basins in the north Sicily continental margin (southern Tyrrhenian Sea): implication for the Drepano Thrust Front. *Tectonophysics* 409, 1–18. http://dx.doi.org/10.1016/j.tecto.2005.05.009.

Piana Agostinetti, N., Steckler, M. S., and F. P., Lucente (2009). Imaging the subducted slab under the Calabrian arc, Italy, from receiver function analysis. *Lithosphere* 1, no. 3, 131–138, doi: 10.1130/L49.1.

Piatanesi, A. and S., Tinti (1998). A revision of the 1693 eastern Sicily earthquake and tsunami. *J. Geophys. Res.-Sol. Ea*, 103(B2), 2749-2758.

Piatanesi, A., and S., Tinti (2002). Numerical modelling of the September 8, 1905 Calabrian (southern Italy) tsunami. *Geophys. J. Int.* 150, no. 1, 271–284, doi: 10.1046/j.1365-246X.2002.01700.x.

Pino, N. A., Palombo, B., Ventura, G., Perniola, B., Ferrari, G. (2008). Waveform modeling of historical seismograms of the 1930 Irpinia earthquake provides insight on “blind” faulting in southern Apennines (Italy). *J. Geophys. Res.-Sol. Ea*, 113(B5).

Pino, N., Piatanesi, A., Valensise, G., Boschi, E. (2009). The 28 December 1908 Messina Straits earthquake (Mw 7.1): a great earthquake throughout a century of seismology. *Seism. Res. Lett.*, 80, 243–259.

Pintore, S., Quintiliani. M., and D.. Franceschi (2005). Teseo: A vectorizer of historical seismograms. *Comp. Geosci.*, 31: 1277–1285.

Platania, G. (1907). I fenomeni in mare durante il terremoto di Calabria del 1905, Società Tipografica Modenese, Modena, Italy.

Polonia A., Torelli, L., Mussoni, P., Gasperini, L., Artoni, A., Klaeschen, D. (2011). The Calabrian Arc subduction complex in the Ionian Sea: regional architecture, active deformation, and seismic hazard. *Tect.*, 30, TC5018, doi:10.1029/2010TC002821.

Polonia, A., Torelli, L., Artoni, A., Carlini, M., Faccenna, C., Ferranti, L., Gasperini, L., Govers, R., Klaeschen, D., Monaco, C., Neri, G., Nijholt, N., Orecchio, B., Wortel, R. (2016). The Ionian and Alfeo-Etna fault zones: New segments of an evolving plate boundary in the central Mediterranean Sea?. *Tectonophysics*, 675, 69–90.

Pondrelli, S., Morelli, A., Ekström, G., Mazza, S, Boschi, E., Dziewonski, A.M. (2002). European-Mediterranean regional centroid-moment tensors: 1997–2000. *Phys. Earth Planet Inter.* 130(1):71–101

Pondrelli, S., Piromallo, C., and E., Serpelloni (2004). Convergence vs. retreat in Southern Tyrrhenian Sea: Insights from kinematics. *Geophys. Res. Lett.*, 31, L06611, doi:10.1029/2003GL019223.

Pondrelli, S., Salimbeni, S., Ekstrom, G., Morelli, A., Gasperini, P., Vannucci, G. (2006). The Italian CMT dataset from 1977 to the present. *Phys. Earth Planet. In.*, 159 (3–4), 286–303.

Pondrelli, S., Salimbeni, S., Morelli, A., Ekström, G., Boschi, E. (2007). European-Mediterranean regional centroid moment tensor catalog: solutions for years 2003 and 2004. *Phys. Earth Planet Inter.* 164(1):90–112

Pondrelli, S., Salimbeni, S., Morelli, A., Ekström, G., Postpischl, L., Vannucci, G., Boschi, E. (2011). European-Mediterranean regional centroid moment tensor catalog: Solutions for 2005–2008. *Phys. Earth Planet. Int.*, 185(3), 74–81.

Pontevivo, A. and G.F., Panza (2006). The Lithosphere-Asthenosphere system in the Calabrian Arc and surrounding seas—Southern Italy. *Pure appl. Geophys.*, 163, 1617–1659.

Presti, D., Troise, C., and G., De Natale (2004). Probabilistic location of seismic sequences in heterogeneous media. *Bull. seism. Soc. Am.*, 94, 2239–2253.

Presti, D., Orecchio, B., Falcone, G., Neri, G. (2008). Linear versus non-linear earthquake location and seismogenic fault detection in the southern Tyrrhenian Sea, Italy. *Geophys. J. Int.* 172, 607–618.

Presti, D., Billi, A., Orecchio, B., Totaro, C., Faccenna, C., Neri, G. (2013). Earthquake focal mechanisms, seismogenic stress, and seismotectonics of the Calabrian Arc, Italy. *Tectonophysics*, 602, 153–175, doi:10.1016/j.tecto.2013.01.030.

Presti, D., Neri, G., Orecchio, B., Scolaro, S., Totaro, C. (2017). The 1905 Calabria, Southern Italy, Earthquake: Hypocenter Location, Causative Process, and Stress Changes Induced in the Area of the 1908 Messina Straits Earthquake. *B. Seismol. Soc. Am.*, 107(6), 2613-2623.

Reitz, M. A., and L., Seeber (2012). Arc-parallel strain in a short rollback subduction system: The structural evolution of the Crotone basin (northeastern Calabria, southern Italy). *Tectonics*, 31, TC4017, doi:10.1029/2011TC003031.

Riuscetti, M., and R., Schick (1975). Earthquakes and tectonics in southern Italy. *Boll. Geof. Teor. Appl.* 17(65), 59–78.

Rizzo, G. B. (1906). Sulla velocità di propagazione delle onde sismiche nel terremoto della Calabria del giorno 8 settembre 1905, C. Clausen, Turin, Italy (in Italian).

Rosenbaum, G., and G. S., Lister (2004). Neogene and Quaternary rollback evolution of the Tyrrhenian sea, the Apennines, and the Sicilian Maghrebides. *Tectonics*, 23, TC1013, doi:10.1029/2003TC001518.

Rovida, A. N., Locati, M., Camassi, R. D., Lolli, B., Gasperini, P. (2016). CPTI15, the 2015 version of the Parametric Catalogue of Italian Earthquakes.

Sabatini, V. (1908). Appunti sul terremoto calabrese del 23 ottobre 1907, Bollettino del R. Comitato Geologico d'Italia, 1, 3-11.

Scherbaum, F. (1996). Of Poles and Zeros: Fundamentals of Digital Seismology, Kluwer, Dordrecht, The Netherlands.

Schlupp, A. (1996). Néotectonique de la Mongolie Occidentale analysée à partir de données de terrain, sismologiques et satellitaires, PhD thesis, ULP, Strasbourg.

Scognamiglio, L., Tinti, E., and A., Michelini (2009). Real-time determination of seismic moment tensor for the Italian region. *Bull. Seismol. Soc. Am.*, 99(4), 2223–2242, doi:10.1785/0120080104.

Selvaggi, G., Chiarabba, C. (1995). Seismicity and P wave velocity image of the southern Tyrrhenian subduction zone. *Geophy. J. Int.*, 121, 818–826. http://dx.doi.org/10.1111/j.1365-246X.1995.tb06441.x.

Serpelloni, E., Bürgmann, R., Anzidei, M., Baldi, P., Mastrolembo Ventura, B., Boschi, E. (2010). Strain accumulation across the Messina Straits and kinematics of Sicily and Calabria from GPS data and dislocation modeling. *Earth Planet. Sc. Lett.* 298, 1–14.

Silwal, V. and Tape, C. (2016). Seismic moment tensors and estimated uncertainties in southern Alaska. *J. Geophys. Res. Solid Earth* 121(4):2772–2797

Snoke, J. A., and J. C., Lahr (2001). Locating earthquakes: At what distance can the earth no longer be treated as flat? *Seismol. Res. Lett.* 72, no. 5, 538–541, doi: 10.1785/gssrl.72.5.538.

Spakman, W., and R., Wortel (2004). A tomographic view on western Mediterranean geodynamics. In: Cavazza, W. (Ed.), The Transmed Atlas: The Mediterranean Region from Crust to Mantle. Springer, New York, pp. 31–52.

Stich, D., Ammon, C. J., and J. Morales (2003a). Moment tensor solutions for small and moderate earthquakes in the Ibero-Maghreb region. J. Geophys. Res.-Sol. Ea, 108(B3).

Stich, D., Batlló, J., Morales, J., Macià, R., Dineva, S. (2003b). Source parameters of the 1910 Mw= 6.1 Adra earthquake (southern Spain). *Geophys. J. Int.*, 155, 539–546.

Stich, D., Batlló, J., Macià, R., Teves-Costa, P., Morales, J. (2005). Moment tensor inversion with single-component historical seismograms: The 1909 Benavente (Portugal) and Lambesc (France) earthquakes. *Geophys. J. Int.*, 162(3), 850-858.

Stich, D., Martín, R., Batlló, J., Macià, R., Mancilla, F., Morales, J. (2018). Normal faulting in the 1923 Berdún earthquake and postorogenic extension in the Pyrenees. *Geophys. Res. Lett.*, 45, doi:10.1002/2018GL077502

Tan, Y., Zhu, L., Helmberger, D., and C., Saikia (2006). Locating and modeling regional earthquakes with two stations. *J. Geophys. Res.*, 111, B01306, doi:10.1029/2005JB003775.

Tanioka, Y., Satake, K., and L., Ruff (1995). Analysis of seismological and tsunami data from the 1993 Guam earthquake, in Tsunamis: 1992–1994, Birkhauser, Basel, Switzerland, 823–837.

Thorndike, R. L. (1953). Who belongs in the family?. *Psychometrika*, 18(4), 267–76.

Tiberti, M. M., Vannoli, P., Fracassi, U., Burrato, P., Kastelic, V., Valensise, G. (2017). Understanding seismogenic processes in the

Southern Calabrian Arc: a geodynamic perspective. *Ital. J. Geosci.*, 136 (3), 365–388, doi: https://doi.org/10.3301/IJG.2016.12

Toda, S., Stein, R. S., Reasenberg, P. A., Dieterich, J. H., Yoshida, A. (1998). Stress transferred by the 1995 Mw 6:9 Kobe, Japan, shock: Effect on aftershocks and future earthquake probabilities. *J. Geophys. Res.* 103, no. B10, 24,543–24,565, doi: 10.1029/98JB00765.

Tortorici, L., Monaco, C., Tansi, C., and O., Cocina (1995). Recent and active tectonics in the Calabrian arc (southern Italy). *Tectonophysics* 243, no. 1, 37–55, doi: 10.1016/0040-1951(94)00190-K.

Totaro, C., Presti, D., Billi, A., Gervasi, A., Orecchio, B., Guerra, I., Neri, G. (2013). The ongoing seismic sequence at the Pollino Mountains, Italy. *Seismol. Res. Lett.*, 84(6), 955–962, doi:10.1785/0220120194.

Totaro, C., Koulakov, I., Orecchio, B., and D., Presti (2014). Detailed crustal structure in the area of the southern Apennines–Calabrian Arc border from local earthquake tomography. *J. Geodyn.*, 82, 87–97, doi:10.1016/j.jog.2014.07.004.

Totaro, C., Seeber, L., Waldhauser, F., Steckler, M., Gervasi, A., Guerra, I., Orecchio, B., Presti, D. (2015). An intense earthquake swarm in the southernmost Apennines: Fault architecture from high-resolution hypocenters and focal mechanisms. *Bull. Seismol. Soc. Am.*, 105(6), 3121–3128, doi:10.1785/0120150074.

Totaro, C., Orecchio, B., Presti, D., Scolaro, S., Neri, G. (2016). Seismogenic stress field estimation in the Calabrian Arc region (south Italy) from a Bayesian approach. *Geophys. Res. Lett.*, 43(17), 8960-8969.

Townend, J. (2006). What do faults feel? Observational constraints on the stress acting on seismogenic faults, in *Earthquakes: Radiated Energy and Physics of Faulting, Geophys*. Monogr. Ser., vol. 170, edited by R. Abercrombie et al., pp. 313–327, AGU, Washington, D. C.

Townend, J., Sherburn, S., Arnold, R., Boese, C., Woods, L. (2012). Three-dimensional variations in present-day tectonic stress along the Australia–Pacific plate boundary in New Zealand. *Earth Planet. Sci. Lett.*, 353–354, 47–59, doi:10.1016/j.epsl.2012.08.003.

Troise, C., De Natale, G., Pingue, F., Petrazzuoli, S. M. (1998). Evidence for static stress interaction among earthquakes in the south–central Apennines (Italy). *Geophys. J. Int.* 134, no. 3, 809–817, doi:10.1046/j.1365-246x.1998.00610.x.

Valensise, G., and D., Pantosti (2001). The investigation of potential earthquake sources in peninsular Italy: a review. *J. Seismol.*, 5(3), 287-306.

Valentine, A.P., and J., Trampert (2012). Assessing the uncertainties on seismic source parameters: towards realistic error estimates for centroid-moment-tensor determinations. *Phys. Earth Planet Inter.* 210:36–49

Van Dijk, J.P. (1992). Late Neogene fore-arc basin evolution in the Calabrian Arc (Central Mediterranean). Tectonic sequence stratigraphy and dynamic geohistory. With special reference to the geology of Central Calabria. *Geol. Ultraj.*, 92, p. 288

Vannoli, P., Vannucci, G., Bernardi, F., Palombo, B., Ferrari, G. (2015). The Source of the 30 October 1930 M w 5.8 Senigallia (Central Italy) Earthquake: A Convergent Solution from Instrumental, Macroseismic, and Geological Data. *B. Seismol. Soc. Am.*, 105(3), 1548-1561.

Vannoli, P., Bernardi, F., Palombo, B., Vannucci, G., Console, R., G., Ferrari (2016). New constraints shed light on strike-slip faulting beneath the southern Apennines (Italy): The 21 August 1962 Irpinia multiple earthquake. *Tectonophysics,* 691, 375-384.

Visini, F., De Nardis, R., Barbano, M. S., Lavecchia, G. (2009). Testing the seismogenic sources of the January 11th 1693 Sicilian earthquake (Io X/XI): insights from macroseismic field simulations. *Boll. Soc. Geol. Ital.*, 128(1), 147-156.

Wells, D. L., and K. J., Coppersmith (1994). New empirical relationships among magnitude, rupture length, rupture width, rupture area, and surface displacement. *Bull. Seismol. Soc. Am.* 84, no. 4, 974–1002.

Wortel, M.J.R., and W., Spakman (2000). Subduction and slab detachment in the Mediterranean– Carpathian region. *Science* 290, 1910–1917.

Zhao, L. S., and D., Helmberger (1994). Source estimation from broad-band regional seismograms. *Bull. Seismol. Soc. Am.*, 85, 590–605.

Zhu, L., and D,. Helmberger (1996). Advancement in source estimation technique using broadband regional seismograms. *Bull. Seismol. Soc. Am.*, 86, 1634–1641.

Zhu, L., Akyol, N., Mitchell, B.J., Sozbilir, H. (2006). Seismotectonics of western Turkey from high resolution earthquake relocations and moment tensor determinations. *Geophys. Res. Lett.* 33(7)

Zoback, M. L. (1992). First- and second-order patterns of stress in the lithosphere: The world stress map project. *J. Geophys. Res.*, 97(B8), 11,703–11,728, doi:10.1029/92JB00132.

DATA AND SHARING RESOURCES

Centroid Moment Tensor Catalog CMT, available at http://www.globalcmt.org/

EuroSeismos database, available at http://storing.ingv.it/es_web/

International Seismological Center catalogue ISC, available at http://www.isc.ac.uk/

Italian Archive of Historical Earthquake Data, available at https://emidius.mi.ingv.it/ASMI/index_en.htm

Italian Parametric Earthquake Catalogue CPTI15, available at https://emidius.mi.ingv.it/CPTI15-DBMI15/

Italian Seismological Instrumental and Parametric Data-Base ISIDe, available at http://cnt.rm.ingv.it/

Regional Centroid Moment Tensor Catalog RCMT, available at http://rcmt2.bo.ingv.it/

Sismos database, available at http://sismos.ingv.it/

Time Domain Moment Tensor Catalog TDMT, available at http://cnt.rm.ingv.it/tdmt